ANCR-NUREG-1287
DATE PUBLISHED — JUNE 1976

IDAHO NATIONAL ENGINEERING LABORATORY

THERMAL-HYDRAULIC ANALYSIS OF THE SEMISCALE MOD-1 BLOWDOWN HEAT TRANSFER TEST SERIES

PREPARED BY AEROJET NUCLEAR COMPANY FOR
U. S. NUCLEAR REGULATORY COMMISSION
AND
ENERGY RESEARCH AND DEVELOPMENT ADMINISTRATION
IDAHO OPERATIONS OFFICE UNDER CONTRACT E(10-1) -1375

DISCLAIMER

Printed in the United States of America
Available from
National Technical Information Service
U. S. Department of Commerce
5285 Port Royal Road
Springfield, Virginia 22161
Price: Printed Copy $5.50; Microfiche $2.25

"The NRC will make available data tapes and operational computer codes on research programs dealing with postulated loss-of-coolant accidents in light water reactors. Persons requesting this information must reimburse the NRC contractors for their expenses in preparing copies of the data tapes and the operational computer codes. Requests should be submitted to the Research Applications Branch, Office of Nuclear Regulatory Research, Nuclear Regulatory Commission, Washington, D.C. 20555."

Approved:

J. O. Zane, Manager
Semiscale Program

P. E. MacDonald /FOR

E. P. Eales, Manager
Systems Research Division

ANCR-NUREG-1287

Distributed Under Category:
NRC-2
Water Reactor Safety Research
Systems Engineering

THERMAL-HYDRAULIC ANALYSIS OF THE SEMISCALE MOD-1 BLOWDOWN HEAT TRANSFER TEST SERIES

by

James M. Cozzuol

AEROJET NUCLEAR COMPANY

Date Published – June 1976

PREPARED FOR THE
U.S. NUCLEAR REGULATORY COMMISSION
AND
ENERGY RESEARCH AND DEVELOPMENT ADMINISTRATION
IDAHO OPERATIONS OFFICE
UNDER CONTRACT No. E(10-1)-1375

ACKNOWLEDGMENTS

The author wishes to express his thanks to the personnel of the Fluids Laboratory Division for their efforts in conducting the tests and gathering the data; to the personnel of the Test Integration and Coordination Section for verification and documentation of the data; to R. F. Farman, R. T. French, and R. W. Shumway for their technical support; and to K. A. Dietz for editing and improving the quality of the overall report.

ABSTRACT

Selected experimental thermal-hydraulic data from the recent Semiscale Mod-1 blowdown heat transfer test series are analyzed from an experimental viewpoint with emphasis on explaining those phenomena which influence core fluid behavior. Comparisons are made between the trends measured by the system instrumentation and the trends predicted by the RELAP4 computer code to aid in obtaining an understanding of the interactions between phenomena occurring in different parts of the system. The analyses presented in this report are valuable for evaluating the adequacy and improving the predictive capability of analytical models developed to predict the system response of a pressurized water reactor during a postulated loss-of-coolant accident (LOCA).

SUMMARY

Data from the Semiscale Mod-1 blowdown heat transfer test series have been analyzed with emphasis on explaining those phenomena which influence core fluid response. In addition, calculations obtained from the RELAP4 computer program have been compared with the data to help in obtaining an understanding of the interactions among phenomena occurring in different parts of the system and to assess the current depth of understanding of the physical processes taking place during a simulated loss-of-coolant accident.

The blowdown heat transfer test series was the second series conducted in the Semiscale Mod-1 program and consisted of ten blowdown tests; nine of these simulated a 200% offset shear of either the hot or cold leg of the broken loop piping, and one of these simulated a small break of the cold leg of the broken loop piping. Each test was conducted by establishing the system fluid conditions at a nominal pressure of 2,260 psia and a core inlet fluid temperature of about 544°F. The core power and intact loop flow rates were controlled for each test to establish the required system temperature differential. Once the piping and various metal components approached the fluid temperature, a rupture in the broken loop piping caused the system fluid to flow out through two rupture nozzles and into a pressure suppression tank. The decompression or blowdown process lasted about 30 seconds for each of the tests. Three of the tests included the injection of emergency core coolant (ECC).

Knowledge of core fluid behavior during blowdown is important to blowdown analyses because the core fluid behavior determines the amount of energy removed from the core. The principal influence on core fluid behavior during a 200% offset shear cold leg break test is the flow in the vessel inlet side of the broken loop, especially during the subcooled portion of blowdown. The high flow rate of subcooled fluid in the vessel inlet side of the broken loop results in an immediate core flow reversal following rupture.

The effect of break location on the overall system response, and in particular on core fluid behavior, was demonstrated to be large when results from a 200% offset shear hot leg break test (Test S-02-1) were compared with those from a 200% offset shear cold leg break test (Test S-02-2). The most significant difference in results for the hot leg break test in comparison with results from the cold leg break test occurred within the core region. For the hot leg break test a positive core flow existed throughout blowdown and the fluid density at the core inlet was high. In contrast, for the cold leg break test the core inlet flow became negative immediately following rupture, and the core inlet fluid density dropped to a small value, indicating a high rate of steam generation within the core.

The effect of the system temperature distribution prior to rupture on system response during blowdown was demonstrated by comparison of results from Test S-01-6 of the previous Semiscale Mod-1 isothermal test series with results from Tests S-02-2 and S-02-4 of the current test series. Each of the three tests was a 200% offset shear cold leg break test with an initial core inlet fluid temperature of about 540°F. The system fluid temperature differentials for the three tests were 0, 48, and 67°F, respectively. Results of these tests

demonstrate that the initial temperature distribution has significant influence on the overall system hydraulic response and, in particular, on the flow from the vessel inlet side of the break during subcooled blowdown. The 200% cold leg break tests with high initial system temperature differentials resulted in higher subcooled flow rates at the vessel inlet side of the break than tests with smaller initial system temperature differentials. The core flow response, being highly sensitive to the vessel inlet side break flow, is thus strongly affected by the initial system temperature distribution.

Results from Tests S-02-3 and S-02-4 were compared to determine the influence of initial core power on the overall system fluid response during blowdown. Results indicate that the initial core power has little, if any, effect on the blowdown response of the system. Variations in the system blowdown performance between Tests S-02-3 and S-02-4 were attributed to the influence of the intact loop pump. The higher pump speed during Test S-02-4 (as compared to that during Test S-02-3) resulted in a reduction in the magnitude of the core flow reversal during the subcooled portion of blowdown.

The interaction of the downcomer and lower plenum fluids with the hot core fluid during the early portion of blowdown for a 200% cold leg break test has significant influence on the subcooled flow response on the vessel inlet side of the broken loop. Mixing of the hot core fluid with the downcomer and lower plenum fluids, and the rate of transport of the mixture up the vessel downcomer and into the broken loop cold leg, determines the length of time that the cold leg fluid remains subcooled. Analysis has shown that a multivolume lower plenum in the RELAP4 model correctly represents the physical phenomena occurring in the lower plenum by allowing hot core fluid to mix with only the upper portion of the lower plenum fluid. Use of a three-volume lower plenum improved the estimate of enthalpy transport to the vessel inlet side of the broken loop, resulting in an improvement in the calculated cold leg flow.

An analysis of the intact loop pressurizer response indicates that the pressurizer did not significantly affect the intact loop hot leg flow during the first 12 seconds of blowdown. After 12 seconds, the high velocity steam flow from the pressurizer had considerable influence on the intact loop hot leg fluid flow and influenced the rewetting of several of the core heater rods.

The intact loop steam generator secondary-to-primary heat transfer during blowdown was found to be small (less than 1%) compared with the energy stored in the primary fluid. An improvement in the calculation of the secondary side response by the RELAP4 program was obtained by using a larger film boiling heat transfer coefficient in the steam generator model. The change in the heat transfer coefficient did not significantly alter the calculations of the primary side response.

The major influence of the intact loop pump on system response during a 200% cold leg break test occurred within seven seconds, following rupture, and resulted in limiting the magnitude of the core flow reversal during the subcooled portion of blowdown. The pump head became fully degraded by seven seconds because of voiding of the fluid at the pump suction.

CONTENTS

ACKNOWLEDGMENTS ii

ABSTRACT iii

SUMMARY iv

I. INTRODUCTION 1

II. EXPERIMENT DESCRIPTION 3

III. RESULTS OF THE DATA ANALYSIS 9

1. CORE FLUID BEHAVIOR 10

2. INFLUENCE OF INITIAL CONDITIONS AND BREAK CONFIGURATION ON SYSTEM AND CORE FLOW BEHAVIOR 14

2.1 Cold Leg Versus Hot Leg Break Configuration 14
2.2 Influence of System Initial Temperature Differential 17
2.3 Influence of Initial Core Power 23

3. RESPONSE OF SYSTEM COMPONENTS 28

3.1 Downcomer and Lower Plenum Fluid Response 28
3.2 Broken Loop Flow Response 34
3.3 Pressurizer Performance and Influence on Intact Loop Hot Leg and Core Fluid Response 43
3.4 Steam Generator Performance 46
3.5 Intact Loop Pump and Cold Leg Response 56

IV. CONCLUSIONS 59

1. CORE FLUID BEHAVIOR 59

2. INFLUENCE OF INITIAL CONDITIONS AND BREAK LOCATION ON CORE FLOW BEHAVIOR 59

3. RESPONSE OF SYSTEM COMPONENTS 60

V. REFERENCES 61

APPENDIX A – RELAP4 COMPUTER CODE AS APPLIED TO SEMISCALE MOD-1 THERMAL-HYDRAULICS ANALYSIS 65

APPENDIX B – DATA RELIABILITY 75

APPENDIX C – REPEATABILITY OF RESULTS 83

FIGURES

1. Semiscale Mod-1 hot leg break configuration – isometric 4

2. Semiscale Mod-1 cold leg break configuration – isometric 5

3. Cross section of vessel with core 6

4. Mass flow rate at the inlet to the core – Tests S-02-3, S-02-4, and S-02-7 11

5. Comparison of mass flow rates at the inlet to the core and near the vessel in the inlet side of the broken loop – Test S-02-4 11

6. Mass flow rate at the inlet to the core – comparison of RELAP4 results with Test S-02-4 data 12

7. Fluid density at the inlet to the core – Tests S-02-3, S-02-4, and S-02-7 13

8. Fluid density at the inlet to the core – comparison of RELAP4 results with Test S-02-4 data 13

9. Pressure response upstream of the break nozzle on the vessel inlet side – Tests S-02-1 and S-02-2 15

10. Pressure response upstream of the break nozzle on the vessel outlet side – Tests S-02-1 and S-02-2 15

11. Mass flow rate near the vessel on the inlet side of the broken loop – Tests S-02-1 and S-02-2 16

12. Mass flow rate near the vessel on the outlet side of the broken loop – Tests S-02-1 and S-02-2 16

13. Mass flow rate at the inlet to the core – Tests S-02-1 and S-02-2 17

14. Fluid density at the inlet to the core – Tests S-02-1 and S-02-2 18

15. Pressure response in the vessel lower plenum – Tests S-01-6, S-02-2, and S-02-4 19

16. Mass flow rate near the vessel on the inlet side of the broken loop – Tests S-01-6, S-02-2, and S-02-4 20

17. Mass flow rate near the vessel on the inlet side of the intact loop – Tests S-01-6, S-02-2, and S-02-4 21

18. Fluid density at the intact loop pump suction – Tests S-01-6, S-02-2, and S-02-4 21

19. Differential pressure across the intact loop pump Tests S-01-6, S-02-2, and S-02-4 22

20. Mass flow rate at the inlet to the core – Tests S 01 6, S 02 2, and S-02-4 22

21. Total core power – Tests S-02-3 and S-02-4 24

22. Mass flow rate near the vessel on the inlet side of the broken loop – Tests S-02-3 and S-02-4 25

23. Mass flow rate near the vessel on the outlet side of the broken loop – Tests S-02-3 and S-02-4 25

24. Total integrated energy leaving vessel – Tests S-02-3 and S-02-4 26

25. Mass flow rate near the vessel on the inlet side of the intact loop – Tests S-02-3 and S-02-4 26

26. Mass flow rate near the vessel on the outlet side of the broken loop – Tests S-02-3 and S-02-4 27

27. Intact loop pump speed – Tests S-02-3 and S-02-4 27

28. Mass flow rate at the inlet to the core – Tests S-02-3 and S-02-4 28

29. Mass flow rate near the vessel on the inlet side of the broken loop – Tests S-02-2 and S-02-3 30

30. Fluid temperature in the vessel downcomer 35 inches below the broken loop cold leg centerline – Tests S-02-2 and S-02-3 30

31. Mass flow rate near the vessel on the inlet side of the broken loop compared with the sum of the mass flows at the core inlet and near the vessel inlet side of the intact loop – Test S-02-4 31

32. Fluid velocities in the vessel downcomer – Test S-02-4 31

33. Fluid temperatures in the vessel lower plenum at 7.5, 14.5, and 27.5 inches above the bottom of the lower plenum – Test S-02-4 32

34. Fluid temperature at the 14.5-inch level in the vessel lower plenum – comparison of RELAP4 calculations using one- and three-volume lower plenum models with Test S-02-4 data 33

35. Fluid temperature in the vessel downcomer 35 inches below the broken loop cold leg centerline – comparison of RELAP4 calculations using one- and three-volume lower plenum models with Test S-02-2 data 33

36. Mass flow rate near the vessel on the inlet side of the broken loop – comparison of RELAP4 calculations using one- and three-volume lower plenum models with Test S-02-2 data 35

37. Fluid density at the inlet to the core – comparison of RELAP4 calculations using one- and three-volume lower plenum models with Test S-02-2 data 35

38. Fluid density in the vessel lower plenum 172 inches below the cold leg centerline – comparison of RELAP4 calculations using one- and three-volume lower plenum models with Test S-02-2 data 36

39. Mass flow rate at the inlet to the core – comparison of RELAP4 calculations using one- and three-volume lower plenum models with Test S-02-2 data 36

40. Fluid temperatures in the vessel downcomer at various elevations – Test S-02-4 37

41. Subcooled blowdown pressure response upstream of the break nozzles on the vessel outlet and inlet sides – Test S-02-4 37

42. Pressure response upstream of the break nozzle on the vessel inlet side – comparison with saturation pressure – Test S-02-4 39

43. Subcooled mass flow rate upstream of the break nozzle on the vessel outlet side – Test S-02-4 39

44. Subcooled mass flow rate near the vessel on the inlet side of the broken loop – Test S-02-4 40

45. Pressure response upstream of the break nozzles on the vessel outlet and inlet sides – Test S-02-4 40

46. Mass flow rate near the vessel on the inlet side of the broken loop compared with the flow rate upstream of break nozzle on the vessel outlet side – Test S-02-4 41

47. Mass flow rate near the vessel on the inlet side of the broken loop loop – comparison of RELAP4 calculation with Test S-02-4 data 42

48. Mass flow rate upstream of the break nozzle on the vessel outlet side – comparison of RELAP4 calculation with Test S-02-4 data 42

49. Differential pressure across the broken loop pump simulator – comparison of RELAP4 calculation with Test S-02-4 data 44

50. Differential pressure across the broken loop steam generator simulator – comparison of RELAP4 results with Test S-02-4 data 44

51. Mass flow rate in the intact loop pressurizer surge line – Test S-02-5 46

52. Intact loop pressurizer schematic 47

53. Fluid densities within the intact loop hot leg – Test S-02-5 48

54. Heater rod cladding temperature response in the upper core region – Test S-02-5 48

55. Pressure response of the intact loop pressurizer – comparison of RELAP4 calculation using pressurizer surge line resistance value of 4,500 $sec^2/ft^3\text{-}in.^2$ with Test S-02-4 data 49

56. Pressure response of the intact loop pressurizer – comparison of RELAP4 calculation using pressurizer surge line resistance of 11,000 sec^2/ft^3-$in.^2$ with Test S-02-4 data 49

57. Mass flow rate near the vessel outlet side of the intact loop – comparison of RELAP4 calculations using pressurizer surge line resistance values of 4,500 and 11,000 sec^2/ft^3-$in.^2$ with Test S-02-4 data 50

58. Mass flow rate downstream of the pressurizer in the intact loop hot leg – comparison of RELAP4 calculations using pressurizer surge line resistance valves of 4,500 and 11,000 sec^2/ft^3-$in.^2$ with Test S-02-4 data 50

59. Intact loop steam generator configuration 52

60. Pressure response in the intact loop steam generator secondary side – Test S-02-4 53

61. RELAP4 intact loop steam generator model 53

62. Pressure response in the intact loop steam generator secondary side – comparison of RELAP4 calculations using secondary-to-primary heat transfer coefficients of 5 and 250 Btu/hr-ft^2-^oF with Test S-02-4 data 54

63. Pressure response near the inlet to the steam generator in the intact loop – comparison of RELAP4 calculations using secondary-to-primary heat transfer coefficients of 5 and 250 Btu/hr-ft^2-^oF with Test S-02-4 data 54

64. Pressure response near the outlet to the steam generator in the intact loop – comparison of RELAP4 calculations using secondary-to-primary heat transfer coefficients of 5 and 250 Btu/hr-ft^2-^oF with Test S-02-4 data 55

65. Differential pressure across the intact loop pump – comparison of RELAP4 calculations with Test S 02-4 data 57

66. Fluid density at the intact loop pump suction – comparison of RELAP4 calculation with Test S-02-4 data 57

67. Mass flow rate at the intact loop pump suction – comparison of RELAP4 calculation with Test S-02-4 data 58

68. Mass flow in intact loop cold leg downstream of the intact loop pump – comparison of RELAP4 calculation with Test S-02-4 data 58

A-1. RELAP4 Semiscale Mod-1 nodalization diagram for Test S-02-4 test prediction – 200% cold leg break configuration 67

A-2. RELAP4 Semiscale Mod-1 nodalization diagram for Test S-02-4 posttest calculation – 200% cold leg break configuration 70

A-3. Semiscale RELAP4 model heated core configuration with hot channel 71

B-1. Mass flow rate near the vessel on the outlet side of the intact loop – comparison of drag disc and turbine flowmeter results – Test S-02-4 76

B-2. Mass flow rate at the intact loop pump suction – comparison of drag disc and turbine flowmeter results – Test S-02-4 76

B-3. Mass flow rate downstream of the intact loop pump – comparison of drag disc and turbine flowmeter results – Test S-02-4 77

B-4. Mass flow rate near the vessel on the inlet side of the intact loop – comparison of drag disc and turbine flowmeter results – Test S-02-4 77

B-5. Mass flow rate at the inlet to the core – comparison of drag disc and turbine flowmeter results – Test S-02-4 78

B-6. Mass flow rate at the inlet to the core (short term) – comparison of drag disc and turbine flowmeter results – Test S-02-4 79

B-7. Mass flow rate near the vessel on the inlet side of the broken loop – comparison of drag disc and turbine flowmeter results – Test S-02-4 79

C-1. System pressure response – showing repeatability of results – Tests S-02-9 and S-02-9A 84

C-2. Mass flow rate downstream of the intact loop pump showing – repeatability of results – Tests S-02-9 and S-02-9A 84

C-3. Mass flow rate near the vessel on the inlet side of the broken loop – showing repeatability of results – Tests S-02-9 and S-02-9A 85

C-4. Mass flow rate at the inlet to the core – showing repeatability of results – Tests S-02-9 and S-02-9A 85

C-5. Fluid density at the inlet to the core – showing repeatability of results – Tests S-02-9 and S-02-9A 86

C-6. Fluid density in the vessel lower plenum 165 inches below the cold leg centerline – showing repeatability of results – Tests S-02-9 and S-02-9A 86

C-7. Fluid density at the intact loop pump suction – showing repeatability of results – Tests S-02-9 and S-02-9A 87

C-8. Fluid density near the vessel on the outlet side of the broken loop – showing repeatability of results – Tests S-02-9 and S-02-9A 87

TABLES

I. Blowdown Heat Transfer Series Test Conditions 7

A-I. RELAP4 Model for Blowdown Heat Transfer Test S-02-4 68

THERMAL-HYDRAULIC ANALYSIS OF THE SEMISCALE MOD-1 BLOWDOWN HEAT TRANSFER TEST SERIES

I. INTRODUCTION

The Semiscale Mod-1 experimental program conducted by Aerojet Nuclear Company is part of the overall U. S. Nuclear Regulatory Commission and Energy Research and Development Administration-sponsored research and development program to investigate the behavior of a pressurized water reactor (PWR) system during a hypothesized loss-of-coolant accident (LOCA). The Semiscale Mod-1 program is intended to provide transient thermal-hydraulic data from a simulated LOCA using a small scale experimental nonnuclear system. The Semiscale Mod-1 program is a major contributor of experimental data that will aid in understanding the response of the system, the response of the individual components, and the interactions that occur between the major components and subsystems. These data provide a means of evaluating the adequacy of the overall system analytical models as well as the models of the individual system components. The objectives of the Semiscale Mod-1 experimental program are to: (a) produce integral and separate effects experimental thermal-hydraulic data that are needed to provide an experimental basis for analytical model assessment, (b) provide data for assessing the requirements and reliability of selected Loss-of-Fluid Test (LOFT) program instrumentation, and (c) produce experimental data to aid in optimizing the selection of test parameters and the evaluation of test results from the LOFT program.

The blowdown heat transfer tests were the second group of tests conducted in the Semiscale Mod-1 program and were the first tests with power applied to the electrically heated core. The primary objectives of the blowdown heat transfer test series were to obtain information required to evaluate the heat transfer characteristics of the Semiscale Mod-1 core and to obtain the information necessary for evaluating the analytical models currently used to calculate core flow and heat transfer coefficients.

In addition to providing information relative to the heat transfer characteristics of the Semiscale Mod-1 core, the blowdown heat transfer test series provided an opportunity to investigate the behavior of the system, specifically: (a) to determine differences in system response caused by initial conditions or system configuration, and (b) to determine component-related thermal-hydraulic phenomena. Those objectives related to differences in system response between tests (in particular, to core hydraulic response) were met through comparisons among tests that demonstrated the influence of: (a) the break location, (b) the cold-leg-to-hot-leg temperature distribution, and (c) initial core power. Those objectives concerned with component-related phenomena were satisfied by tests which investigated: (a) the phenomena occurring within the vessel region, (b) the phenomena occurring in the broken loop, (c) the heat transfer in the intact loop steam generator, (d) the response of the intact loop pressurizer, and (e) the response of the intact loop pump.

The Semiscale Mod-1 test apparatus is a small high-pressure system designed to simulate a LOCA in a PWR. The apparatus consists of a pressure vessel with simulated reactor internals and an electrically heated core; an intact loop with an active pump, steam generator, and pressurizer; and a broken loop with a simulated pump, a simulated steam generator, and break assemblies.

The Semiscale Mod-1 blowdown heat transfer test series consisted of one double-ended offset shear hot leg break test, eight double-ended offset shear cold leg break tests, and one single-ended "small" break test. Two of these tests (Tests S-02-6 and S-02-8) were conducted as standard problems[a] for the U. S. Nuclear Regulatory Commission and, therefore, are not discussed in this report. Each of the tests was conducted by establishing system core inlet fluid conditions at about 544°F and 2,262 psia, adjusting the core power and core flow to achieve the desired core differential temperature, and then rupturing the piping in the broken loop to cause the system fluid to flow out through two rupture nozzles and into a pressure suppression tank. The depressurization (blowdown) lasted about 30 seconds. Emergency core coolant (ECC) was injected during blowdown for Tests S-02-5, S-02-9, and S-02-9A; however, the results of an analysis of the effects of ECC injection are not discussed in this report. The prerupture conditions, test procedures, and uninterpreted results for the blowdown heat transfer tests are provided in a series of experiment data reports[1-7].

This report provides an evaluation of the thermal-hydraulic response of the Semiscale Mod-1 system relative to the specific blowdown heat transfer test objectives. Experimental data and results calculated through use of the RELAP4[8] computer code are presented to aid in understanding the complex phenomena occurring during a LOCA. A companion report relating to the core thermal-hydraulic response is presented in Reference 9.

Section II of this report presents a description of the blowdown heat transfer tests and the experiment system configurations. Section III presents results of data analysis of the core fluid hydraulic behavior, the influence of initial conditions and break configuration on system and core flow response, and the response of individual system components. Section IV presents the more significant conclusions arising out of the analysis. Appendix A presents the RELAP4 analytical model employed throughout the report. Appendices B and C present discussions of the data reliability and repeatability, respectively.

---

[a] A Nuclear Regulatory Commission standard problem test is a test conducted to establish an experimental data base for the purpose of comparison with analytical calculations supplied by the standard problem program participants.

II. EXPERIMENT DESCRIPTION

The Semiscale Mod-1 test apparatus is a high-pressure system designed to operate at typical PWR temperatures and pressures. The system consists of a pressure vessel with simulated reactor internals (upper plenum, core region, lower plenum, and downcomer); an intact loop with an active pump, steam generator, and pressurizer; a broken loop with a simulated steam generator, simulated pump, and pipe rupture assemblies; a pressure suppression system with a header and suppression tank; and a coolant injection system with injection pumps, accumulators, and delivery piping. The broken loop design is such as to allow simulation of either hot or cold leg breaks. Total system liquid volumes for the hot-and-cold-leg-break configuration tests of the blowdown heat transfer series were approximately 7.7 and 7.8 ft^3, respectively. The experimental system configurations for the hot-and-cold-leg-break tests are shown in Figures 1 and 2. Detailed descriptions of the system components, including volumes and flow resistances, and of the measurement and data acquisition systems are contained in Reference 10.

The Semiscale Mod-1 vessel assembly consists of a pressure vessel, vessel filler, vessel filler insulator, core barrel, core barrel insulator, and 40-electrical-heater-rod core. The vessel assembly forms the following internal regions: inlet annulus, downcomer annulus or gap, lower plenum, core, and upper plenum. A cross-sectional view of the vessel with core is shown in Figure 3.

The intact loop is a 1/300-volume scale model of three loops of a commercial four-loop PWR and consists of primary coolant piping, a steam generator, a pressurizer, and a circulating pump. The piping is primarily 3-inch Schedule 160 pipe. The steam generator is a tube-in-shell heat exchanger.

The blowdown loop is a volume-scaled representation of one loop of a four-loop PWR and consists of an inactive pump and steam generator simulators, two discharge nozzles, and two rupture assemblies which provide a simulated double-ended offset shear. The associated piping is primarily 2-inch Schedule 160 stainless steel. The simulated steam generator and simulated pump consist of piping with orifices to achieve the desired hydraulic resistances. The rupture assemblies contain a converging-diverging blowdown nozzle (to provide the desired break area) and two diaphragm rupture discs.

The pressure suppression system consists of a 91.7-ft^3 pressure tank which is used to simulate the backpressure created by a containment building in a PWR system. The tank was maintained partially full of subcooled water, and the downcomer pipe projected below the water surface to accommodate the blowdown effluent. A 16-inch header connects the pressure suppression tank to the primary coolant system.

The Semiscale Mod-1 blowdown heat transfer tests discussed in this report consisted of one double-ended hot leg break configuration test and seven double-ended cold leg break configuration tests. Table I summarizes the test configurations and initial conditions.

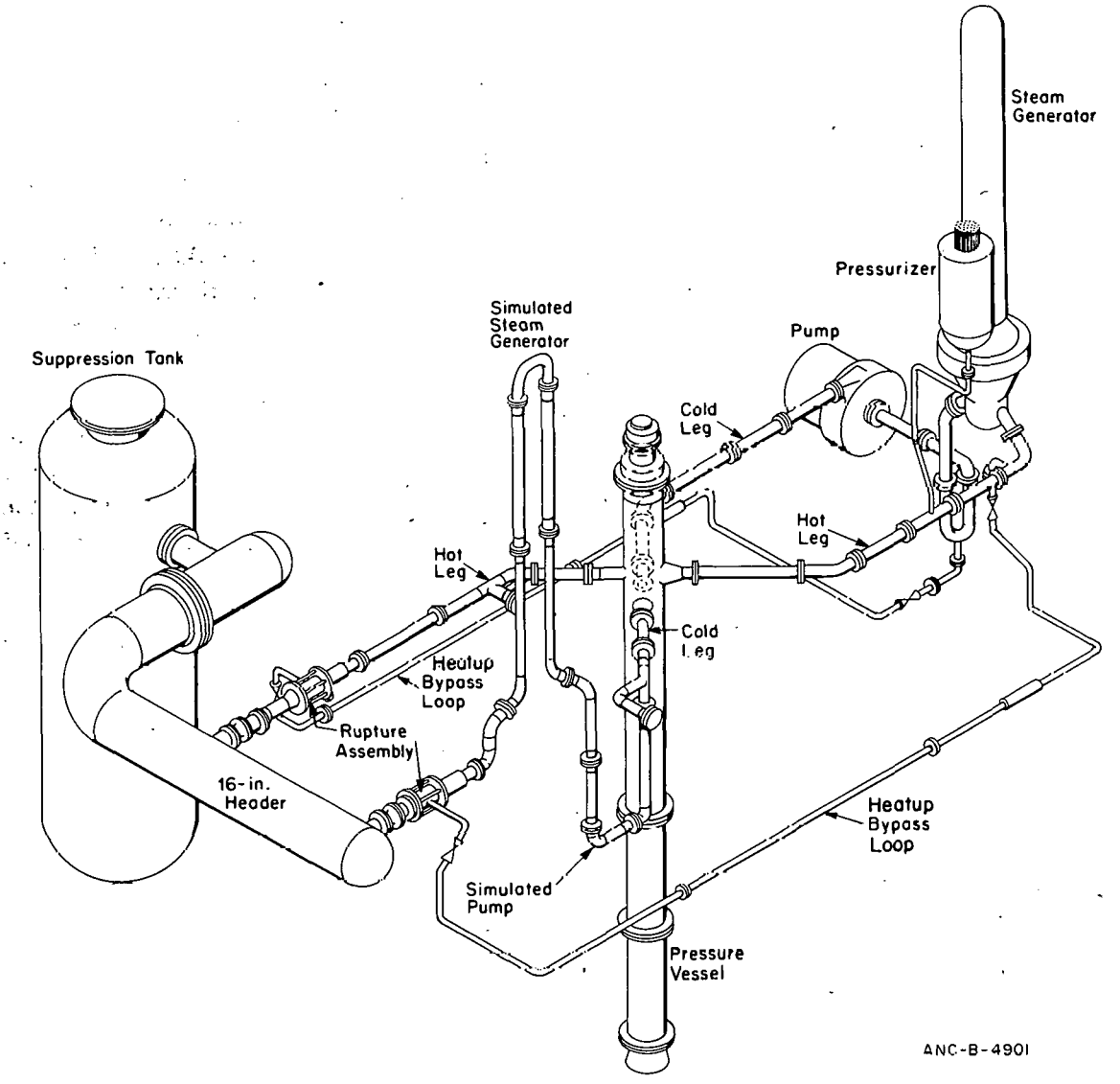

Fig. 1 Semiscale Mod-1 hot leg break configuration – isometric.

All tests in the blowdown heat transfer test series were initiated at a nominal system pressure of 2,265 psia. Test S-02-1 was performed to investigate system response to a depressurization transient caused by a simulated 200% offset shear hot leg break. The core power was 1.18 megawatts, and the core temperature differential was about 49°F. Test S-02-2 had essentially the same initial fluid conditions (flow rates and temperature distribution) as Test S-02-1, but the break configuration represented a simulated 200% offset shear cold leg break. Test S-02-3 was conducted with a simulated 200% offset shear cold leg break and a moderately heated core (1.19 megawatts). However, the system flow for this test was set at 75% of the design flow to achieve a core temperature differential of 68°F. Test S-02-4 was conducted with a 200% offset shear cold leg break and was the first test in the series with full design core power (1.6 MW). The system flow for this test was set to achieve the design core temperature differential of 67°F. Test S-02-5 employed essentially the same initial conditions and break configuration as Test S-02-4, except that

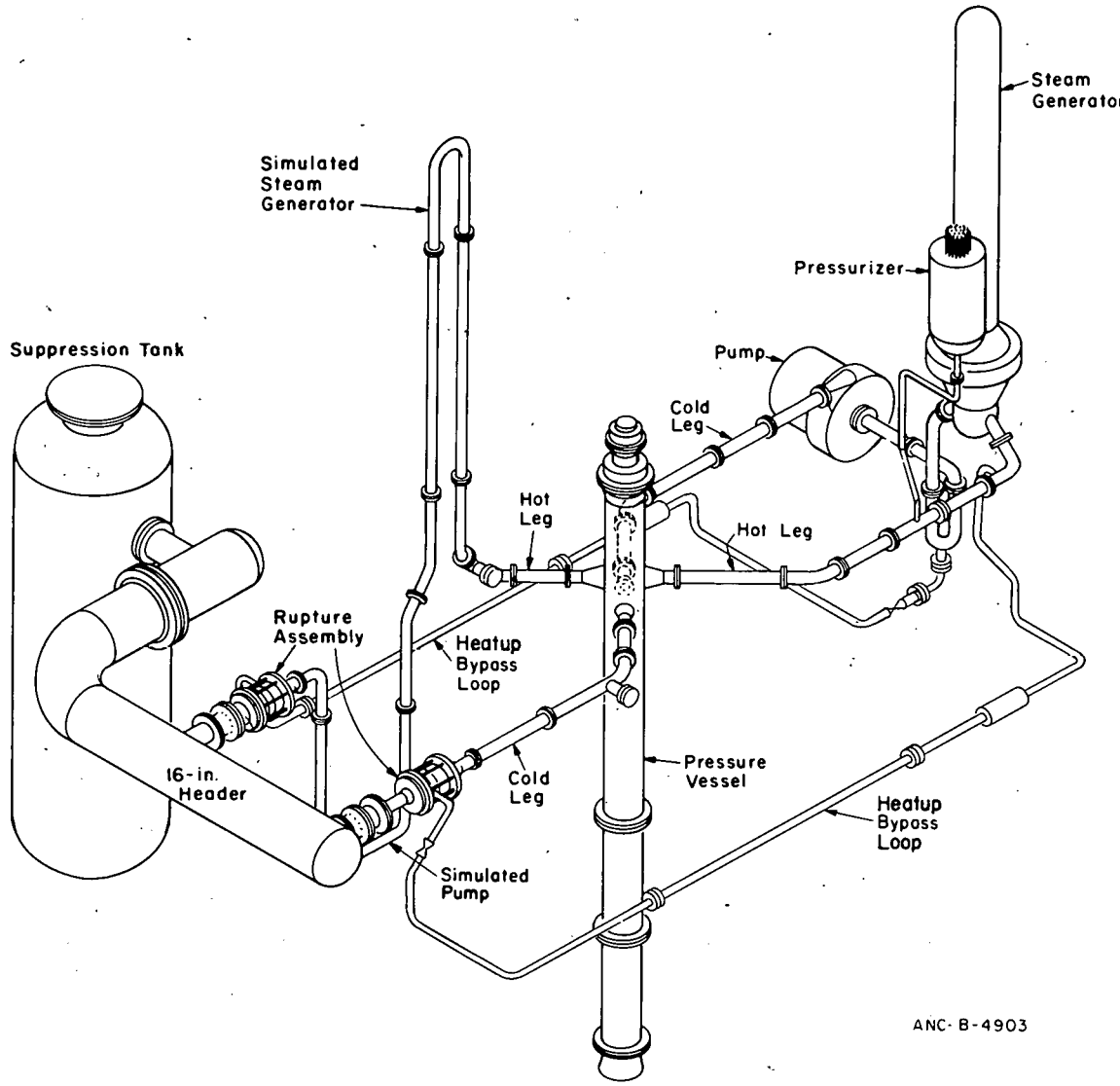

Fig. 2 Semiscale Mod-1 cold leg break configuration – isometric.

the core power decay transient was more severe than that used during Test S-02-4 and previous tests. Also emergency core coolant (ECC) was injected into both the intact and broken loop legs. Test S-02-7 was conducted with a 200% offset shear cold leg break and with full design core power and core differential temperature. However, core power was set to provide a flat radial power profile. Conditions for Tests S-02-9 and S-02-9A were essentially the same as those for Test S-02-7, except emergency core coolant was injected into both the intact and broken loops. Test S-02-9A, an initial attempt to conduct Test S-02-9, was a test in which, contrary to test specifications, a valve in the emergency core coolant line to the lower plenum was inadvertently left open.

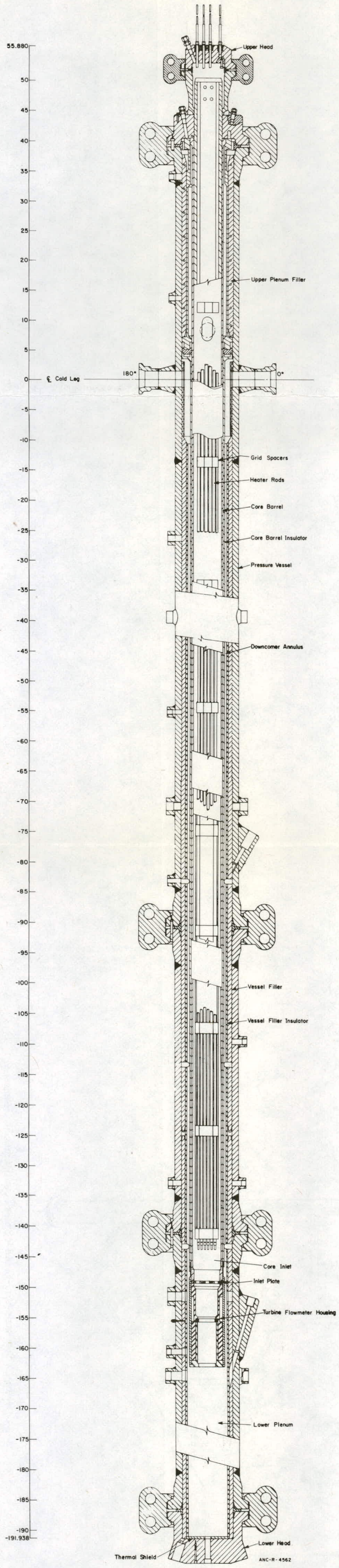

Fig. 3 Cross section of vessel with core.

TABLE I

BLOWDOWN HEAT TRANSFER SERIES TEST CONDITIONS

Condition or Configuration	Tests[a] S-02-1	S-02-2	S-02-3	S-02-4	S-02-5	S-02-7	S-02-9	S-02-9A
Core								
Power (MW)	1.18	1.20	1.19	1.60	1.60	1.61	1.56	1.56
Differential Temperature (°F)	49	48	68	67	66	68	68	65
Nominal System Pressure (psia)	2,265	2,272	2,263	2,263	2,253	2,263	2,253	2,263
Cold Leg Fluid Temperature (°F)	545	542	543	542	543	541	542	542
Core Inlet Flow Rate (gpm)	166	162	119	156	155	154	146	148
Break								
Location	hot leg	cold leg	cold leg	cold leg	cold leg	cold leg	cold leg	cold leg
Type	double-ended offset shear	double-ended offset shear	double-ended offset shear	double-ended offset shear	double-ended offset shear	double-ended offset shear	double-ended offset shear	double-ended offset shear
Size (%)[b]	200	200	200	200	200	200	200	200
Coolant Injection Location	---	---	---	---	intact and broken loop cold legs	---	intact and broken loop cold legs	intact and broken loop cold legs (and lower plenum)
System Pressure at Initiation of Coolant Injection								
From Accumulator (psig)	---	---	---	---	600	---	600	600
From Low-Pressure Injection System (psia)	---	---	---	---	150	---	150	150
From High-Pressure Injection System (psia)	---	---	---	---	---	---	---	---

[a] Tests S-02-6 and S-02-8 were U. S. Nuclear Regulatory Commission standard problem tests and are not discussed in this report.

[b] The references areas for defining total break-area are: 0.00291 ft^2 = 100% for a hot leg break and 0.00262 ft^2 = 100% for a cold leg break.

The test sequence for the blowdown heat transfer experiments was essentially the same for each blowdown. Warmup to the initial test conditions was accomplished with the heaters in the vessel core. The system fluid was circulated through the intact loop and vessel at between 120 and 160 gpm to establish the required core temperature differential. The intact loop steam generator was maintained in an active condition, in which the steam generator secondary pressure and water level were automatically adjusted to control the water temperature in the cold leg of the intact loop. Heatup of the broken loop piping was accomplished with bypass lines which served to allow circulation through the broken loop. Once the initial conditions were established, the tests were initiated by breaking rupture discs in both the vessel inlet and vessel outlet sides of the broken loop. System flow rates during the blowdown transient were controlled by the phenomena occurring in the coverging-diverging nozzles immediately upstream of the rupture discs in the broken loop, as well as by the intact loop pump.

III. RESULTS OF THE DATA ANALYSIS

The results of the data analysis are presented in three parts. The core fluid response during a 200% offset shear cold leg break test is discussed in the first part. Included within this section are comparisons between the test data and results from the RELAP4 computer program.

Analysis related to the effects of various system initial conditions on overall system response and core flow response are discussed in the second part. Since the core flow behavior is of major importance in determining the magnitude of the heat transfer from the heater rods, particular emphasis is placed on the influence of system phenomena on core flow behavior. Included are discussions of the results obtained from investigating the differences in system and core behavior caused by changes in: (a) the break location, (b) the initial system temperature distribution, and (c) the initial core electrical power.

The results of analysis related to the response of individual system components and the effect of the component response on overall system response during the 200% cold leg break tests are discussed in the third part of this section. Although all the blowdown heat transfer tests were evaluated, the discussion has been primarily limited to Test S-02-4, because this test produced typical results and represented the most severe case, with respect to core flow. Included within this discussion are results from an investigation of: (a) phenomena occurring within the vessel region, with emphasis on downcomer and lower plenum fluid behavior, (b) phenomena occurring in the broken loop with emphasis on flow response, (c) intact loop steam generator heat transfer, (d) intact loop pressurizer response, and (e) intact loop pump response. Results from other tests which deviate significantly from those observed during Test S-02-4 are discussed. In addition, comparison of experimental results and results calculated by the RELAP4 computer code are included within this section. When calculated results deviate significantly from test data, an attempt is made to explain the reasons for the discrepancy. Also, a discussion of the changes made to the RELAP4 model to improve respresentation of the Semiscale Mod-1 system is included.

Data from the blowdown heat transfer tests have been analyzed to determine their reliability and repeatability. Discussion of the data reliability and repeatability between tests with similar initial conditions are presented in Appendices B and C. In general, turbine flowmeter results (rather than drag disc flowmeter results) are considered to be more representative of the actual long term flow behavior. Thus, unless otherwise specified, long term flow data presented in this section are from turbine flowmeter measurements. For the core inlet flow, however, composite results from drag discs and turbine flowmeters are presented. The fast response time of the drag disc allows the drag disc to follow the transient core flow during the early portion of blowdown more accurately than can the turbine flowmeter. Thus, the first two to three seconds of the data for the core mass flow results represent the drag disc measurement, and the remainder represents the turbine flowmeter measurement.

1. CORE FLUID BEHAVIOR

Results of the analysis associated with core flow response during blowdown are discussed in this section. The amount of energy removed from the core during blowdown is highly sensitive to the flow rate and quality of fluid in the core. Thus, knowledge of the core fluid behavior is important in determining the severity of a postulated LOCA. The core fluid behavior is influenced by the response of other components within the system, principally the break and the intact loop pump.

The general response of the core inlet flow during blowdown for several of the 200% cold leg break tests is shown in Figure 4. The core inlet flow data from these tests indicate a negative flow within 100 msec after rupture, with the flow remaining negative until three to six seconds into the blowdown. The core fluid then stagnates until between 9 and 12 seconds and then becomes slightly negative for the remainder of blowdown. The large negative core inlet flows during the first 3.5 to 6 seconds following rupture are directly attributable to the large flow rates in the vessel inlet side of the broken loop. Variations between tests in the magnitude of the core inlet flow rates and the duration that the core flows remained negative were due to differences in break flow rates and, to a lesser degree, to the pump response.

The flow in the vessel inlet side of the broken loop was the dominant influence on core flow behavior, especially during the subcooled portion of blowdown. An example of the influence of the broken loop subcooled flow on core flow behavior is shown in Figure 5, which compares the flow rate in the vessel inlet side of the broken loop with the core inlet flow rate for Test S-02-4. The influence of the subcooled flow occurring in the broken loop during the first three seconds is evidenced by the response of the core inlet flow. The intact loop cold leg flow during this period of time decreased only slightly, indicating that the major influence on core flow was the vessel inlet side break flow. Once fluid in the vessel inlet side of the broken loop became saturated, however, the flow rate there dropped sufficiently to allow the intact loop cold leg flow (by means of the vessel inlet annulus) to supply the major portion of the break demand. As a result, the core inlet flow dropped to essentially zero.

The mass flow rate at the inlet to the core for Test S-02-4 and that calculated by the RELAP4 program are compared in Figure 6. The somewhat large discrepancy between the data and the RELAP4 calculation during the first second following rupture can apparently be attributed to the inability of the core inlet drag disc to adequately measure the magnitude of the sudden core flow reversal at rupture[a]. Mass balances using data from Test S-02-4 and results from the RELAP4 calculation indicate that the RELAP4 calculation represents the best estimates of core inlet flow. The discrepancy between the calculated core inlet flow and the data between one and three seconds, however, can be attributed to an underprediction of the cold leg broken loop mass flow rate. Studies of the influence of the

[a] Similar discrepancies between data and the RELAP4 calculated core inlet flow value occurred for other tests in the series.

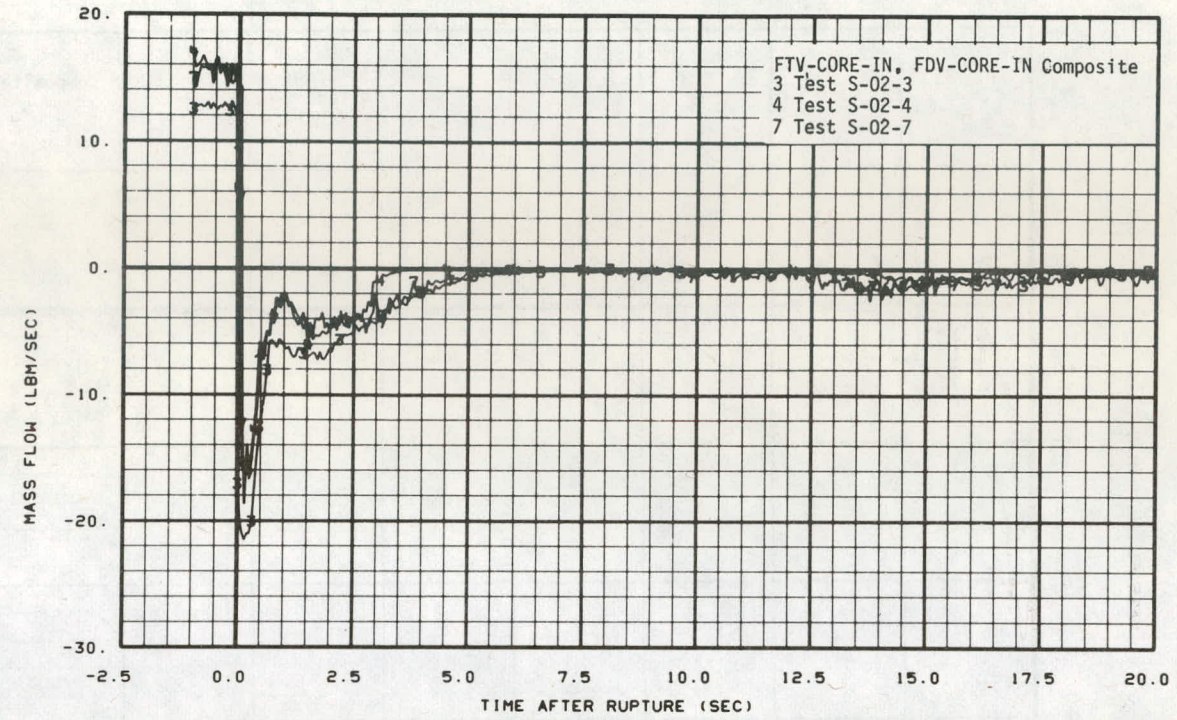

Fig. 4 Mass flow rate at the inlet to the core – Tests S-02-3, S-02-4, and S-02-7.

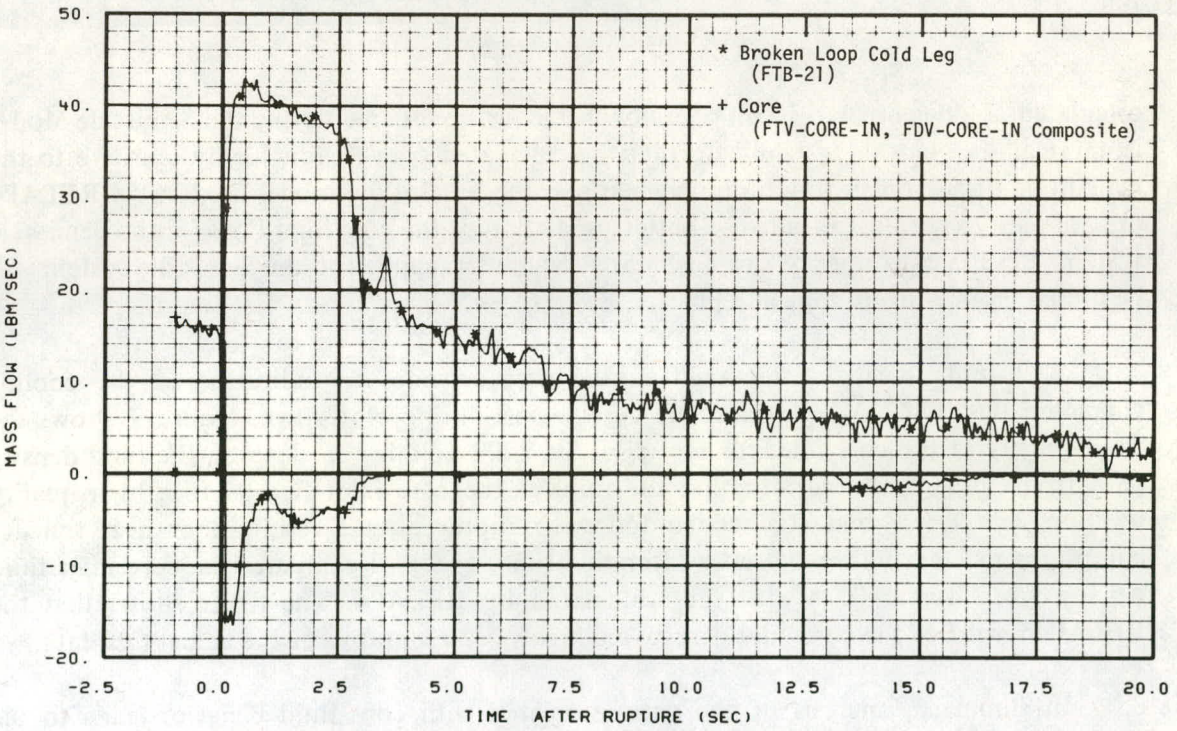

Fig. 5 Comparison of mass flow rates at the inlet to the core and near the vessel on the inlet side of the broken loop – Test S-02-4.

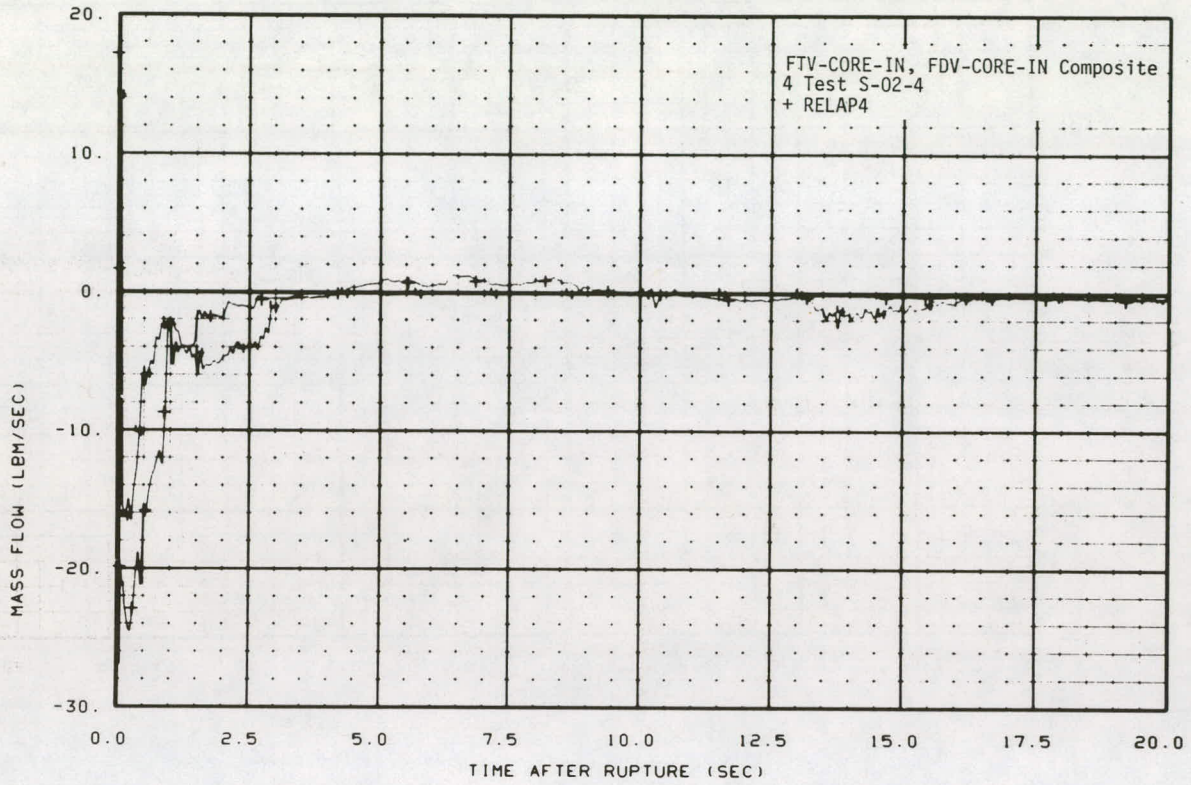

Fig. 6 Mass flow rate at the inlet to the core – comparison of RELAP4 results with Test S-02-4 data.

calculated cold leg break flow on core flow behavior, conducted during the Semiscale Mod-1 isothermal test series[11], indicate that the calculated core flow is highly sensitive to the magnitude of the break flow. Improvements in the break flow model used in the RELAP4 program are expected to lead to a better prediction of the core inlet flow for the Semiscale system. Results of studies of various break flow models applied to the Semiscale system will be presented in a future topical report.

The fluid density at the inlet to the core provides an indication of the cooling characteristics that existed within the core region during blowdown. Figure 7 shows the fluid density at the core inlet for several of the 200% cold leg break tests. The fluid density data from these tests indicate that the fluid at the core inlet flashed to a high quality mixture within less that 0.5 second following rupture. As a result, poor heat transfer conditions existed within the core after this time. Figure 8 compares the core inlet fluid density from Test S-02-4 with that calculated by RELAP4. The figure shows that the RELAP4 results of the core inlet density are highly representative of the actual test data.

In summary, analysis of the data associated with core fluid behavior leads to the conclusion that the large negative core flow rates during the first several seconds of blowdown (for the 200% cold leg break tests) are directly attributable to the large

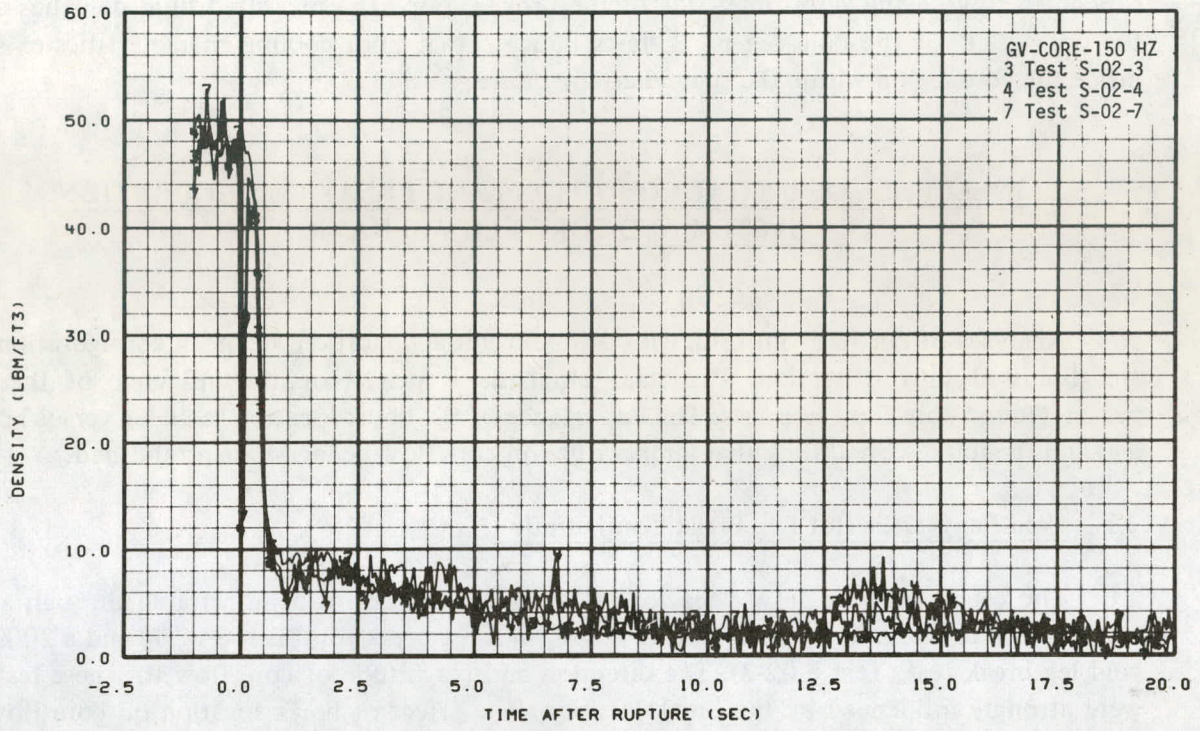

Fig. 7 Fluid density at the inlet to the core – Tests S-02-3, S-02-4, and S-02-7.

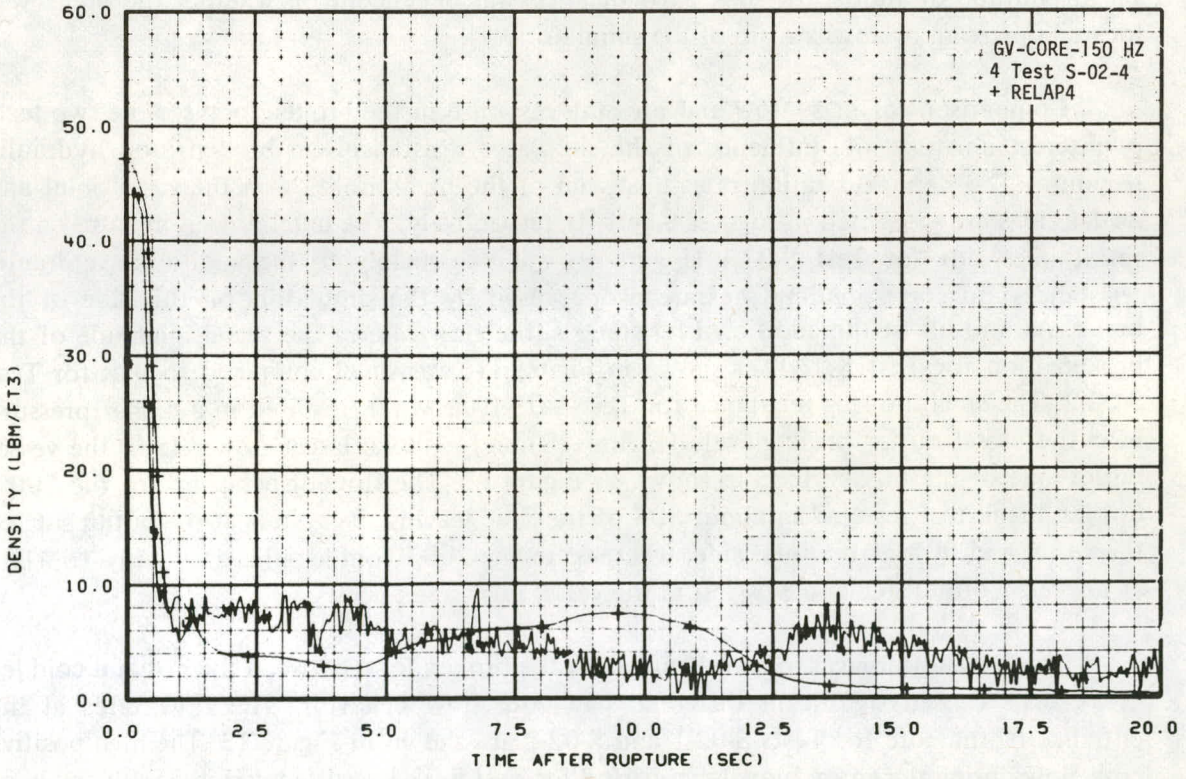

Fig. 8 Fluid density at the inlet to the core – comparison of RELAP4 results with Test S-02-4 data.

subcooled flow in the vessel inlet side of the broken loop. The measured fluid densities at the core inlet for the cold leg break tests indicate that poor cooling characteristics exist inside the core region within 0.5 second after rupture.

2. INFLUENCE OF INITIAL CONDITIONS AND BREAK CONFIGURATION ON SYSTEM AND CORE FLOW BEHAVIOR

Analyses of results from tests with different initial conditions or break configurations are discussed in this section. Particular emphasis is placed on the influence of these parameters on core fluid response. The importance of the break location (cold leg versus hot leg) and the initial core differential temperature on core flow behavior are established.

2.1 Cold Leg Versus Hot Leg Break Configuration

The effect on core flow behavior of the break location is demonstrated through an analysis and comparison of results from a 200% hot leg break test (Test S-02-1) and a 200% cold leg break test (Test S-02-2). The direction and magnitude of core flow for these tests were strongly influenced by the break location. The effect of break location on core flow was principally due to the influence of the pump and steam generator simulators on the distribution of flow out the two sides of the broken loop. Since the simulators consisted of large hydraulic resistances and represented the principal pressure drops in the broken loop, the magnitude of fluid flow in a particular leg was dependent on whether the break was located upstream or downstream of the simulators.

Comparisons of mass flow and pressure response in the broken loop for the two tests of interest illustrate the influence of the simulator resistances on broken loop hydraulic response. The depressurization rates upstream of the break nozzles on the vessel inlet and outlet sides are presented in Figures 9 and 10, respectively. The much lower pressure on the vessel inlet side for Test S-02-1 (Figure 9) was due mainly to the additional hydraulic resistance and corresponding pressure drop caused by the simulators on this side of the break. As a result of the additional resistances, the flow rate in the vessel inlet side of the broken loop for Test S-02-1, as shown in Figure 11, was small compared to that for Test S-02-2. The small hot leg resistance for Test S-02-1, however, resulted in a higher pressure near the vessel outlet break nozzle (Figure 10) and a much larger flow rate in the vessel outlet side of the broken loop as shown in Figure 12. The flow distribution for the 200% hot leg break test resulted in about 80% of the fluid leaving the system at the outlet side of the vessel and 20% at the inlet side, whereas for the 200% cold leg break test only 18% left at the vessel outlet side and 82% left at the vessel inlet side.

The large differences in flow behavior in the broken loop between the hot and cold leg break tests caused significant differences in core flow behavior. The flow rates at the entrance to the core for Tests S-02-1 and S-02-2 are shown in Figure 13. The high positive core flow during the entire blowdown period for Test S-02-1 resulted directly from the large

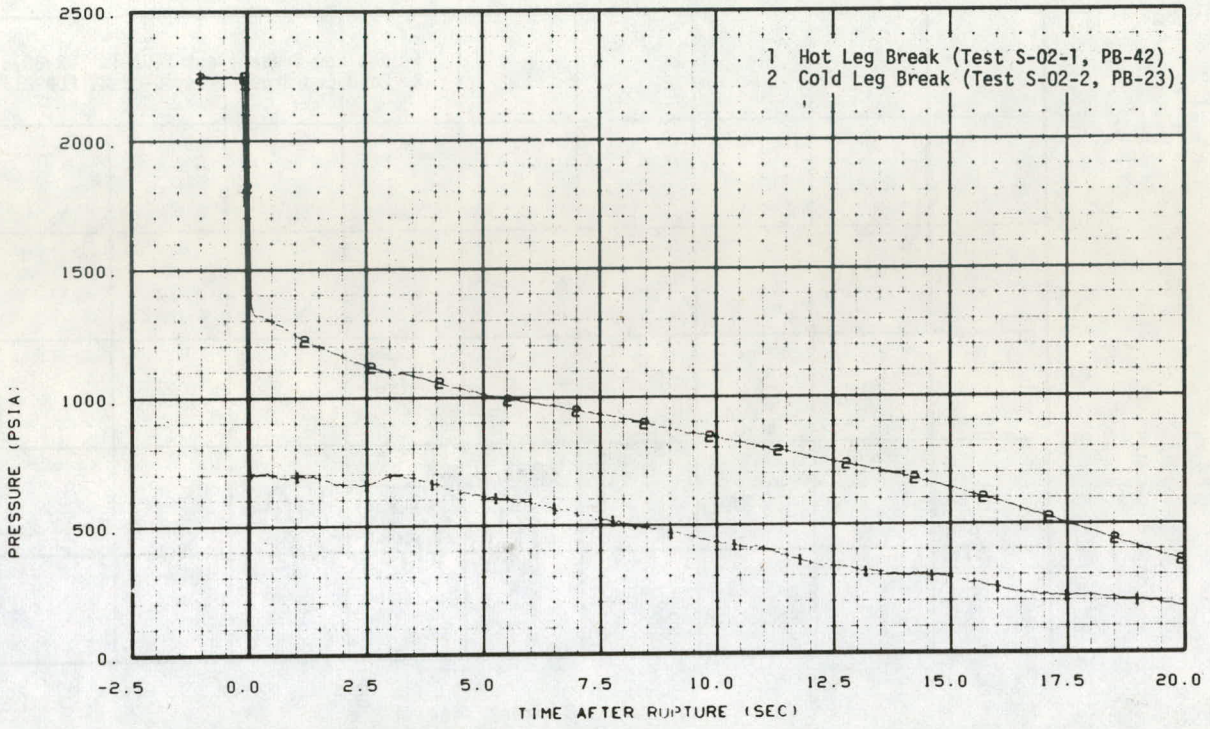

Fig. 9 Pressure response upstream of the break nozzle on the vessel inlet side – Tests S-02-1 and S-02-2.

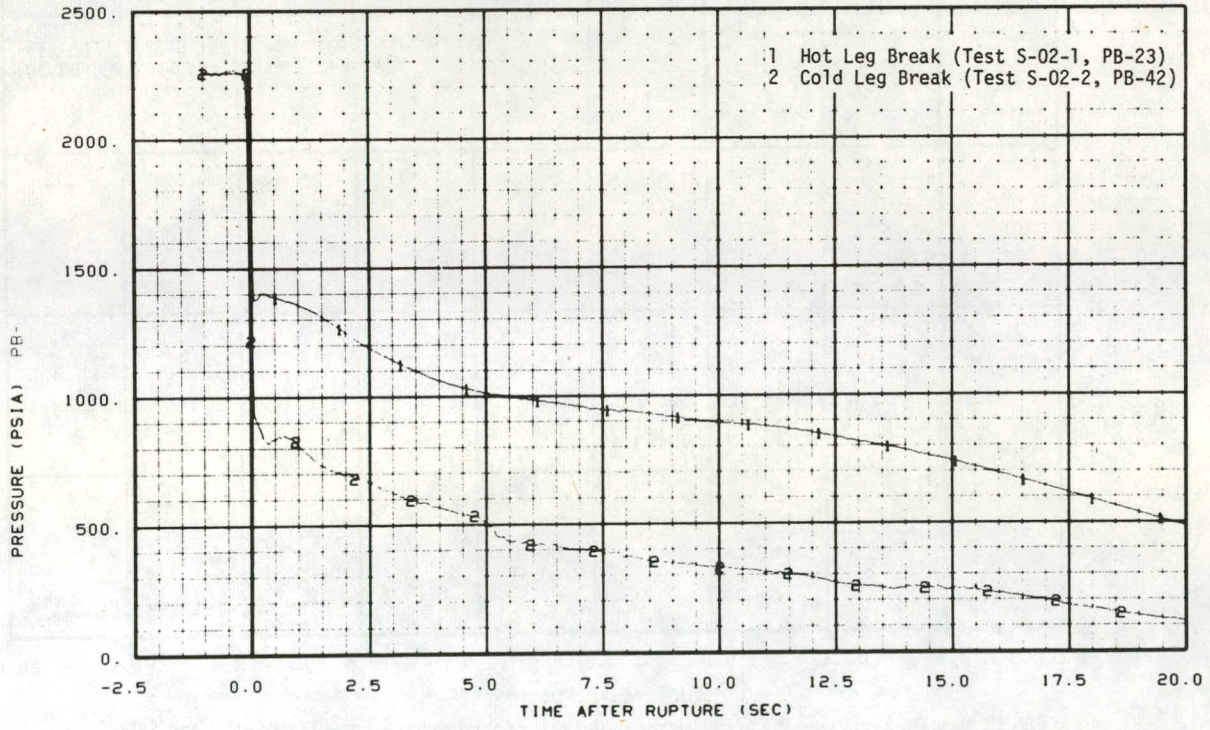

Fig. 10 Pressure response upstream of the break nozzle on the vessel outlet side – Tests S-02-1 and S-02-2.

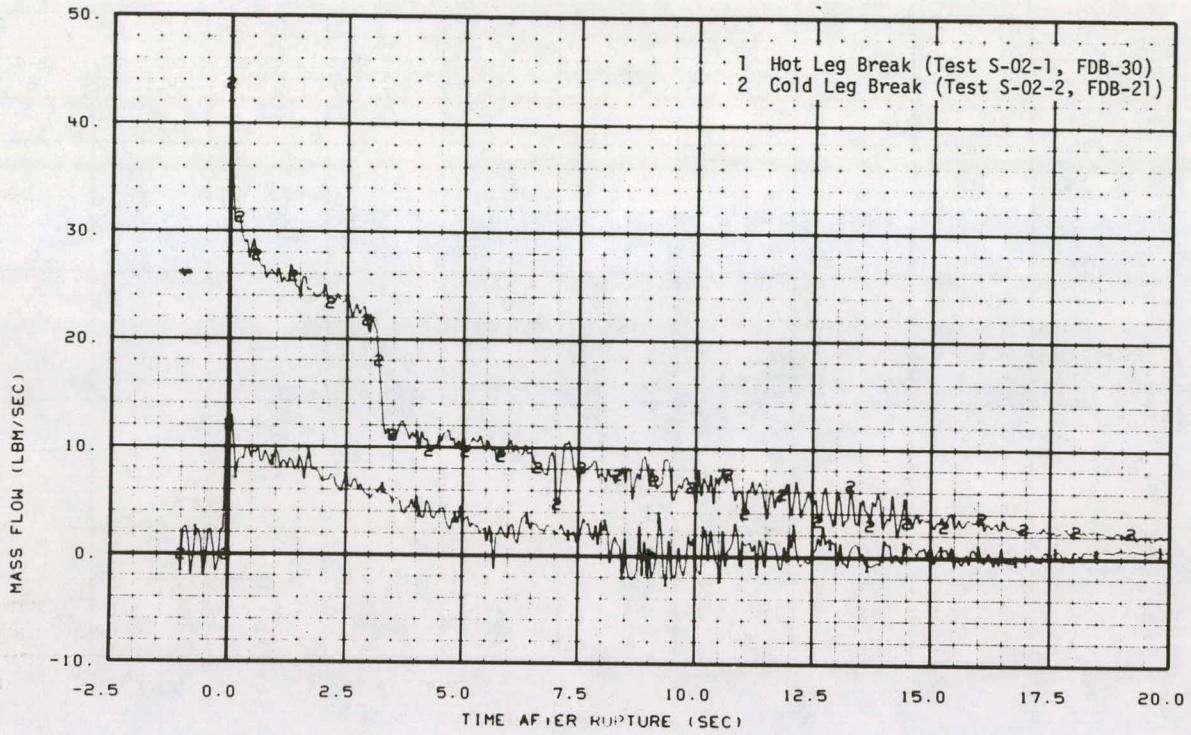

Fig. 11 Mass flow rate near the vessel on the inlet side of the broken loop – Tests S-02-1 and S-02-2.

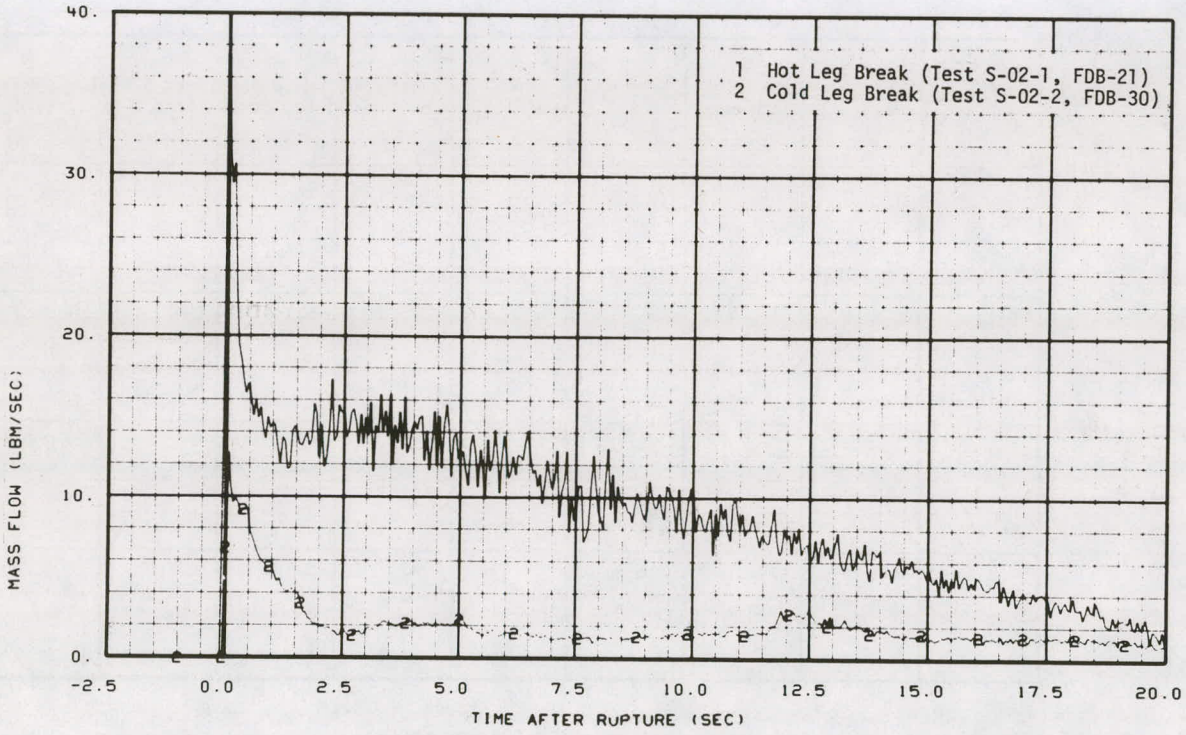

Fig. 12 Mass flow rate near the vessel on the outlet side of the broken loop – Tests S-02-1 and S-02-2.

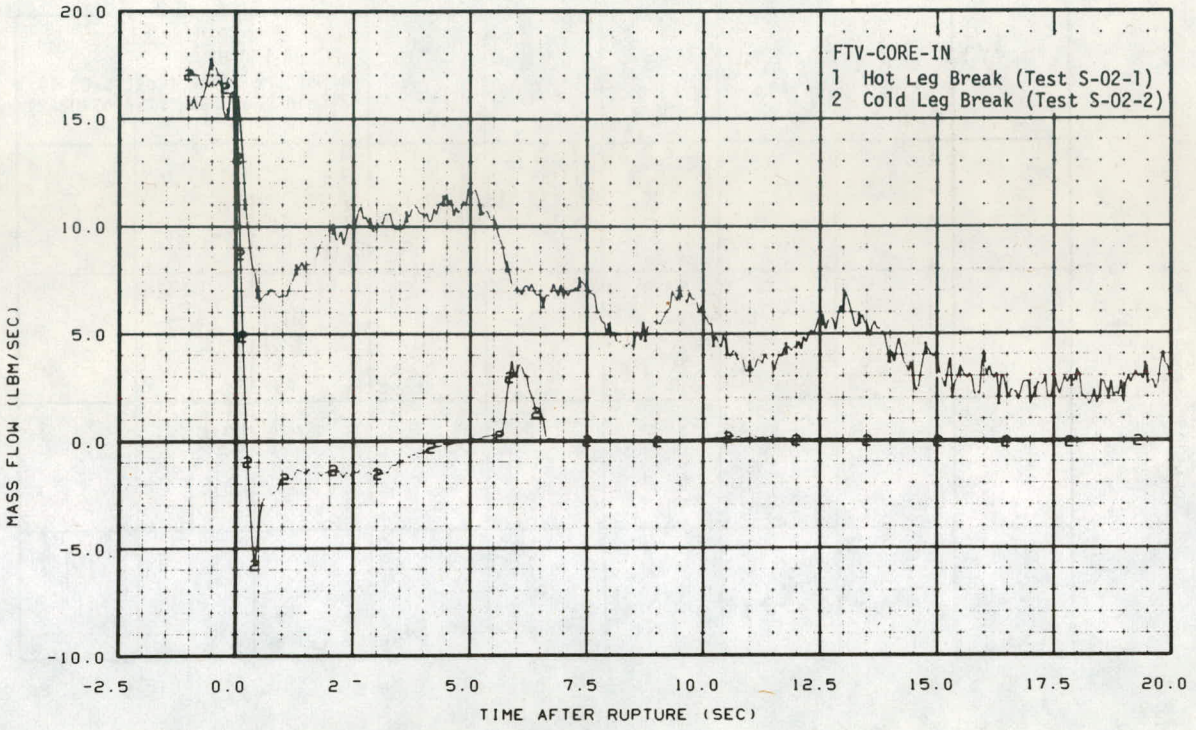

Fig. 13 Mass flow rate at the inlet to the core – Tests S-02-1 and S-02-2.

flow rate in the broken loop vessel outlet side combined with the parallel influence of the intact loop pump.

As shown in Figure 14, the positive core flow for the hot leg break case resulted in a much higher density fluid at the core inlet than existed for the cold leg break case. As a result of the core flow behavior for the hot leg break test, the core heat transfer remained in the nucleate boiling regime maintaining excellent cooling in the core during blowdown. The core thermal response is discussed in detail in Reference 9.

In summary, the 200% hot leg break test was much less severe, with respect to the core thermal response, than was the 200% cold leg break test. This less severe response resulting from the hot leg break was due to the high positive core flow and the resulting excellent heat transfer from the core heater rods to the coolant fluid.

2.2 Influence of System Initial Temperature Differential

The magnitude of the system fluid temperature differential prior to rupture for 200% cold leg break tests had considerable effect on system response and core flow behavior during the ensuing blowdown transient and hence on the amount of cooling provided to the core, especially early in the blowdown period. Variations in the core flow among tests in the series with dissimilar system initial temperature differentials were principally caused by differences in the system saturation pressures and differences in the flow behavior in the

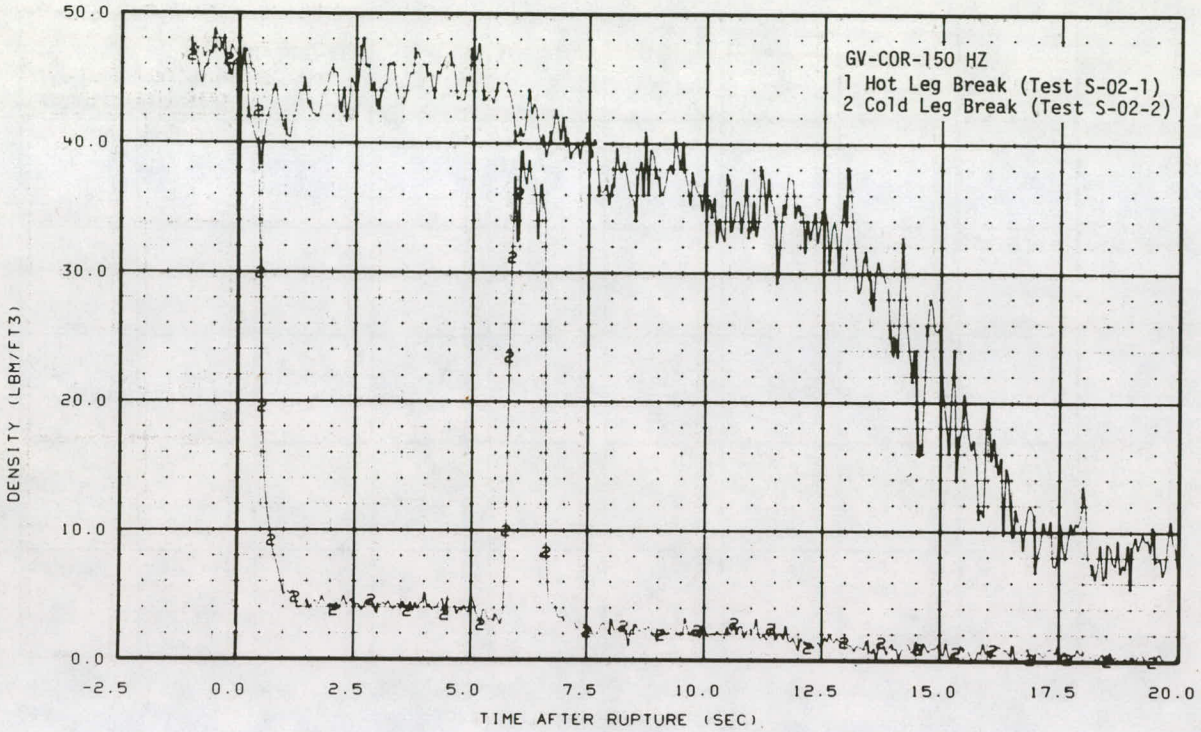

Fig. 14 Fluid density at the inlet to the core – Tests S-02-1 and S-02-2.

vessel inlet sides of the intact and broken loop resulting from the varying degrees of subcooling that existed in these components at rupture.

Results from Test S-01-6[12] (of the isothermal test series) and from Tests S-02-2 and S-02-4 are compared to illustrate the influence of the system initial temperature differential. The core inlet fluid temperature for each of the tests was about 540°F, and the system temperature differentials were 0°F for Test S-01-6, 48°F for Test S-02-2, and 67°F for Test S-02-4. (Since the core inlet fluid temperatures were about the same for all tests, the differences in system behavior presented in this section are discussed only in terms of the system fluid temperature differential. However, the core inlet fluid temperature is expected to have considerable influence on system behavior during blowdown, due to its effect on system saturation pressure.)

System depressurization rates for Tests S-01-6, S-02-2, and S-02-4, as measured in the vessel region, are shown in Figure 15 and illustrate the influence of the initial system fluid temperature differential on the pressure response. After rupture, the system pressure dropped immediately from an initial value of about 2,265 psia to a saturation pressure corresponding to the vessel upper plenum or hot leg fluid temperature. The uniform fluid temperature throughout the system for Test S-01-6 resulted in the entire system fluid becoming saturated within 100 milliseconds after rupture. The system temperature differential and corresponding high upper plenum saturation pressures for Tests S-02-2 and S-02-4, however, caused fluids in the vessel inlet sides of the intact and broken loops, as well

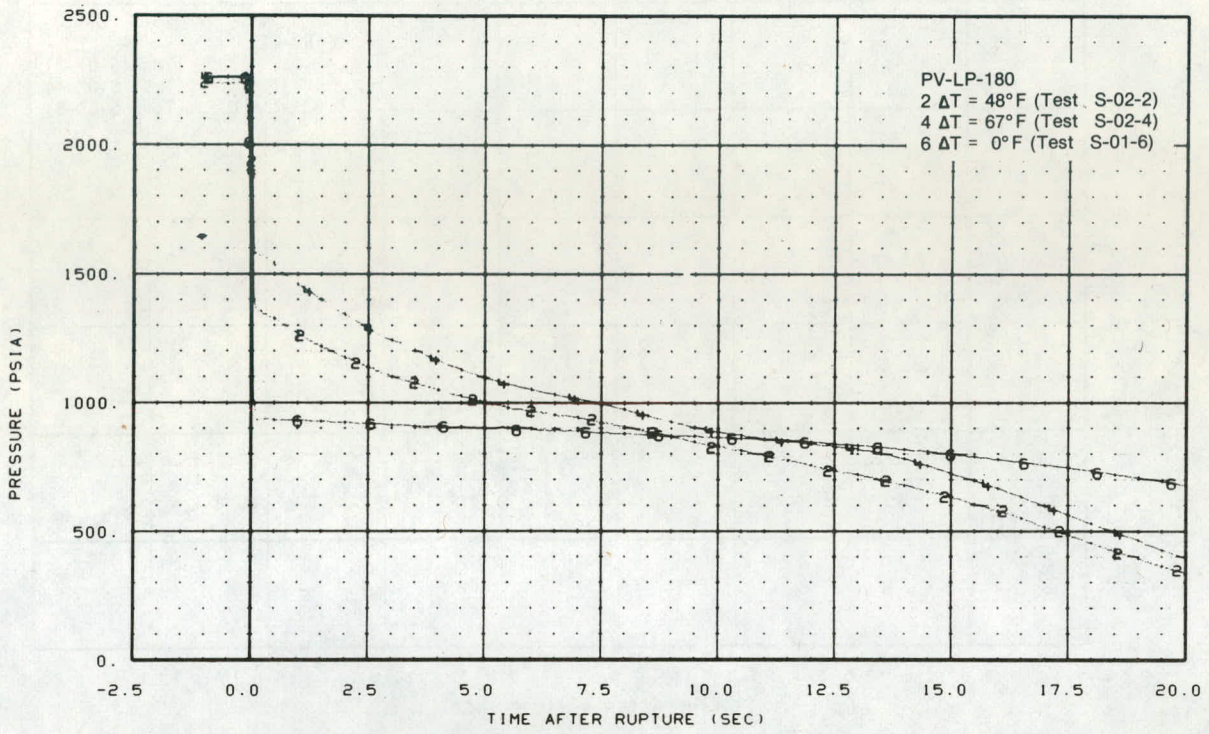

Fig. 15 Pressure response in the vessel lower plenum – Tests S-01-6, S-02-2, and S-02-4.

as in the vessel downcomer and lower plenum, to remain subcooled for considerable time after rupture (until between three and six seconds, depending on location).

The principal effect of the differences in hot leg saturation pressure following rupture for the three tests was to cause variations in the intact and broken loop vessel inlet side flow rates. The presence of subcooled fluid in the intact and broken loop vessel inlet legs for Tests S-02-2 and S-02-4 resulted in pronounced differences in the response of these components, compared to that of Test S-01-6. Figure 16 shows the mass flow rates[a] in the vessel inlet side of the broken loop near the vessel for the three tests. For Test S-01-6, the fluid in the leg became saturated immediately following rupture, resulting in a rapid reduction in flow rate. For Tests S-02-2 and S-02-4, however, the fluid in the vessel inlet side of the broken loop remained subcooled during the first three seconds following rupture, and the flow rates were high. The subcooled flow rate for Test S-02-4 was considerably larger than for Test S-02-2 because of the high system saturation pressure. Once the pressure in the vessel inlet side of the broken loop fell to the saturation pressure of the fluid, choking commenced, and the flow rates were greatly reduced. The high subcooled flow rate in the vessel inlet side of the broken loop for Test S-02-4 resulted in hot fluid from the core region

[a] Turbine flowmeter results in the vessel inlet side of the broken loop were questionable for Test S-02-2. Thus, for comparison purposes drag disc results for the three tests are presented. However, the magnitudes of the mass flow rates obtained from the drag disc measurements are considered to be about 25% low.

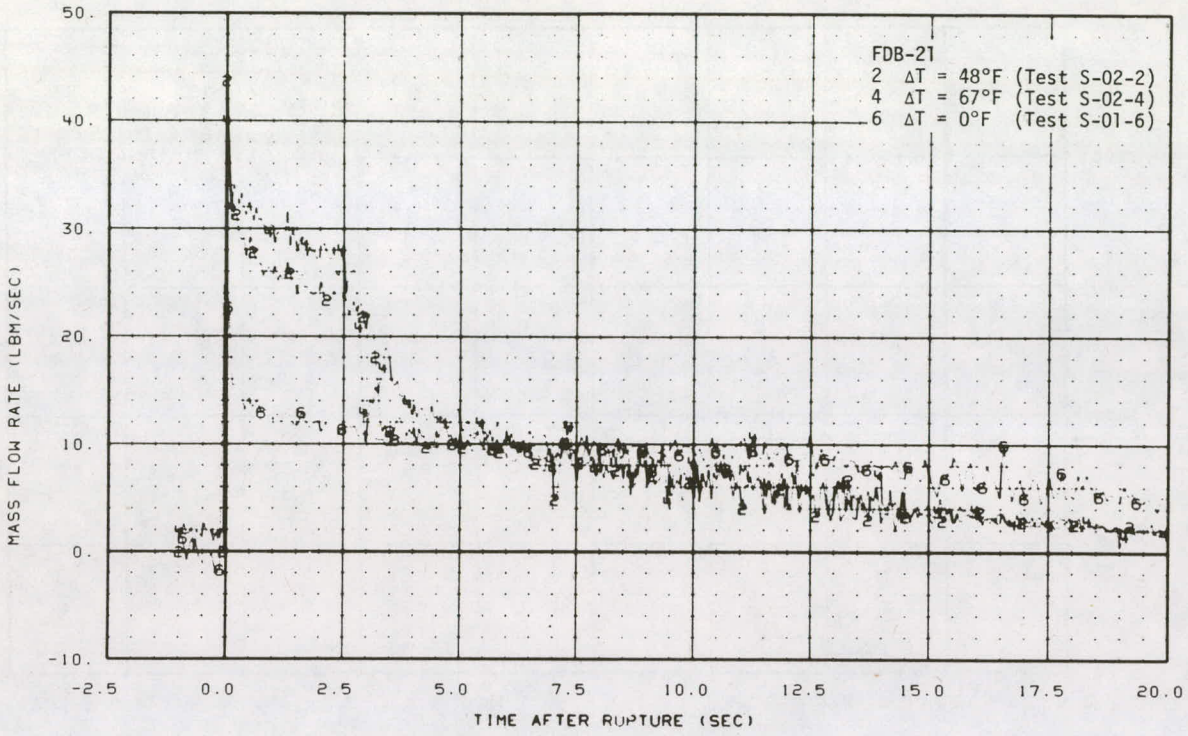

Fig. 16 Mass flow rate near the vessel on the inlet side of the broken loop – Tests S-01-6, S-02-2, and S-02-4.

reaching the leg about 0.5 second earlier than for Test S-02-2. Thus saturation in the vessel inlet side of the broken loop, and the corresponding reduction in flow rate, occurred somewhat sooner for Test S-02-4.

Figure 17 shows the mass flow rates in the intact loop near the vessel inlet for the three tests of interest. The differences in flow response during the first seven seconds were principally due to variations in pump behavior caused by the degree of fluid subcooling at the pump suction. The presence of a two-phase fluid mixture at the pump suction resulted in a reduction of the pump head and a corresponding decrease in the capability of the pump to force fluid around the loop. Figure 18 shows fluid densities at the pump suction for the three tests, and Figure 19 shows the pump differential pressures. For Test S-01-6, the fluid at the pump suction became saturated immediately following rupture (as indicated by the rapid decrease in fluid density), whereas for Tests S-02-2 and S-02-4 the fluid remained subcooled until about 5.5 seconds. As a result, the pump head remained considerably higher in Tests S-02-2 and S-02-4 than in Test S-01-6, and mass flow rates in the intact loop were maintained higher until approximately 6.5 seconds after rupture.

The core flow response for Tests S-01-6, S-02-2, and S-02-4 can be analyzed in terms of the differences between the intact and broken loop vessel inlet flow rates. Figure 20

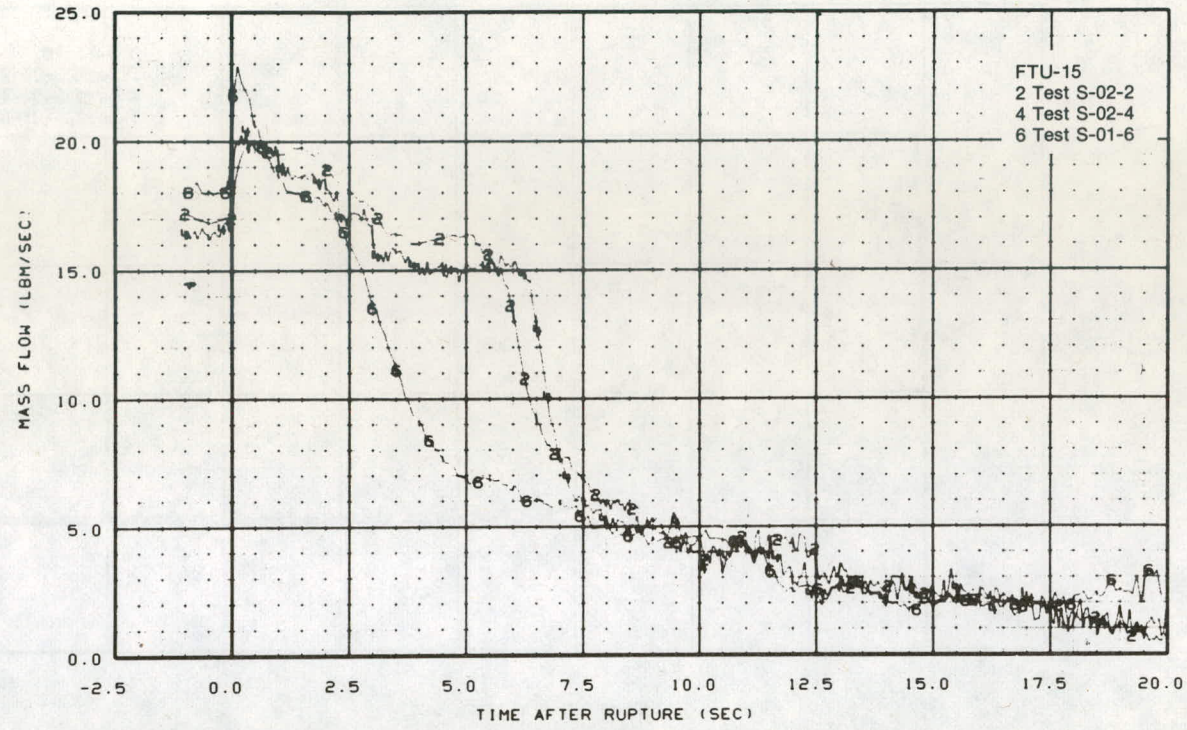

Fig. 17 Mass flow rate near the vessel on the inlet side of the intact loop – Tests S-01-6, S-02-2, and S-02-4.

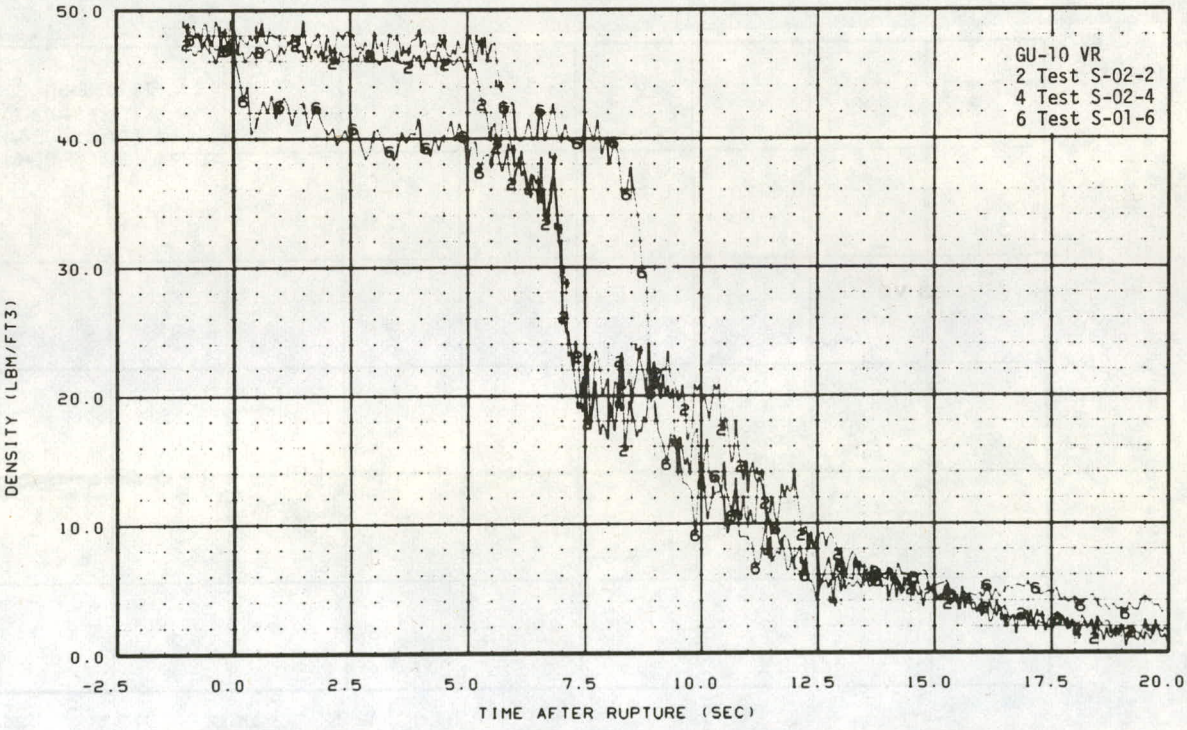

Fig. 18 Fluid density at the intact loop pump suction – Tests S-01-6, S-02-2, and S-02-4.

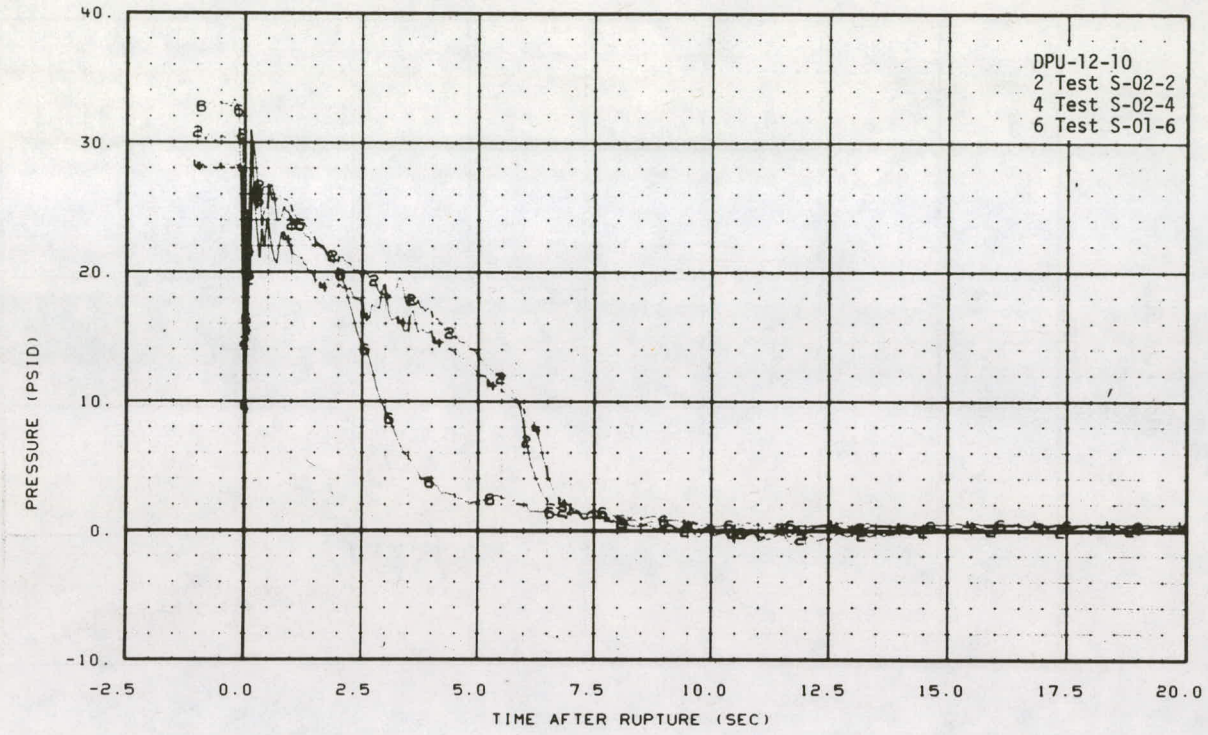

Fig. 19 Differential pressure across the intact loop pump – Tests S-01-6, S-02-2, and S-02-4.

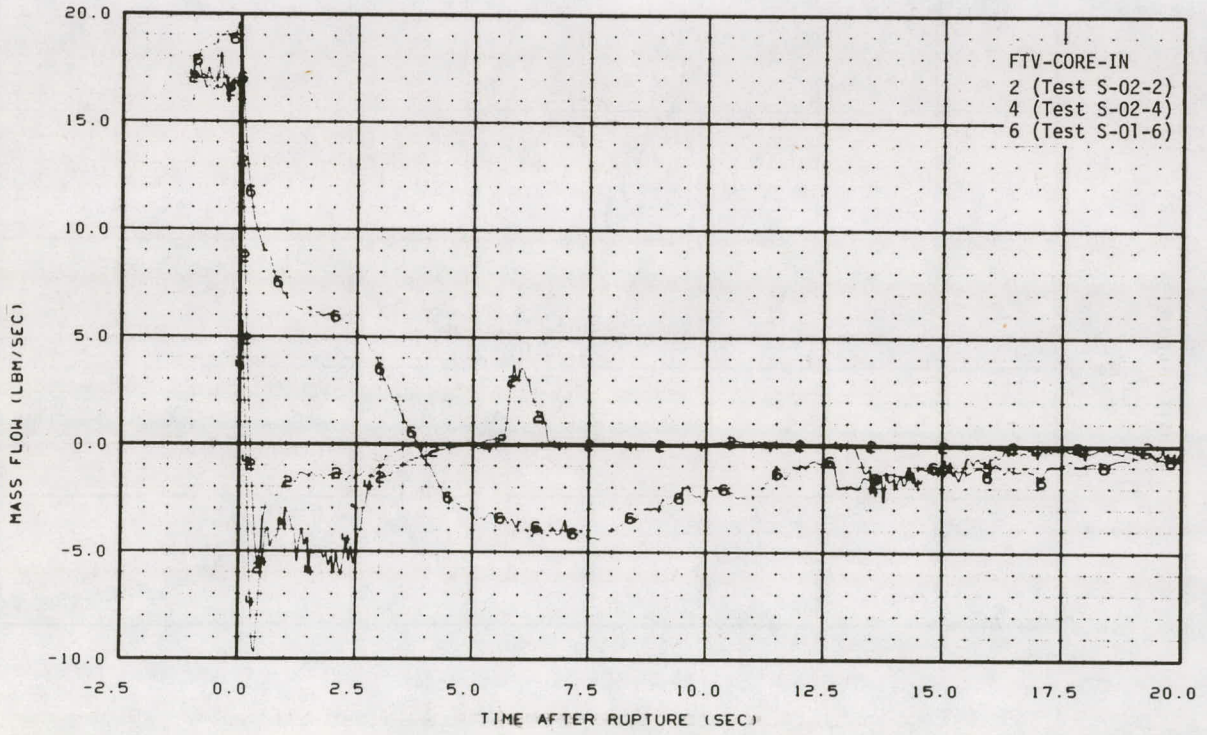

Fig. 20 Mass flow rate at the inlet to the core – Tests S-01-6, S-02-2, and S-02-4.

shows the mass flow rates[a] at the inlet to the core for the three tests. For Test S-01-6, the core inlet flow remained positive until about 3.5 seconds after rupture, because the intact loop cold leg flow was sufficiently large to supply both the broken loop vessel inlet side flow demand and the core inlet flow demand. After 3.5 seconds, the intact loop cold leg flow rate dropped below the broken loop vessel inlet side flow, and core flow reversal occurred. For Tests S-02-2 and S-02-4, however, the broken loop mass flow on the vessel inlet side exceeded the intact loop cold leg flow considerably immediately following rupture, and a large negative core flow resulted. The larger negative core inlet flow for Test S-02-4 (as compared to that for Test S-02-2) resulted directly from the higher flow rate of subcooled fluid out the vessel inlet side of the broken loop. The similarity of the flow rates near the vessel in the intact loop cold leg for Tests S-02-2 and S-02-4 indicates that the intact loop flow was not influential in causing the differences in core flow that were observed. The time after rupture at which the core flow began to decrease for both tests depended directly on the time at which fluid in the vessel inlet side of the broken loop changed from a subcooled to a saturated state. After saturation of the fluid in the vessel inlet side of broken loop occurred, the magnitudes of the break flow rates were sufficiently reduced to allow the intact loop cold leg flow to supply the break demand (through the vessel inlet annulus), and the core inlet mass flow dropped nearly to zero.

In summary, an analysis of phenomena occurring in the Semiscale Mod-1 system during 200% cold leg break tests has led to the conclusion that the overall system flow behavior is strongly influenced by the initial system temperature distribution. The initial system temperature differential, and resulting system saturation pressure, to a large extent determined the subcooled flow rate in the vessel inlet side of the broken loop and thus directly influenced the core flow response. The core inlet flow behavior was highly sensitive to the magnitude of the flow rate in the vessel inlet side of the broken loop during the subcooled portion of blowdown. After saturation occurred in the vessel inlet side of the broken loop, the intact loop cold leg flow was sufficient to supply the break demand causing the core flow to drop nearly to zero.

2.3 Influence of Initial Core Power

The effect of initial core power on system response and the resulting core flow response, for the 200% cold leg break tests, is demonstrated by comparison of results from Tests S-02-3 and S-02-4. Test S-02-3 was run with an initial core power of 1.19 MW (75% Of the full design core power), and an initial intact loop flow rate of 119 gpm. Test S-02-4 was run with an initial core power of 1.60 MW (100% of the design core power) and an initial intact loop flow rate of 156 gpm. The total power supplied to the core during blowdown for the tests is shown in Figure 21. The hot-to-cold-leg temperature differential prior to rupture was the same for both tests (about 68°F) and thus was not a factor in causing any differences in the resulting flow distribution that occurred during blowdown.

---

[a] The core inlet drag disc flow results were questionable for Test S-02-2 and were not available for Test S-01-6. Thus, the turbine flowmeter results for all three tests are presented for comparison purposes.

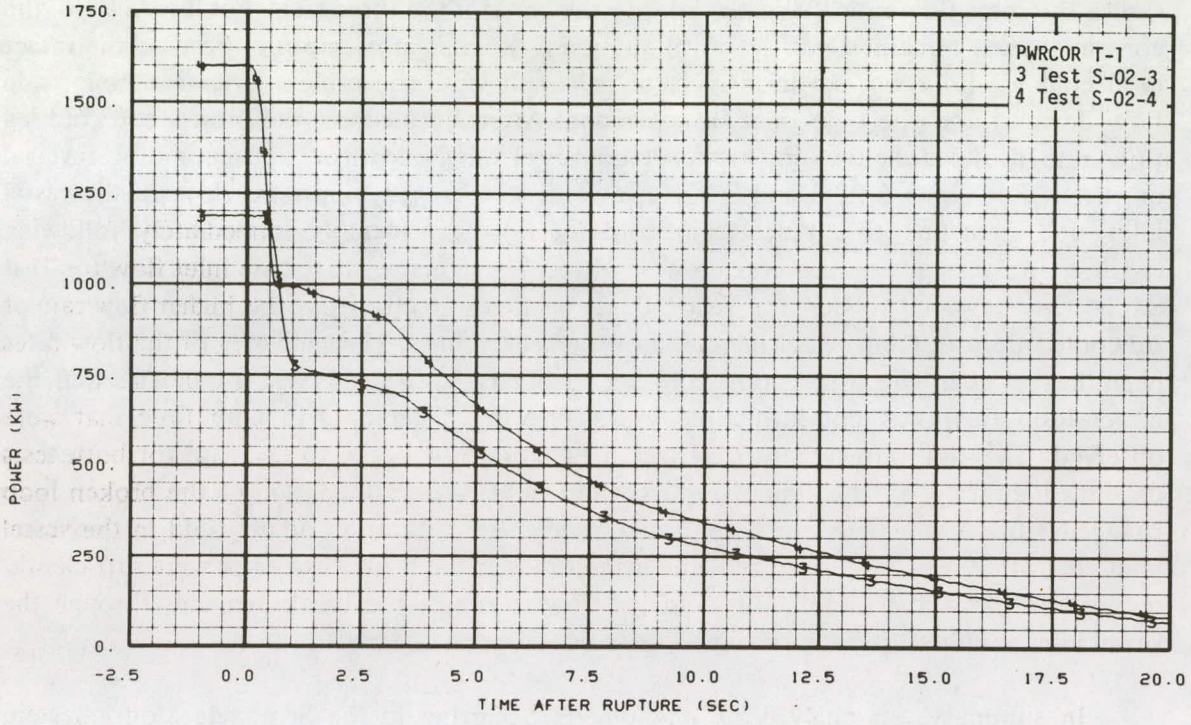

Fig. 21 Total core power – Tests S-02-3 and S-02-4.

The initial core power was found to have little effect on the overall system thermal-hydraulic response during the blowdown period. Figures 22 and 23 show the mass flow rates near the vessel inlet and outlet sides of the broken loop for Tests S-02-3 and S-02-4. The similarity of the flow rates in the broken loop legs for the two tests indicates that equivalent amounts of energy were removed from the vessel by means of the flow through the breaks during the blowdown period. An energy balance using the vessel as a control volume, and the hot and cold leg vessel penetrations as junctions across which mass and energy transfer occurred, supports this conclusion. Figure 24 shows the total integrated energy leaving the vessel as a function of time for the two tests. Apparently, the higher initial core power for Test S-02-4 did not result in additional energy transfer to the coolant fluid during blowdown.

Differences in the core flow and intact loop flow response between Tests S-02-3 and S-02-4 can be attributed to the influence of the intact loop pump, rather than to an effect of the initial core power. The mass flow rates near the vessel in the intact loop cold and hot legs, respectively, are shown in Figures 25 and 26. The higher mass flow rates for Test S-02-4 at both of these locations correspond directly to the higher pump speed shown in Figure 27 for that test. The mass flow rates at the core inlet, compared in Figure 28 for the two tests, indicate that the additional fluid supplied by the pump during the early portion of blowdown for Test S-02-4 led directly to a less negative core mass flow rate.

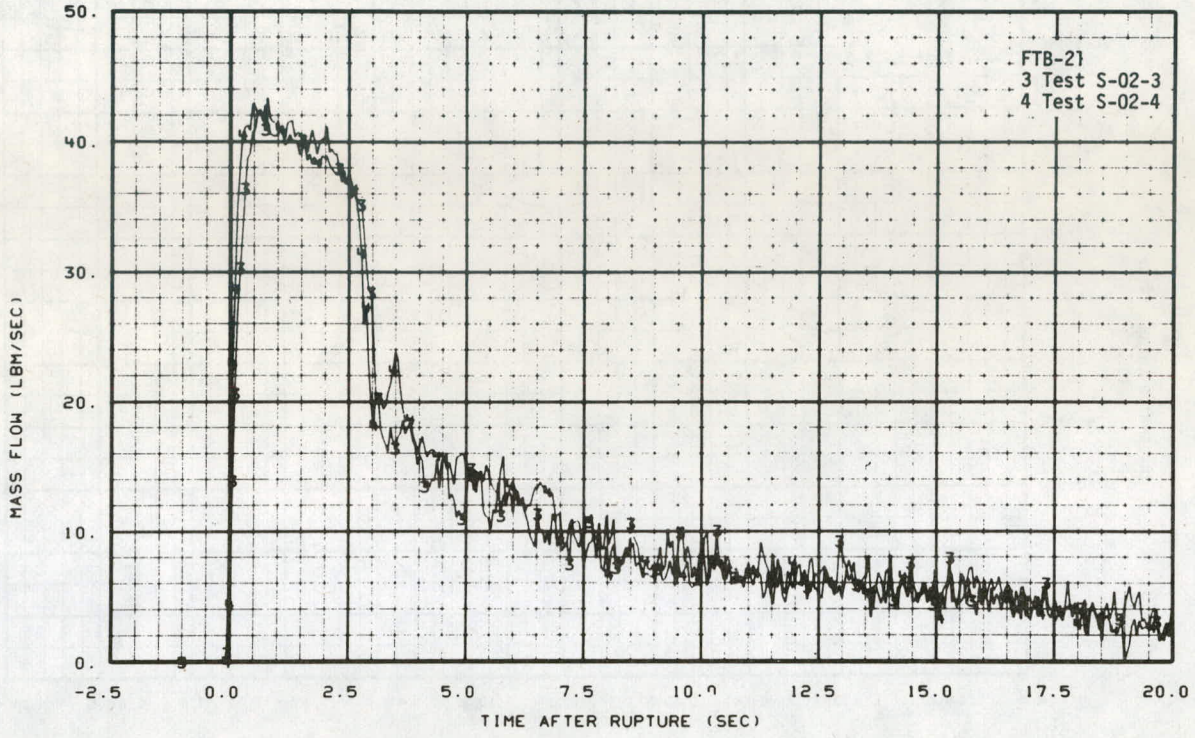

Fig. 22 Mass flow rate near the vessel on the inlet side of the broken loop – Tests S-02-3 and S-02-4.

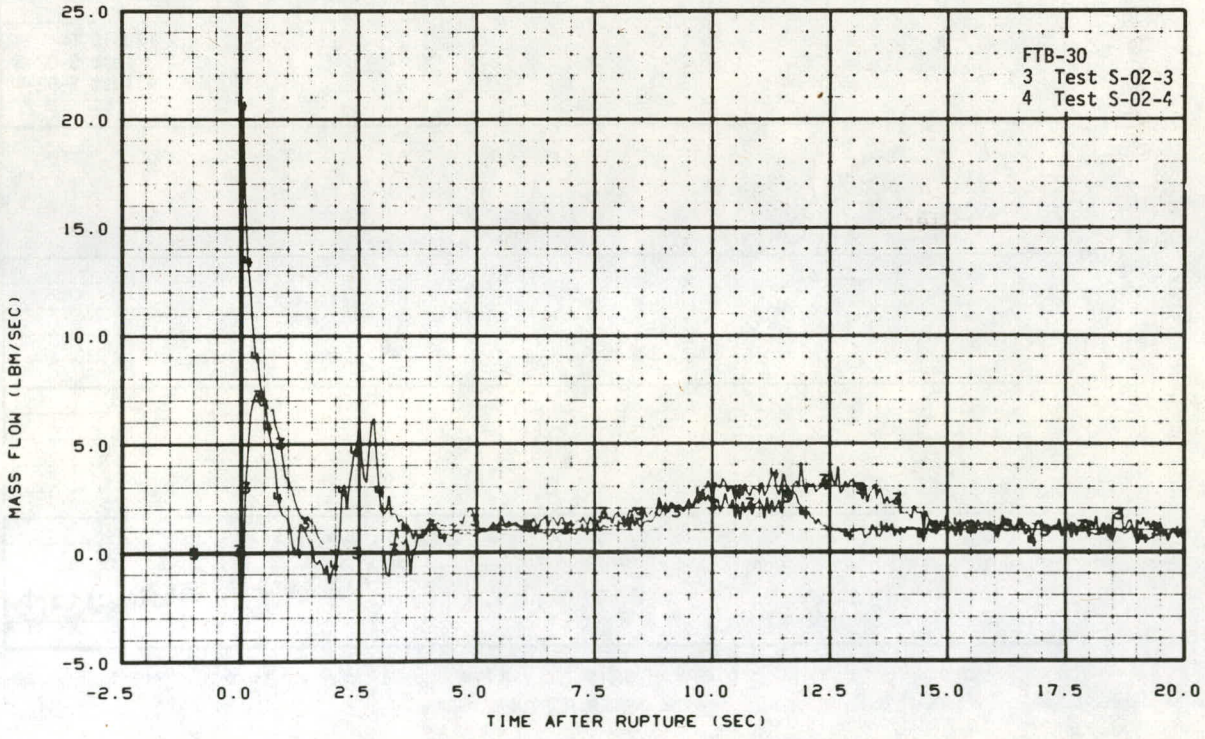

Fig. 23 Mass flow rate near the vessel on the outlet side of the broken loop – Tests S-02-3 and S-02-4.

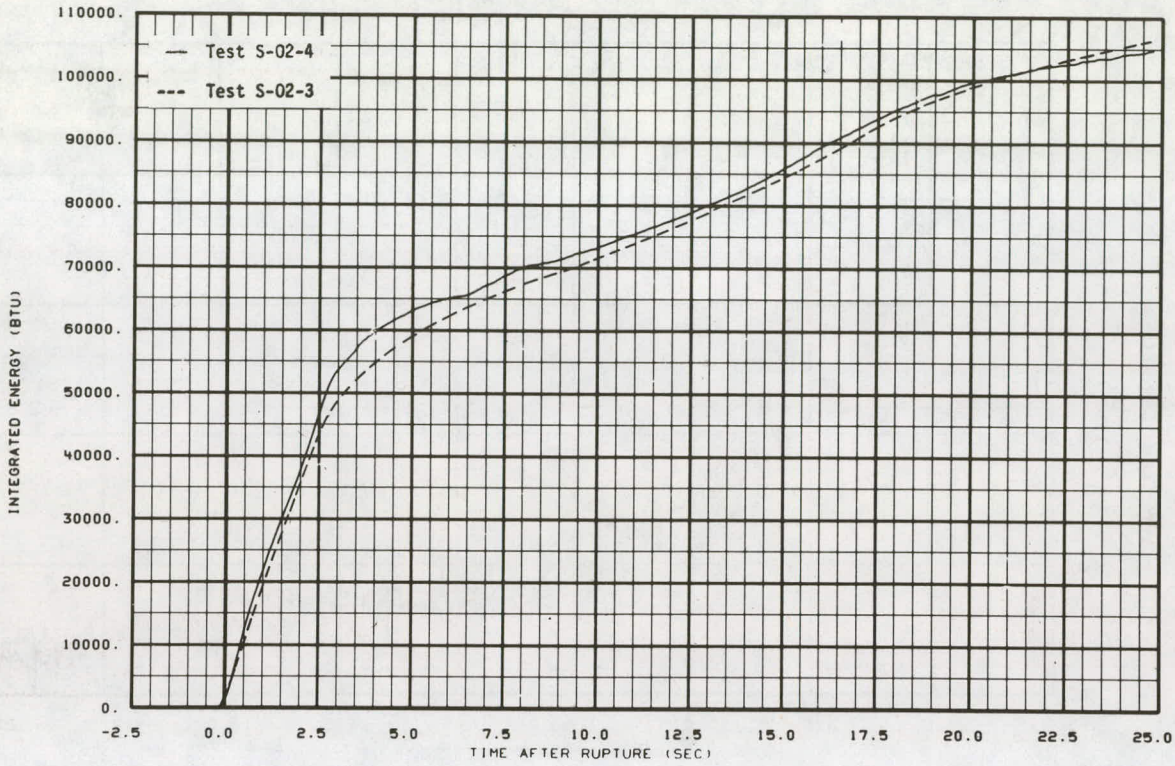

Fig. 24 Total integrated energy leaving vessel – Tests S-02-3 and S-02-4.

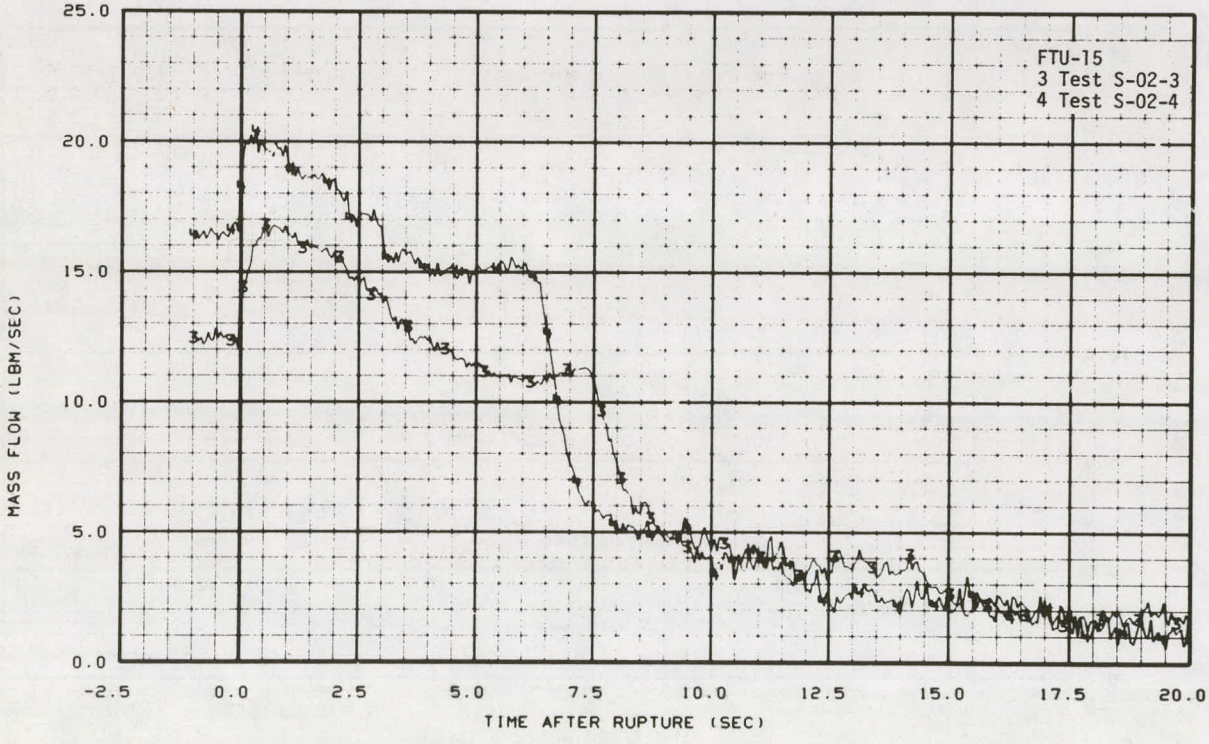

Fig. 25 Mass flow rate near the vessel on the inlet side of the intact loop – Tests S-02-3 and S-02-4.

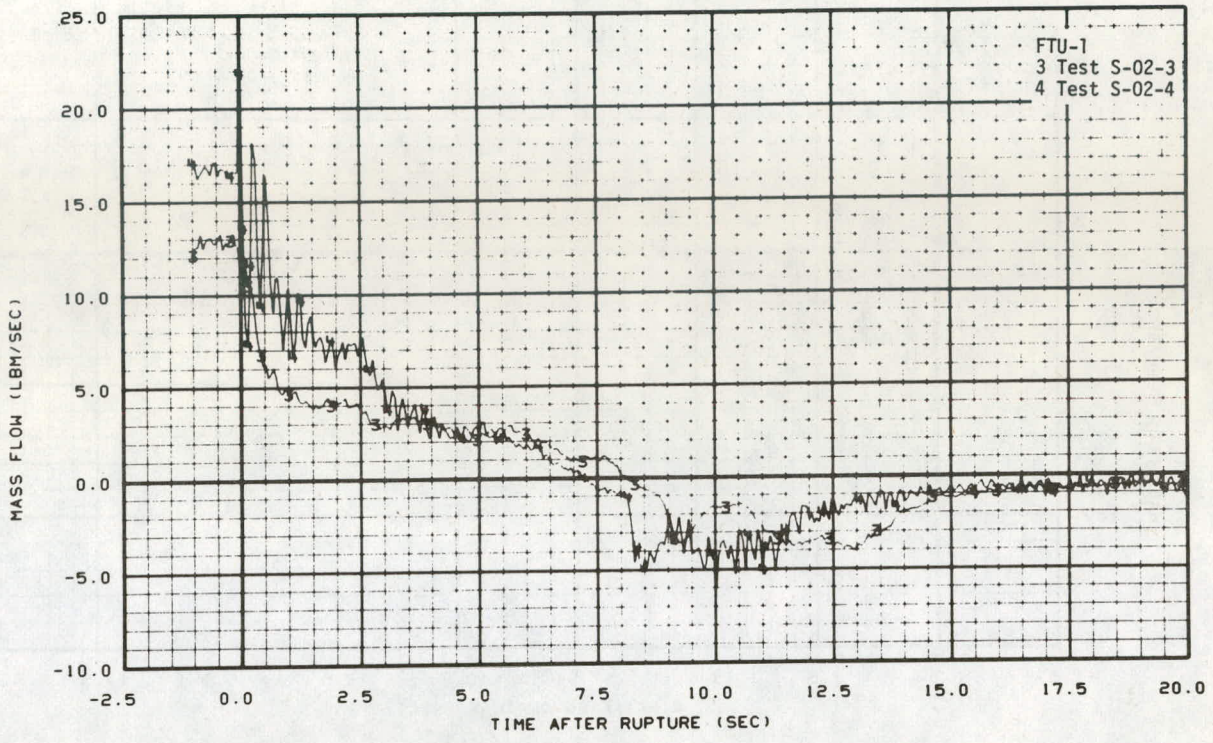

Fig. 26 Mass flow rate near the vessel on the outlet side of the intact loop – Tests S-02-3 and S-02-4.

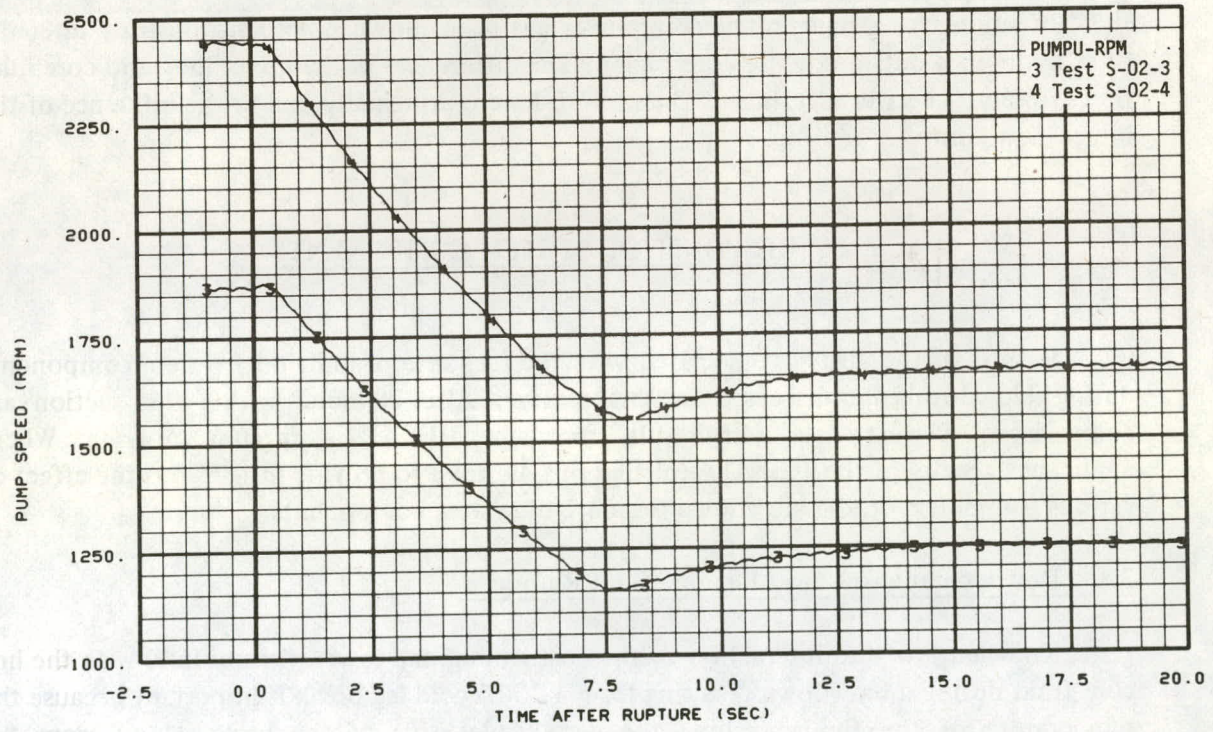

Fig. 27 Intact loop pump speed – Tests S-02-3 and S-02-4.

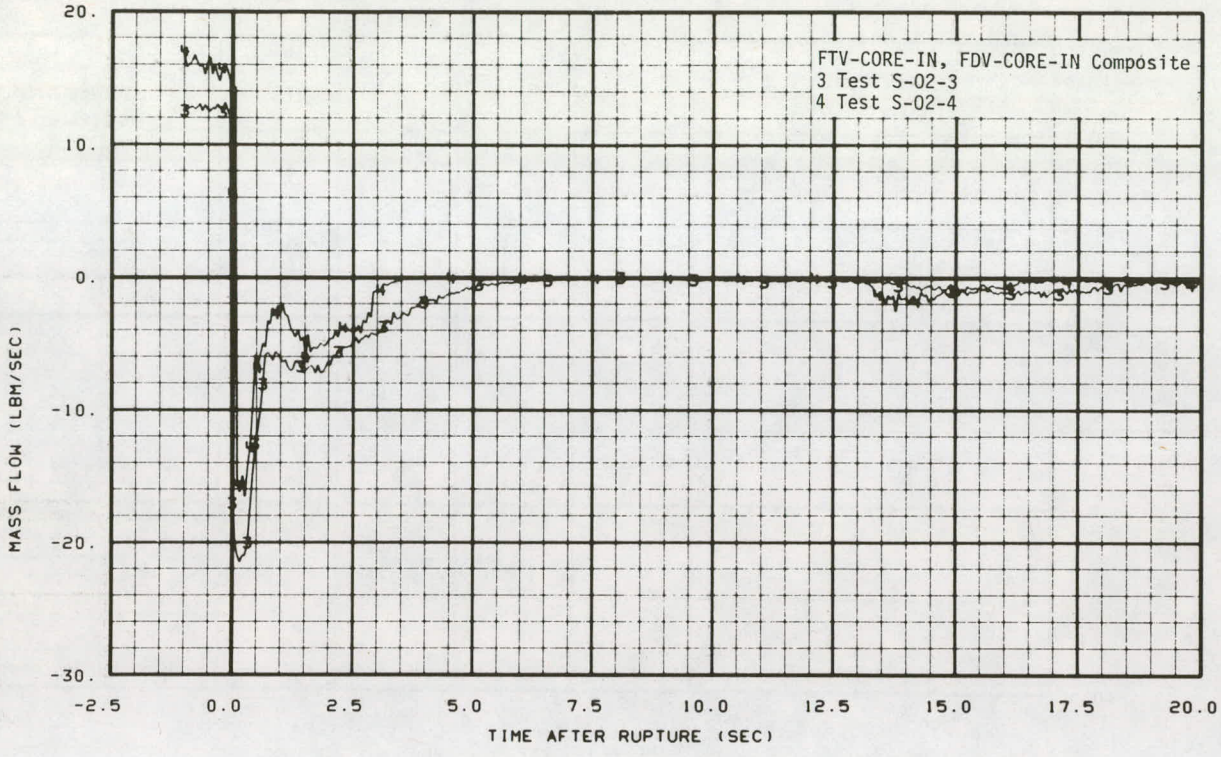

Fig. 28 Mass flow rate at the inlet to the core – Tests S-02-3 and S-02-4.

In summary, a high initial core power has been shown not to significantly alter the fluid hydraulics outside of the core region. The differences in the intact loop and core inlet flows observed between Tests S-02-3 and S-02-4 were principally due to the influence of the intact loop pump.

3. RESPONSE OF SYSTEM COMPONENTS

Results of the analysis associated with the response of individual system components during blowdown are discussed in this section. Also included within this section are comparisons of test data with results from the RELAP4 computer program. Where applicable, results of the RELAP4 calculations are used to provide insight into the effect of various parameters on the blowdown response of system components.

3.1 Downcomer and Lower Plenum Fluid Response

Knowledge of the interaction of the downcomer and lower plenum fluid with the hot core fluid during a blowdown resulting from a 200% cold leg break is important because the temperature of the fluid reaching the vessel inlet side of the broken loop from the downcomer and lower plenum regions has significant influence on the duration of the subcooled flow. Mixing of the hot core fluid with the lower plenum and downcomer fluid results in an increase in the temperature of the fluid in the vessel inlet side of the broken

loop as blowdown progresses. The rate of increase of the fluid temperature determines the duration that the fluid remains subcooled and thus influences the flow rate.

Comparison of results from Tests S-02-2 and S-02-3 demonstrates the effect of the rate of increase in fluid temperature in the vessel inlet side of the broken loop on the subcooled blowdown response. The mass flow rates in the vessel inlet side of the broken loop for the two tests are shown in Figure 29. The considerably higher mass flow for Test S-02-3 causes the hot core and lower plenum fluid mixture to reach the upper downcomer and broken loop cold leg regions earlier than was the case for Test S-02-2. Figure 30 shows the fluid temperatures in the downcomer beneath the broken loop cold leg for the two tests, illustrating the early increase in downcomer fluid temperature for Test S-02-3. As a result of the more rapid increase in fluid temperature, the fluid in the vessel inlet side of the broken loop for Test S-02-3 becomes saturated earlier than for Test S-02-2, causing a somewhat earlier decrease in the flow rate as shown by the flow responses in Figure 29.

The lower plenum and downcomer during the first three to four seconds following rupture were considerably depleted of fluid by the subcooled vessel inlet side break flow demand. Figure 31 compares the flow rate in the vessel inlet side of the broken loop and the sum of flows at the inlet to the core and in the intact loop cold leg. The results indicate that a significant percentage (about 40%) of the fluid flow out the vessel inlet side of the broken loop is supplied by the downcomer and lower plenum fluid during this period. Once the fluid in the vessel inlet side of the broken loop became saturated, however, the intact loop cold leg flow was sufficiently large to supply the demand of the break. As a result, a stagnation in the downcomer fluid occurred, as is shown in Figure 32, which illustrates the downcomer fluid velocities. The increase in fluid velocities in the downcomer that occurs at about 7.5 seconds corresponds to the degradation of the pump head and is caused by steam flow resulting from vaporization of the lower plenum fluid. Steam from the vaporization of fluid in the lower plenum is sufficient to make up the differences between the vessel inlet side break flow demand and the intact loop cold leg flow through the remainder of blowdown as shown in Figure 31.

Fluid temperatures at locations 7.5, 14.5, and 27.5 inches above the bottom of the lower plenum for Test S-02-4, compared in Figure 33, illustrate the degree of mixing of hot core fluid with the lower plenum fluid. The increase in fluid temperatures at the 27.5- and 14.5-inch elevations in the lower plenum during the first several seconds following rupture indicates that the core fluid mixed with at least the upper 50% of the liquid in the lower plenum volume. The mixture of the lower plenum and core fluid traveled up the downcomer and into the broken loop cold leg, resulting in an increase in the cold leg fluid temperature.

A study was performed using the RELAP4 computer code to determine the influence on system blowdown response of the degree of mixing of hot core fluid with the cooler lower plenum fluid during a cold leg break test. Calculations were made using both a single-volume and a three-volume lower plenum in the RELAP4 model of the Semiscale system. Use of a single- volume lower plenum in the RELAP4 model forced the core fluid to mix with the entire lower plenum volume of fluid, whereas, use of a three-volume lower plenum in the model allowed mixing of the core fluid with only the upper volume of the

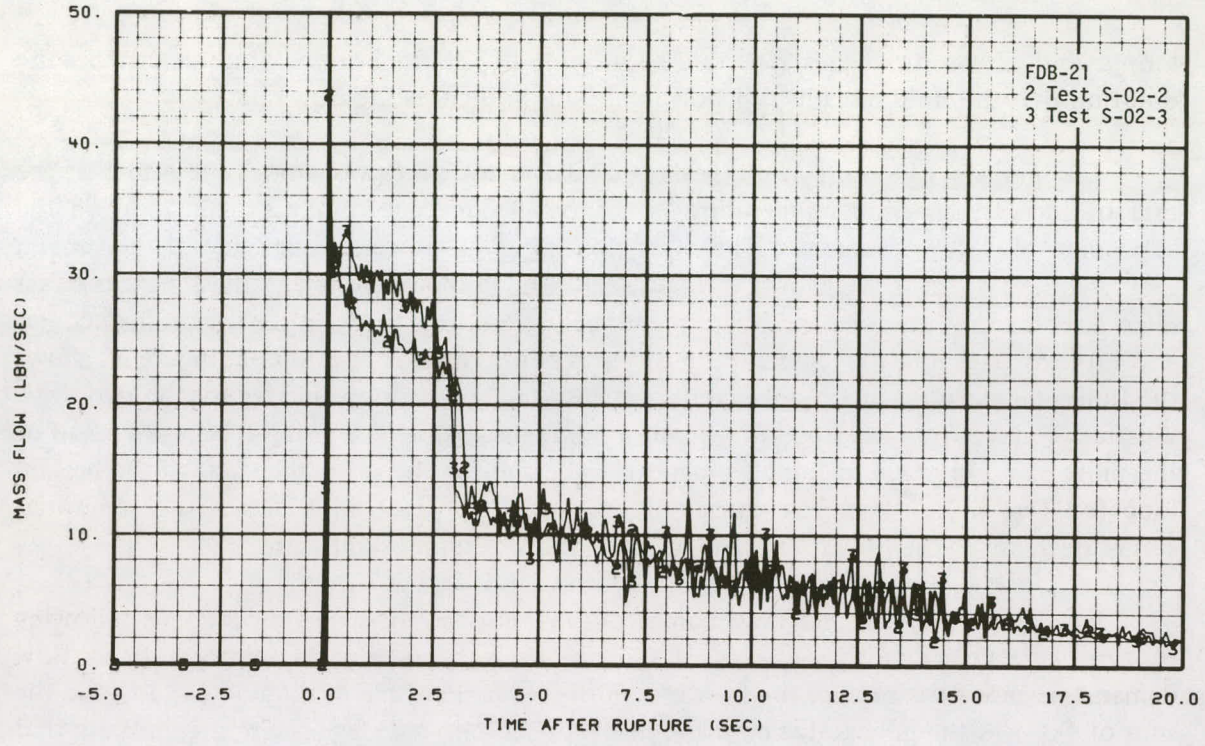

Fig. 29 Mass flow rate near the vessel on the inlet side of the broken loop – Tests S-02-2 and S-02-3.

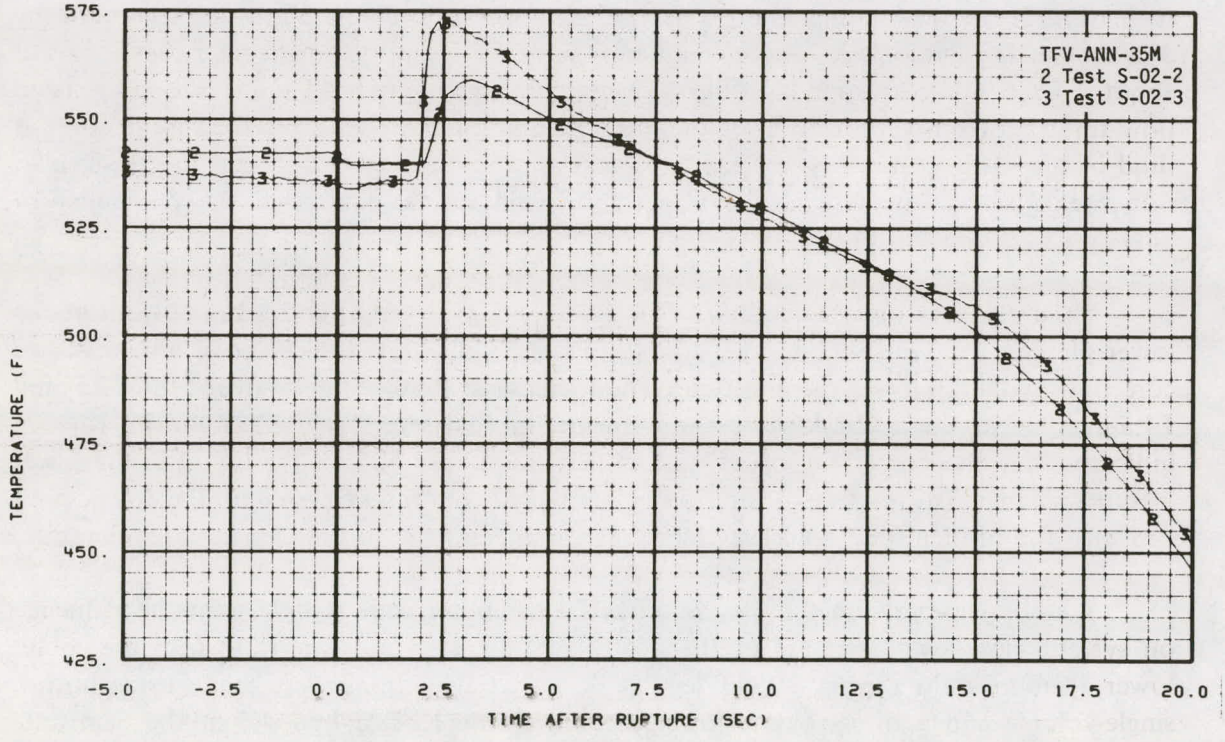

Fig. 30 Fluid temperature in the vessel downcomer 35 inches below the broken loop cold leg centerline – Tests S-02-2 and S-02-3.

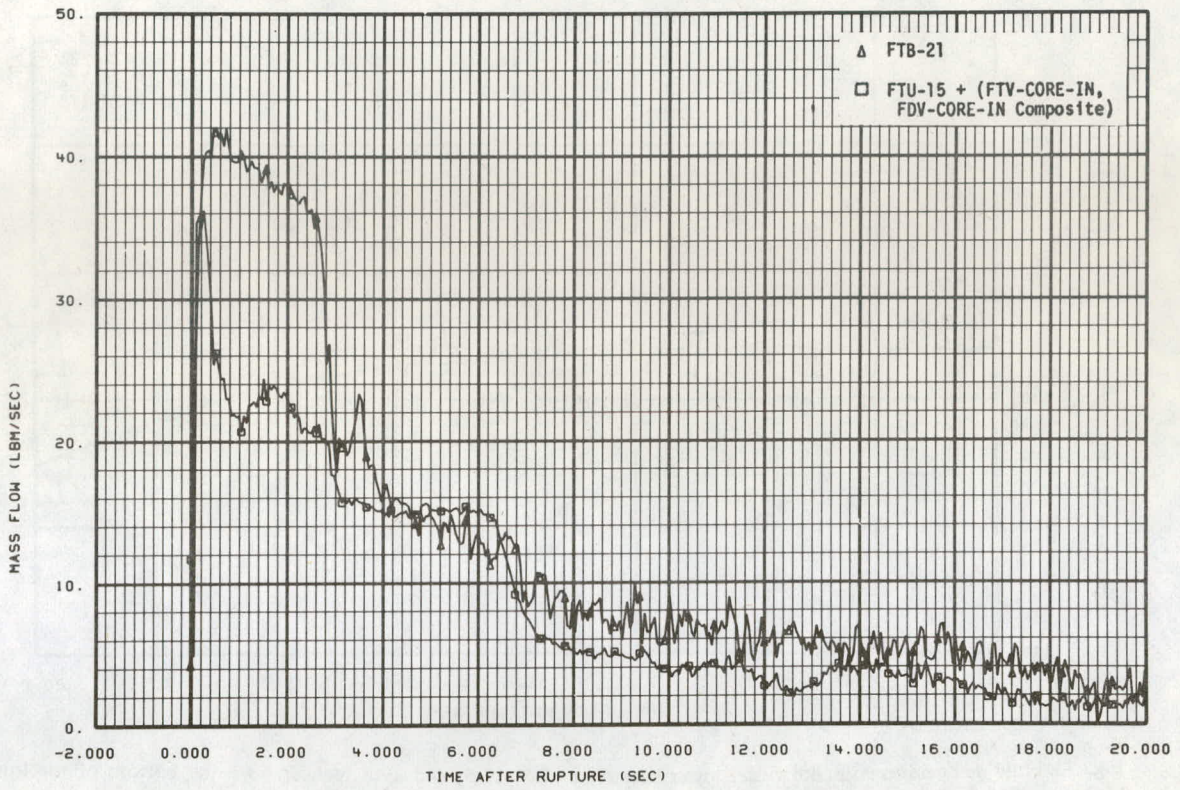

Fig. 31 Mass flow rate near the vessel on the inlet side of the broken loop compared with the sum of the mass flows at the core inlet and near the vessel inlet side of the intact loop – Test S-02-4.

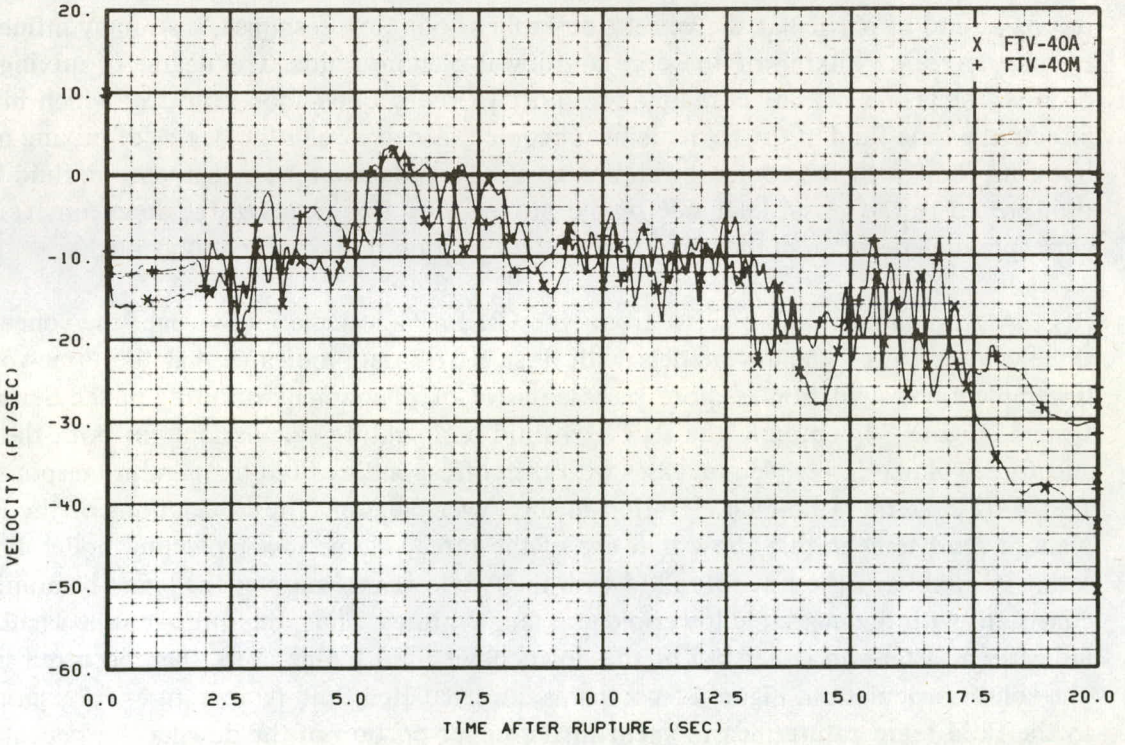

Fig. 32 Fluid velocities in the vessel downcomer – Test S-02-4.

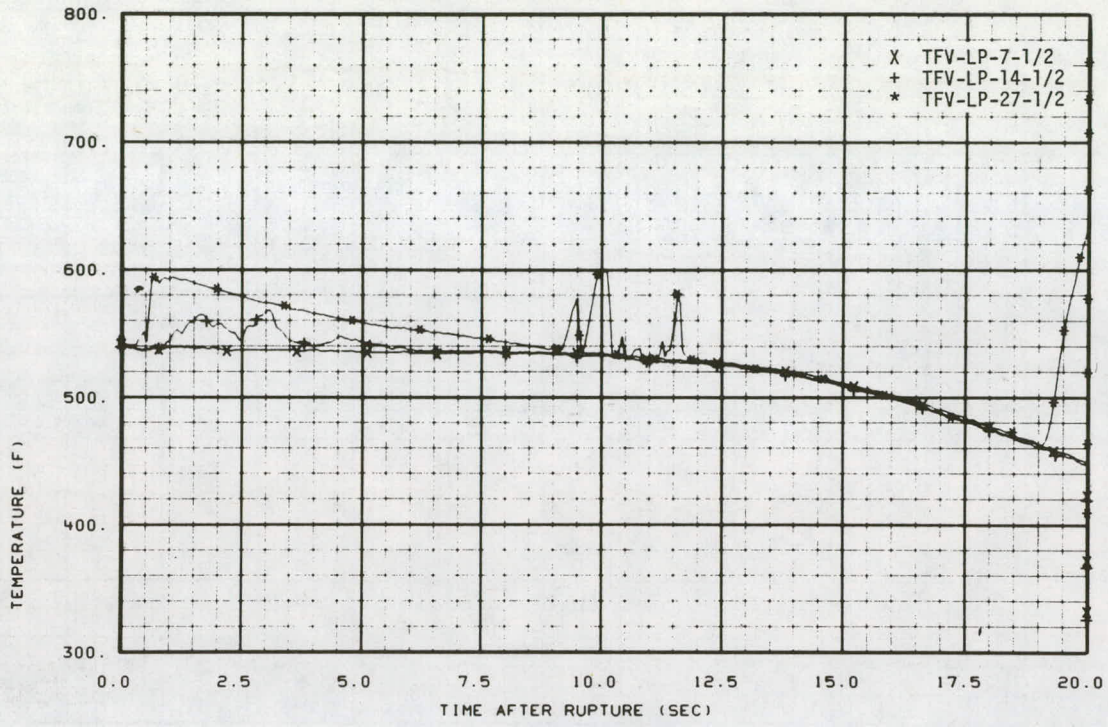

Fig. 33 Fluid temperatures in the vessel lower plenum at 7.5, 14.5, and 27.5 inches above the bottom of the lower plenum – Test S-02-4.

three lower plenum volumes. Results of the calculations show that the overall system response, and in particular the vessel side broken loop flow response, is strongly influenced by the degree of mixing of the core and lower plenum fluids. The degree of mixing that occurs affects the rate of enthalpy transport to the broken loop cold leg, which in turn affects the time fluid in the leg remains subcooled. A decrease in the degree of mixing of the hot core fluid with the cooler lower plenum fluid results in a higher temperature fluid being transported to the vessel inlet side of the broken loop (by means of the downcomer) and a corresponding decrease in the time that the broken loop fluid remains subcooled.

A comparison of results from the RELAP4 calculations using the one- and three-volume lower plenum models with Test S-02-2 data indicates that the three-volume lower plenum calculation is more representative of phenomena occuring in the Semiscale system. Figure 34 compares the RELAP4 fluid temperature calculations for both the one- and three-volume lower plenum cases with the corresponding fluid temperature response for Test S-02-2 at the 14.5-inch elevation in the lower plenum. The calculations of the lower plenum fluid temperature show that use of the three-volume lower plenum model did not result in mixing of the hot core fluid with the two lower volumes of the lower plenum, as is consistant with the measured lower plenum temperatures. Thus, the three-volume caculation indicates a faster and larger rise of the downcomer fluid temperature than occurred in the one-volume calculation. Figure 35 compares the calculated fluid temperatures corresponding to the fluid temperature measurement in the upper portion of the downcomer beneath the broken loop cold leg for Test S-02-2 and shows the more rapid increase in temperature for the three-volume lower plenum case. As a result of the faster increase in the downcomer

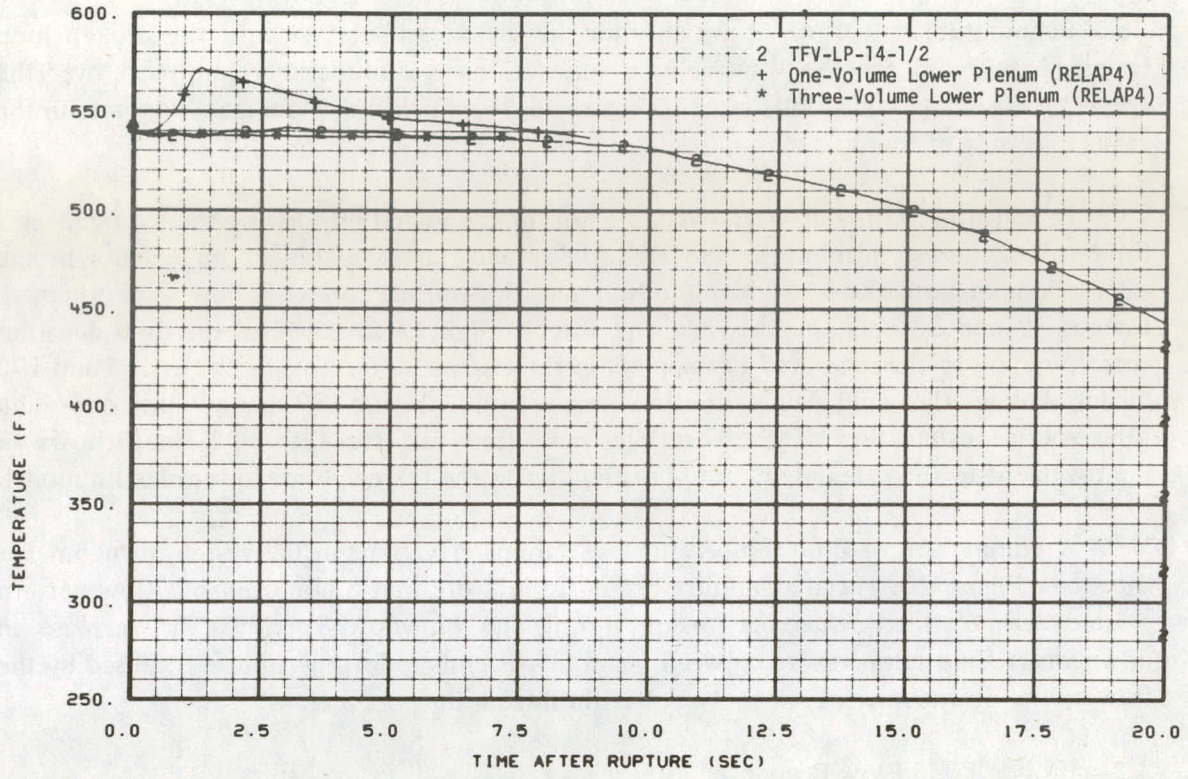

Fig. 34 Fluid temperature at the 14.5-inch level in the vessel lower plenum – comparison of RELAP4 caclulations using one- and three-volume lower plenum models with Test S-02-4 data.

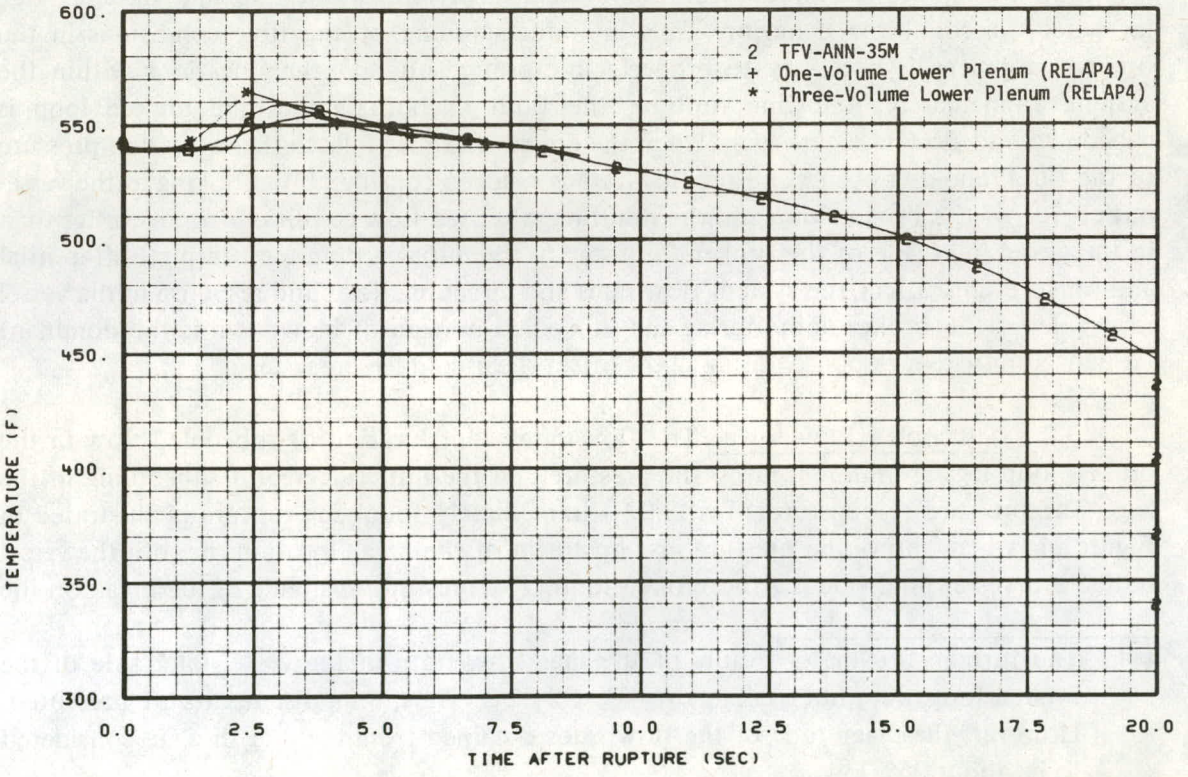

Fig. 35 Fluid temperature in the vessel downcomer 35 inches below the broken loop cold leg centerline – comparison of RELAP4 calculations using one- and three-volume lower plenum models with Test S-02-2 data.

fluid temperature, the time at which fluid in the vessel inlet side of the broken loop becomes saturated for the three-volume calculations is considerably improved over the one-volume calculation as illustrated in Figure 36[a], which shows the mass flow rate in the vessel inlet side of the broken loop.

In addition to the improvements noted in the calculated responses obtained by using a three-volume lower plenum in the RELAP4 model, considerable improvements in the calculations of both the lower plenum fluid densities and the core inlet flow were obtained. Figures 37 and 38 compare the one- and three-volume calculations of the fluid densities corresponding to the measured lower plenum fluid densities for Test S-02-2 at 165 and 172 inches below the cold leg centerline, respectively. Figure 39 shows the one- and three-volume calculation of the core inlet mass flow rate for Test S-02-2 and shows an improvement in the calculated core inlet flow using the three-volume lower plenum model.

A comparison of fluid temperatures at various elevations in the vessel downcomer is shown in Figure 40. The temperature responses indicate that a homogeneous flow pattern existed within the downcomer region during the blowdown period. The increase in downcomer fluid temperature between 1 and 2.5 seconds following rupture is caused by the flow up the downcomer of relatively hotter fluid from the core region.

3.2 Broken Loop Flow Response

The phenomena occurring in the broken loop legs and, in particular at the break location, during blowdown control the system depressurization rate and have a large influence on core flow behavior. Thus an understanding of the flow conditions in the broken loop legs is necessary to properly interpret results at other locations within the system. Immediately following rupture, the fluid in both legs of the broken loop is subcooled and flow rates are high. When the pressure in a leg falls to the saturation pressure of the fluid, choking occurs and the flow rate is reduced considerably. Choking in the vessel outlet side of the broken loop and the resulting saturated flow conditions occur earlier than in the vessel inlet side of the broken loop due to the initial system temperature differential and, in so doing, affect the system flow rates and direction. The fluid response in the vessel inlet side of the broken loop during the subcooled portion of blowdown is the dominant influence on system response during 200% offset shear cold leg break tests.

3.2.1 Subcooled Blowdown. The flow rates and duration of subcooled flow in the broken loop legs are influenced by the pressure and the initial degree of subcooling in the legs. The pressure response for Test S-02-4 immediately following rupture is illustrated in Figure 41, which shows the pressure just upstream of the break locations in both the vessel outlet and vessel inlet sides of the broken loop. The pressure upstream of the break on the

[a] The turbine flowmeter results of the mass flow rate in the vessel inlet side of the broken loop were not available for Test S-02-2. Thus, drag disc results are presented. However, the magnitude of the flow rates obtained from the drag disc are considered to be about 25% low.

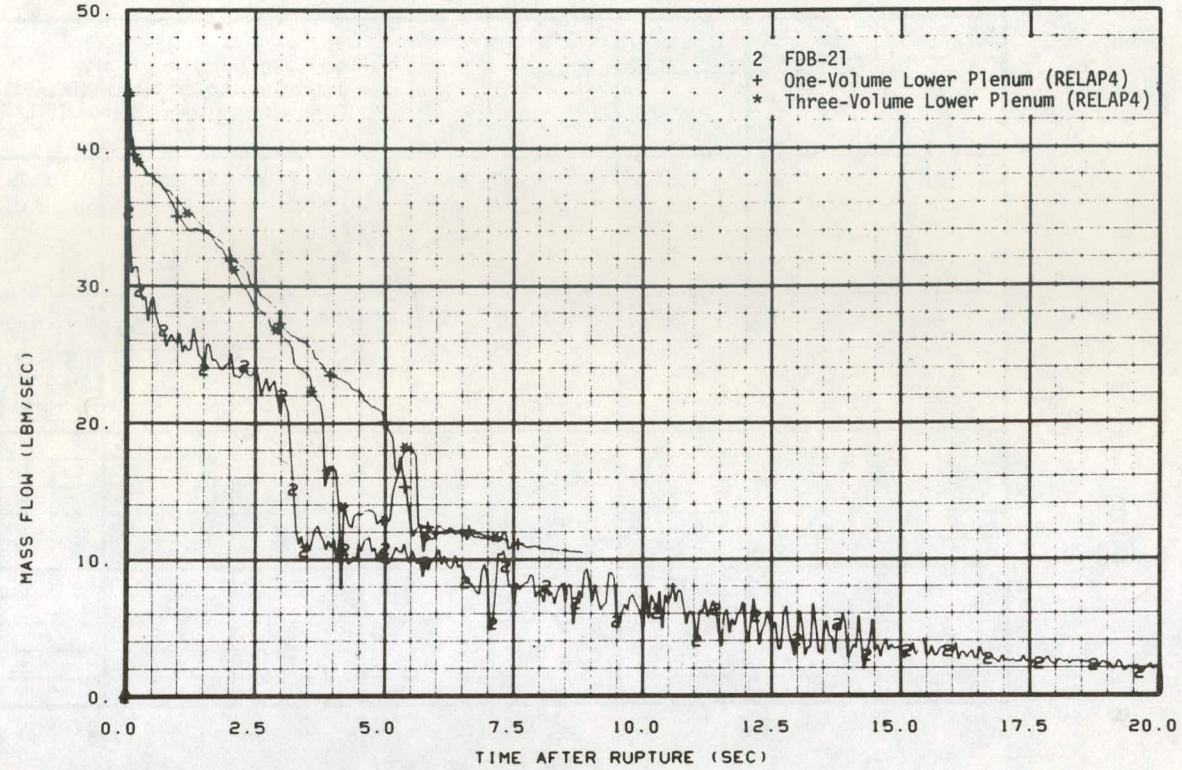

Fig. 36 Mass flow rate near the vessel on the inlet side of the broken loop – comparison of RELAP4 calculations using one- and three-volume lower plenum models with Test S-02-2 data.

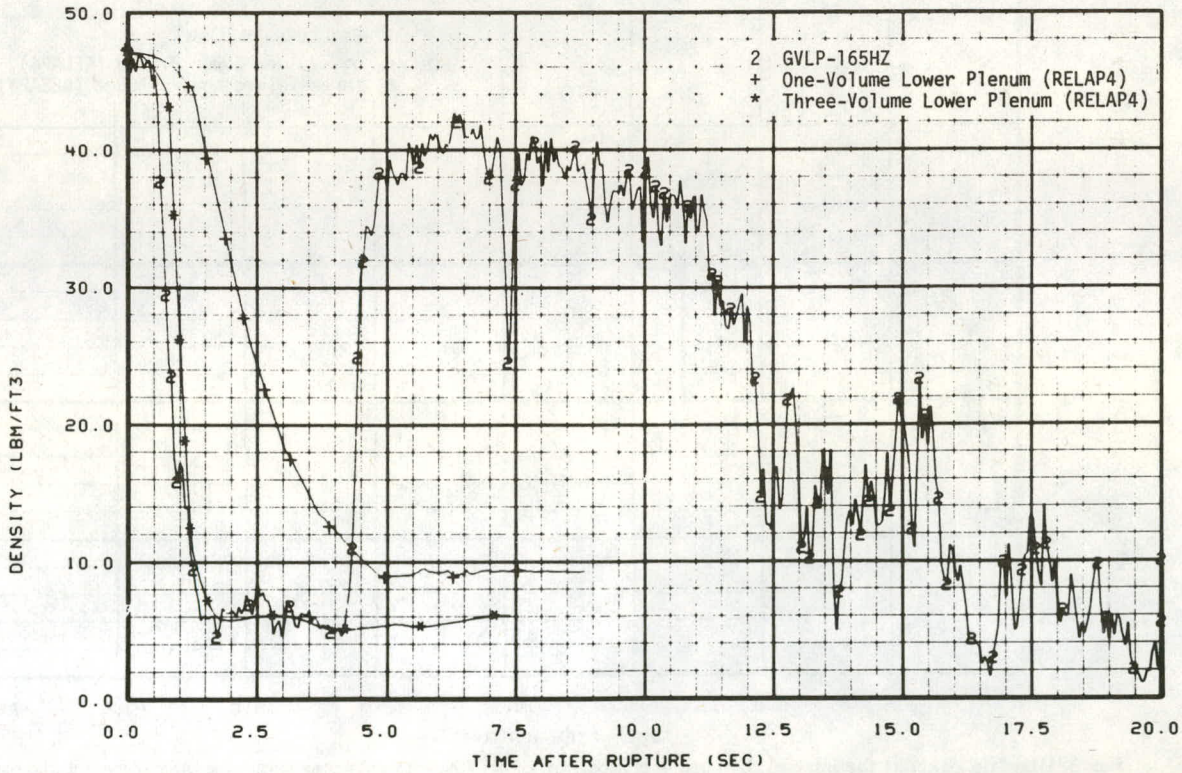

Fig. 37 Fluid density at the inlet to the core – comparison of RELAP4 calculations using one- and three-volume lower plenum models with Test S-02-2 data.

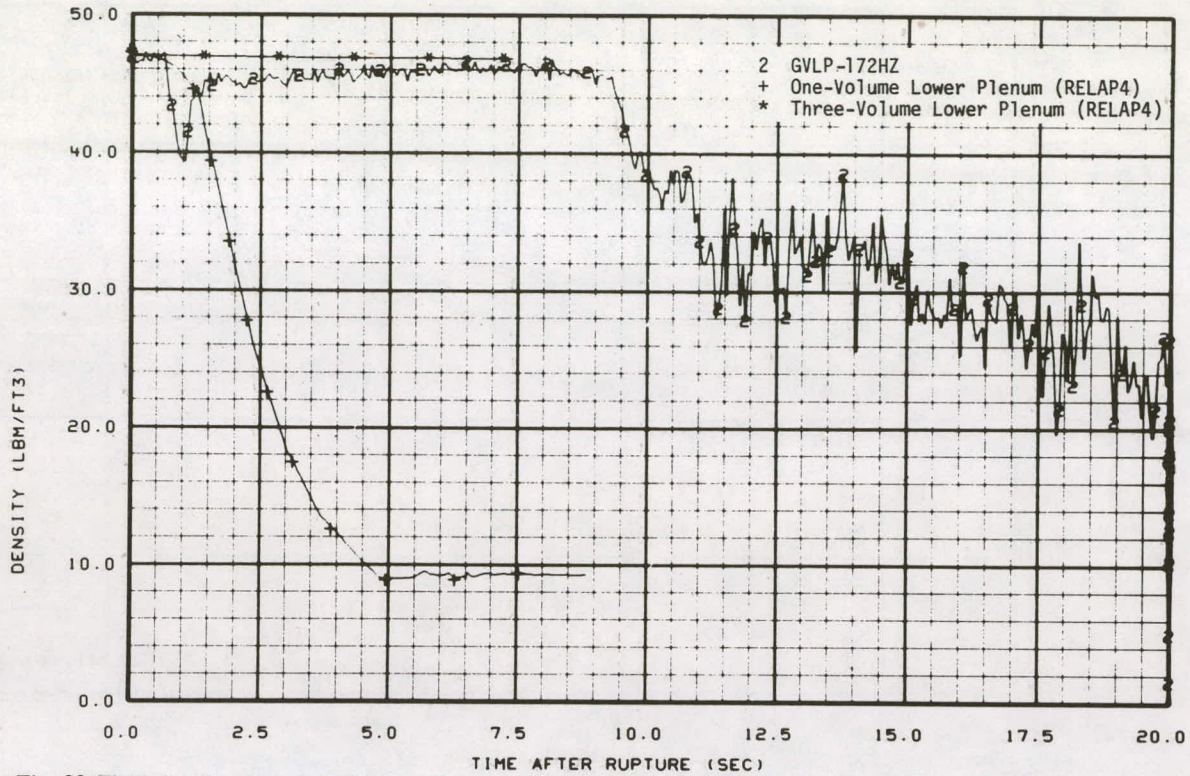

Fig. 38 Fluid density in the vessel lower plenum 172 inches below the cold leg centerline – comparison of RELAP4 calculations using one- and three-volume lower plenum models with Test S-02-2 data.

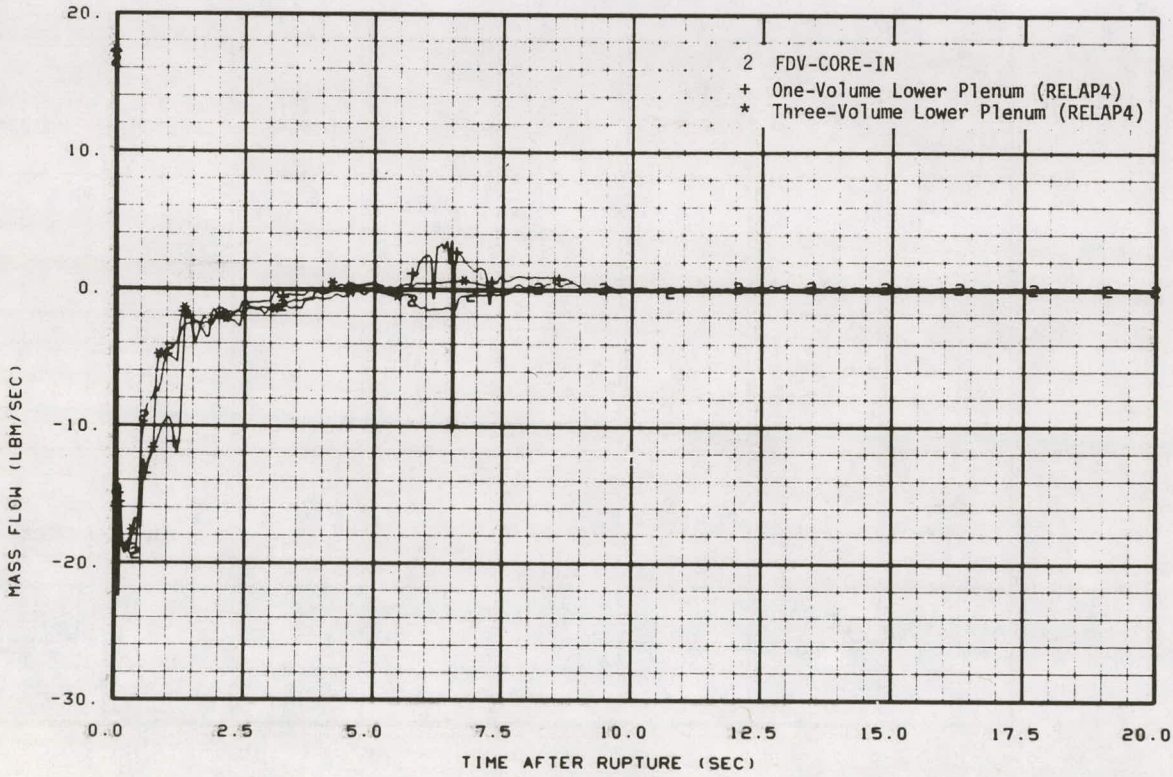

Fig. 39 Mass flow rate at the inlet to the core – comparison of RELAP4 calculations using one- and three-volume lower plenum models with Test S-02-2 data.

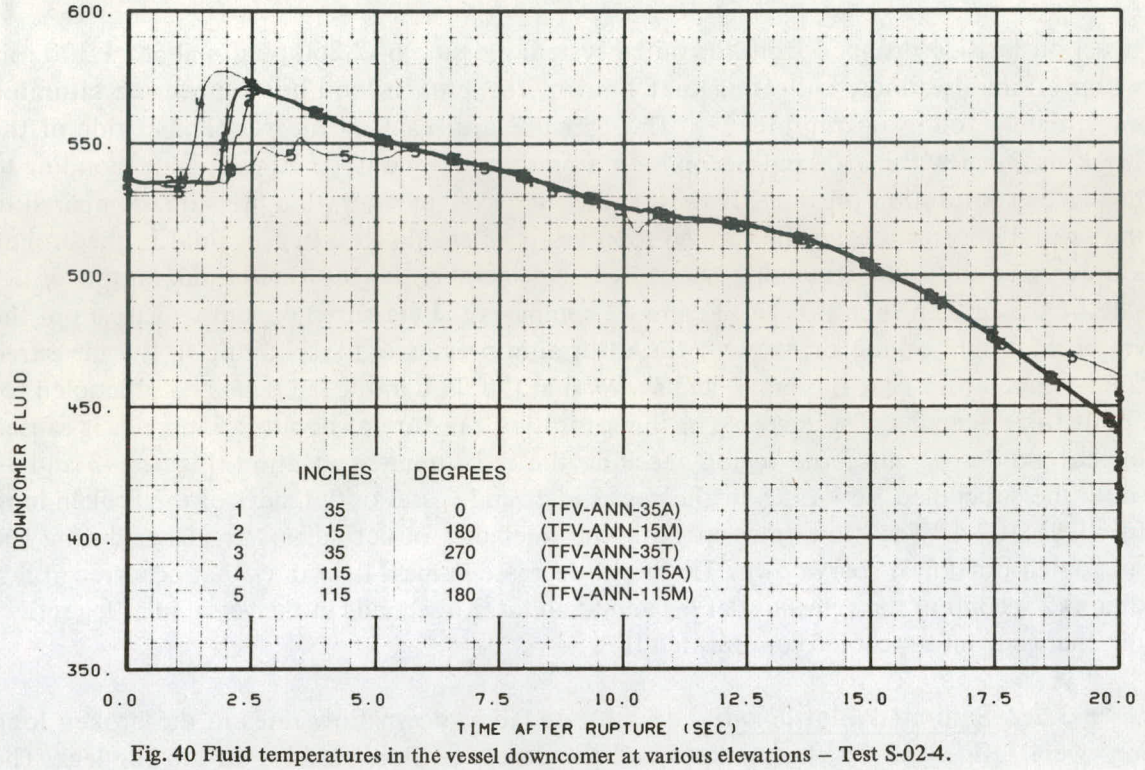

Fig. 40 Fluid temperatures in the vessel downcomer at various elevations – Test S-02-4.

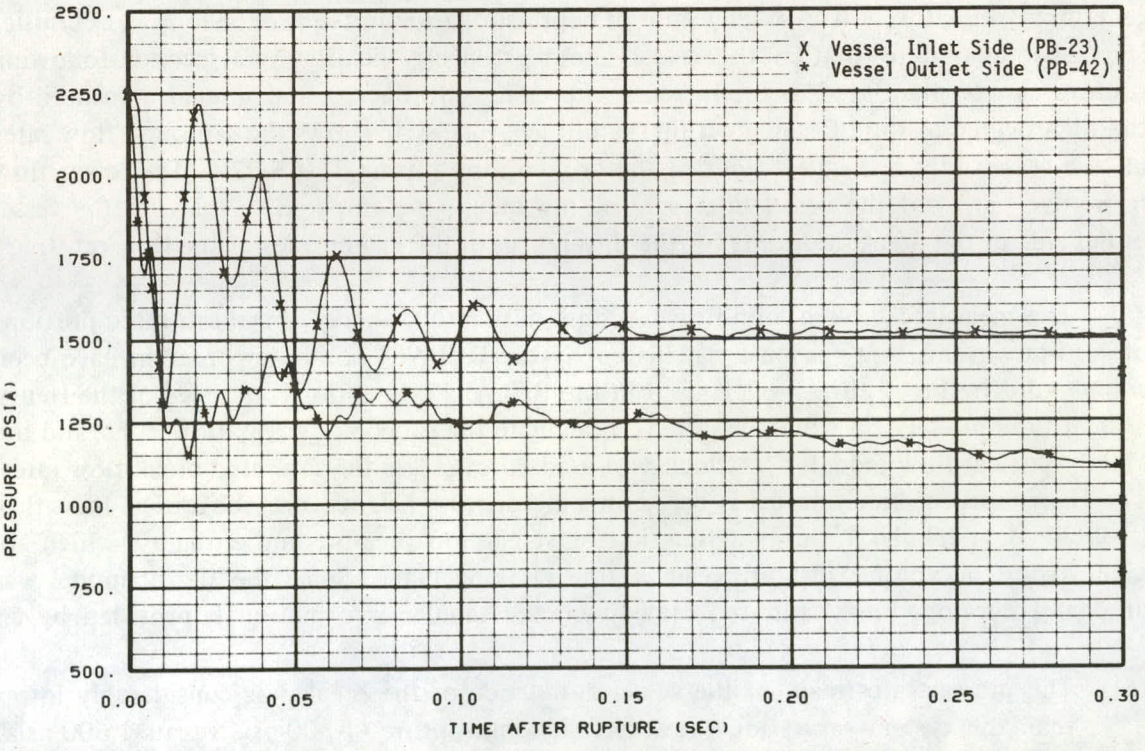

Fig. 41 Subcooled blowdown pressure response upstream of the break nozzles on the vessel outlet and inlet sides – Test S-02-4.

vessel outlet side dropped from the initial system pressure of 2,260 psia to about 1,300 psia within 10 milliseconds, indicating that fluid in the broken loop hot leg became saturated immediately following rupture[a] . The pressure upstream of the vessel inlet side of the break dropped within 100 milliseconds to a pressure of about 1,600 psia, corresponding to the system saturation pressure. However, the high system saturation pressure (compared to the saturation pressure on the broken loop vessel inlet side) resulted in fluid in the broken loop vessel inlet side remaining subcooled considerably longer than fluid in the outlet side of the broken loop hot leg. Figure 42 compares the measured pressure upstream of the vessel inlet side of the break with the saturation pressure corresponding to the measured fluid temperature near the break and shows that the fluid in the leg remained subcooled for about three seconds. The increase in the saturation pressure at about 2.5 seconds is caused by hot fluid from the core region reaching the measurement location. Figures 43 and 44 show the subcooled flow rates in the vessel inlet and vessel outlet sides of the broken loop for Test S-02-4. The flow rates in both the inlet and outlet sides were large during the subcooled portion of blowdown. The rapid decrease in mass flow rates that occurred at less than 0.2 second in the vessel outlet leg and at about 2.6 seconds in the vessel inlet leg reflect the change from subcooled to saturated flow.

3.2.2 Saturated Blowdown. The saturated blowdown flow rates in the broken loop legs were influenced by the pressure and the degree of fluid flashing within the legs. The saturated blowdown pressure responses upstream of the break nozzles for Test S-02-4 are shown in Figure 45. The much lower pressure throughout blowdown upstream of the break on the vessel outlet side is caused by the large pressure drops across the pump and steam generator simulators. The higher rate of depressurization in the broken loop vessel outlet leg (as compared to that in the vessel inlet leg) during the first two seconds following rupture can be attributed to the increase in pressure drop across the simulators caused by the high degree of fluid flashing within the hot leg. Figure 46 shows the saturated flow rates on the vessel inlet and outlet sides of the broken loop during Test S-02-4. The lower flow restrictive path out the vessel inlet side of the break, as compared to that out the vessel outlet side of the break, accounts for the differences in the magnitudes of the flow rates.

The measured broken loop flow response during the subcooled and saturated portions of blowdown and that response calculated by the RELAP4 computer program have been compared. The break flow models used in the RELAP4 calculations consisted of the Henry critical flow model[13] which was used to calculate the subcooled break flow rates, and the Moody critical flow model[14] which was used to calculate the saturated break flow rates. The Henry critical break model is based on a momentum balance, and the critical mass flux is obtained in tabular form as a function of stagnation pressure and enthalpy, which are taken from the volume just upstream of the choking plane. Since the Henry model was originally developed for saturated blowdown, the tabular information is provided by an

[a] The pressure upstream of the vessel outlet side of the break was considerably lower than the system saturation pressure following rupture (1,300 psia versus 1,600 psia) due to the large pressure drops across the pump and steam generator simulators.

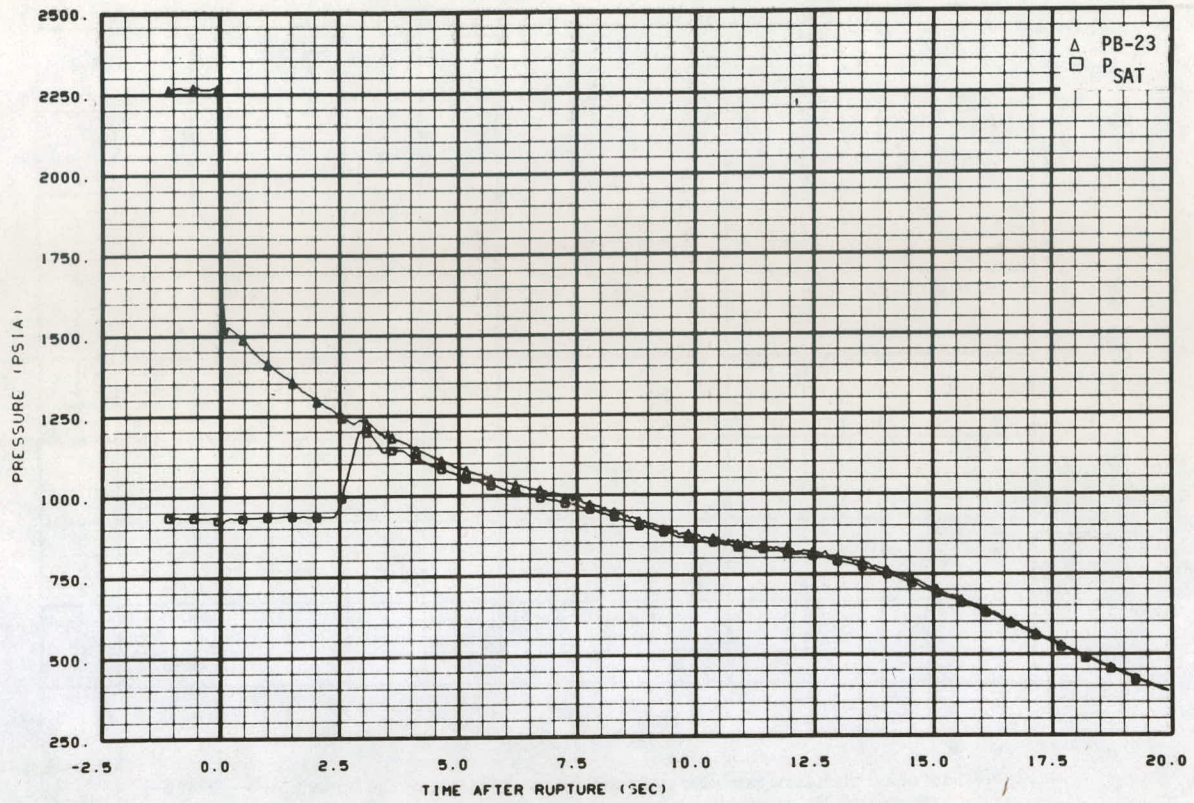

Fig. 42 Pressure response upstream of the break nozzle on the vessel inlet side – comparison with saturation pressure – Test S-02-4.

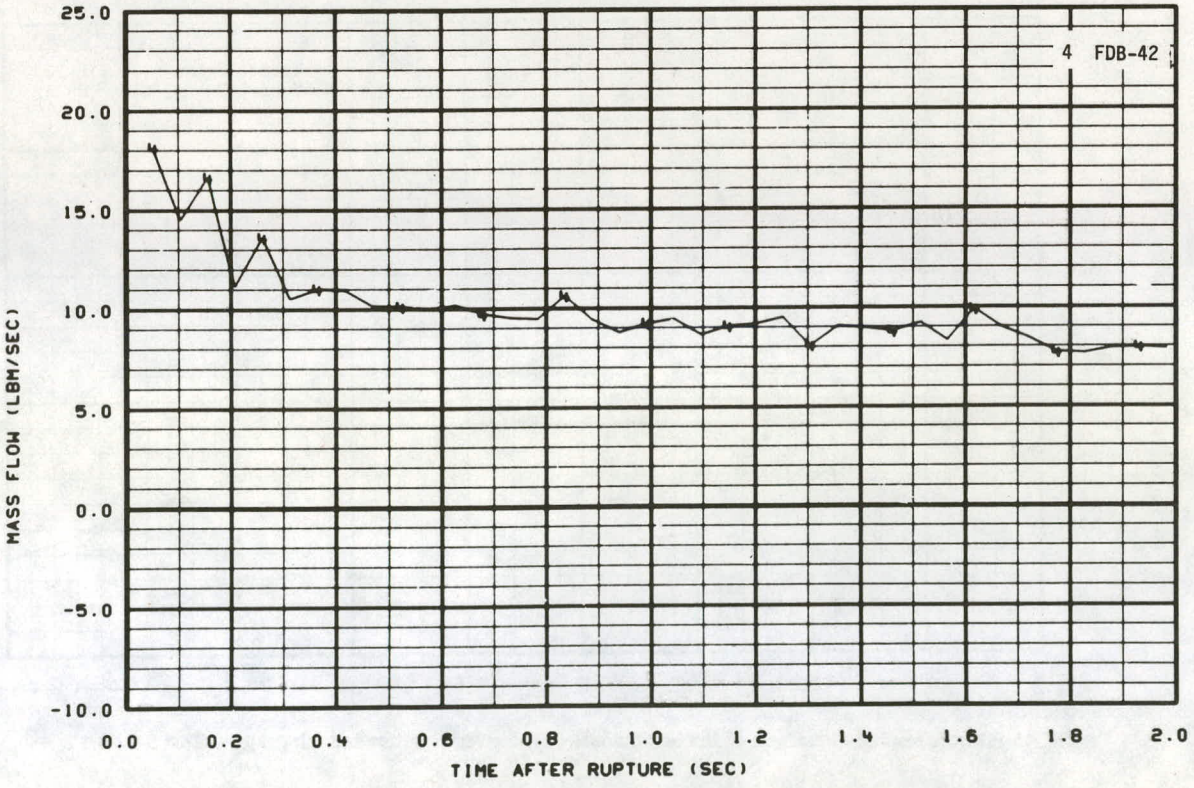

Fig. 43 Subcooled mass flow rate upstream of the break nozzle on the vessel outlet side – Test S-02-4.

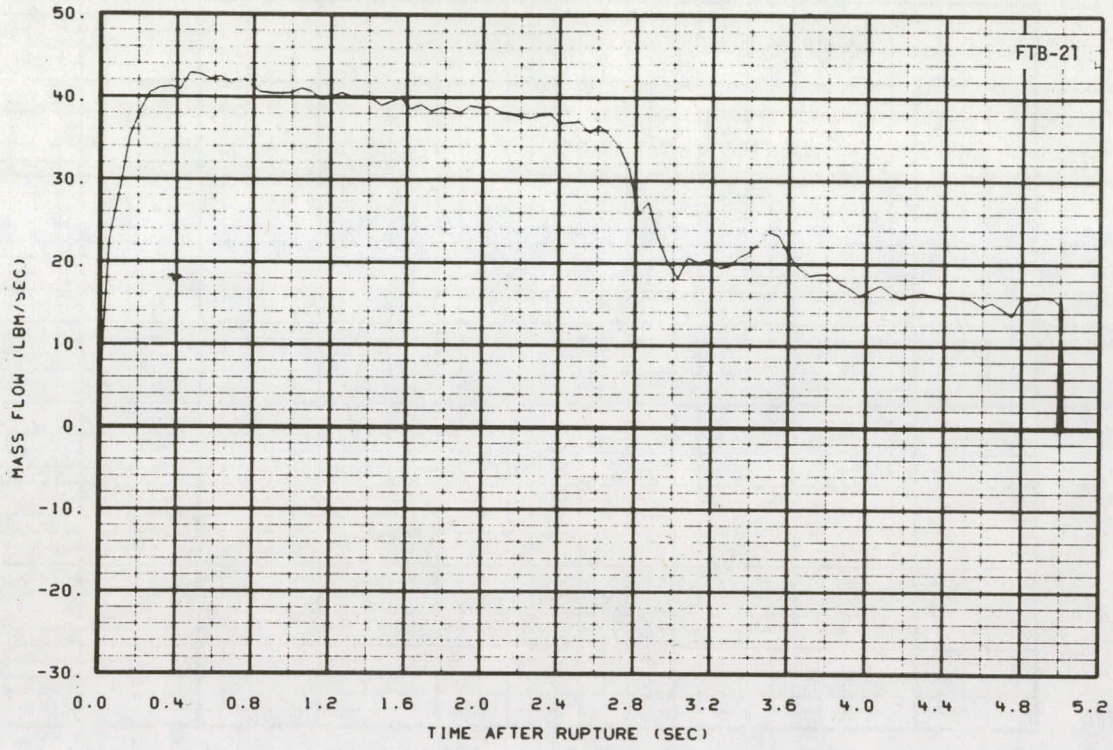

Fig. 44 Subcooled mass flow rate near the vessel on the inlet side of the broken loop – Test S-02-4.

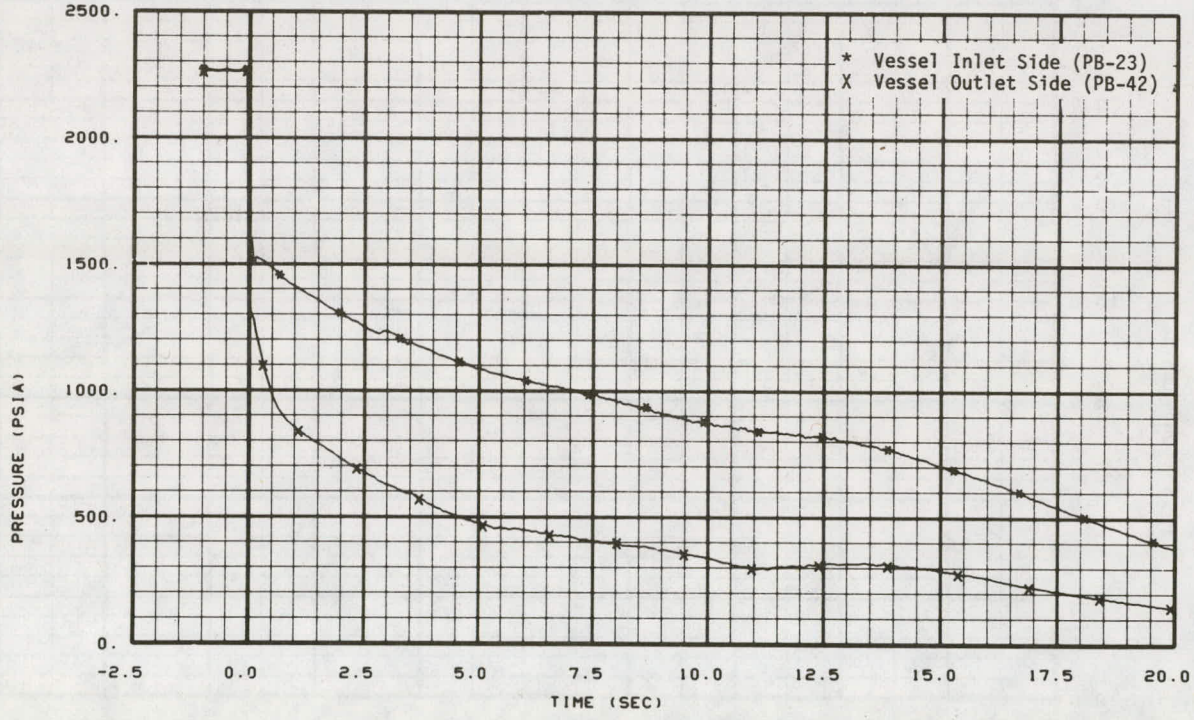

Fig. 45 Pressure response upstream of the break nozzles on the vessel outlet and inlet sides – Test S-02-4.

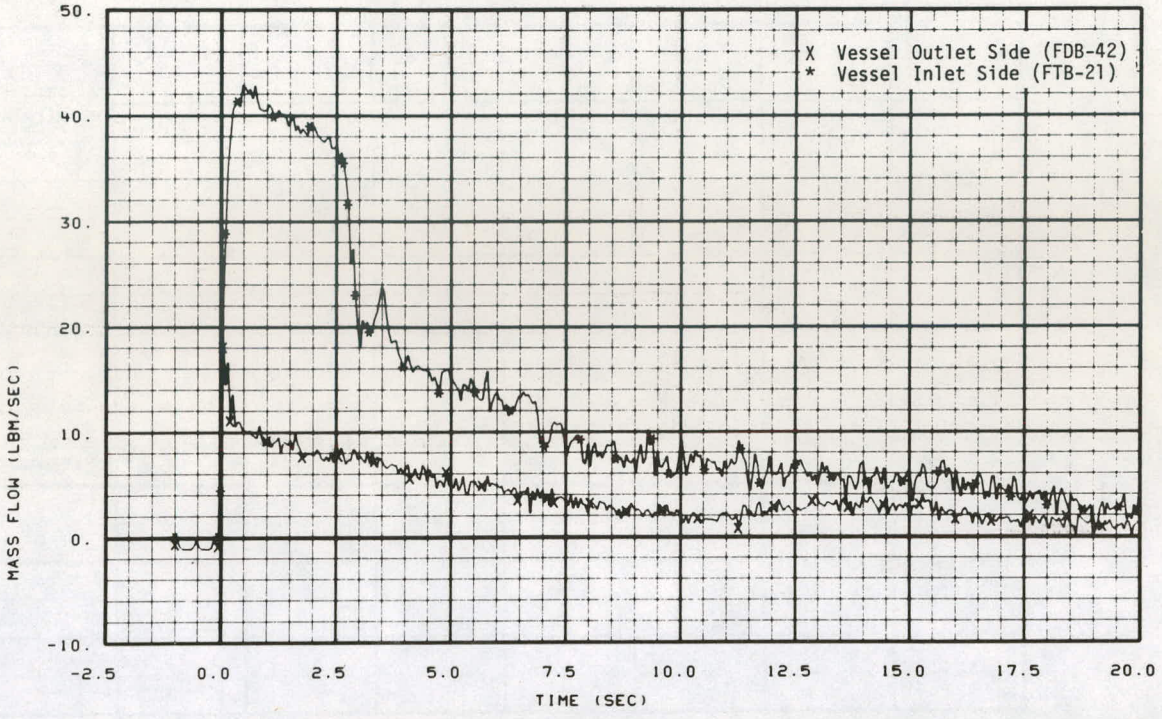

Fig. 46 Mass flow rate near the vessel on the inlet side of the broken loop compared with the flow rate upstream of break nozzle on the vessel outlet side – Test S-02-4.

extended Henry table of values applicable to subcooled conditions. Once the mass flux is obtained, a contraction coefficient (multiplier) is used to account for flow losses encountered in the fluid going through the break nozzle. The multiplier value of 1.0 was determined to be appropriate for the nozzle configuration used in the Semiscale system. The Moody critical flow model is based on an energy balance using the first law of thermodynamics and takes into account slip within the two-phase mixture in calculating the break flow rate. The critical mass flux is obtained in tabular form as a function of stagnation pressure and enthalpy, which are taken from volumes just upstream of the choking plane. A multiplier of 0.6 for the Moody critical mass flux was determined to be appropriate for the Semiscale nozzle configuration.

The RELAP4 calculations of the mass flow rates on the vessel inlet and outlet sides of the broken loop are compared with Test S-02-4 data in Figures 47 and 48. The calculated values are in generally good agreement with the data. However, variations between the calculated subcooled blowdown time and the data for the broken loop vessel inlet leg do exist. A thorough investigation of various break flow models for the Semiscale system has been made and will be presented in a future topical report.

3.2.3 Influence of Broken Loop Pump and Steam Generator Simulators. The pump and steam generator simulators located in the broken loop of the Semiscale Mod-1 system were designed to be geometrically similar to the LOFT simulators. The steam generator simulator consists of a housing in the shape of an inverted "U" in which are installed 14

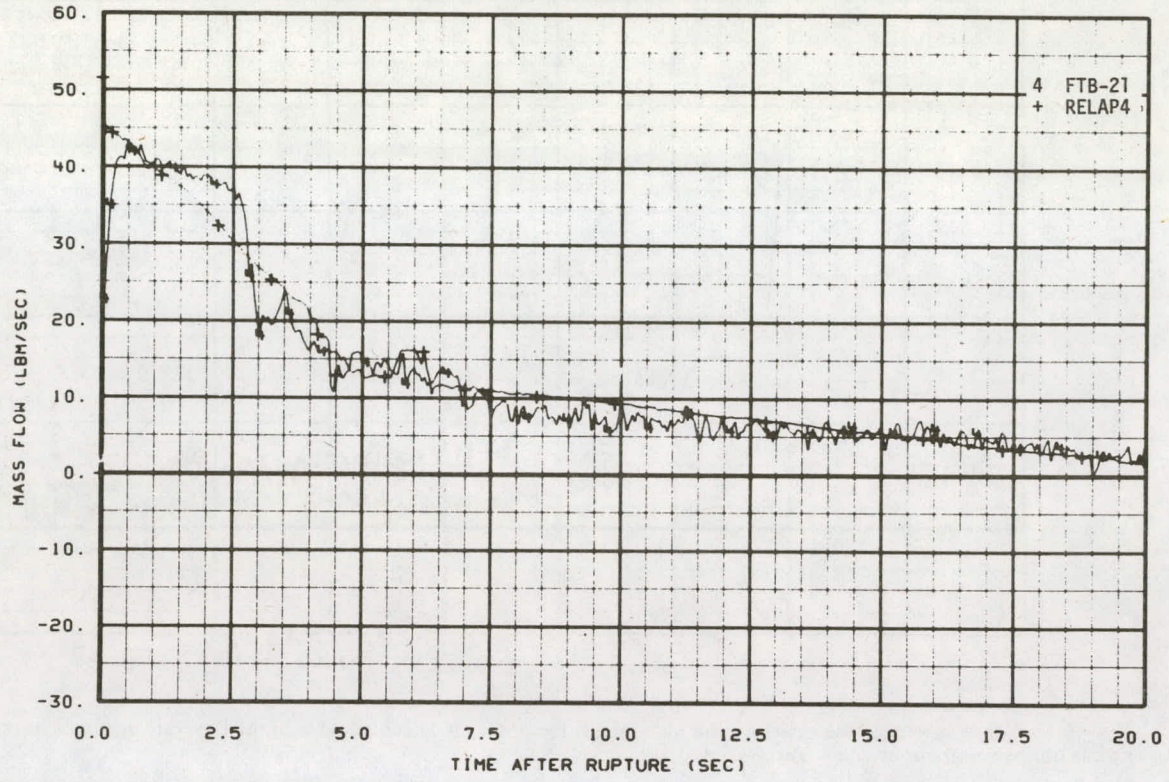

Fig. 47 Mass flow rate near the vessel on the inlet side of the broken loop – comparison of RELAP4 calculation with Test S-02-4 data.

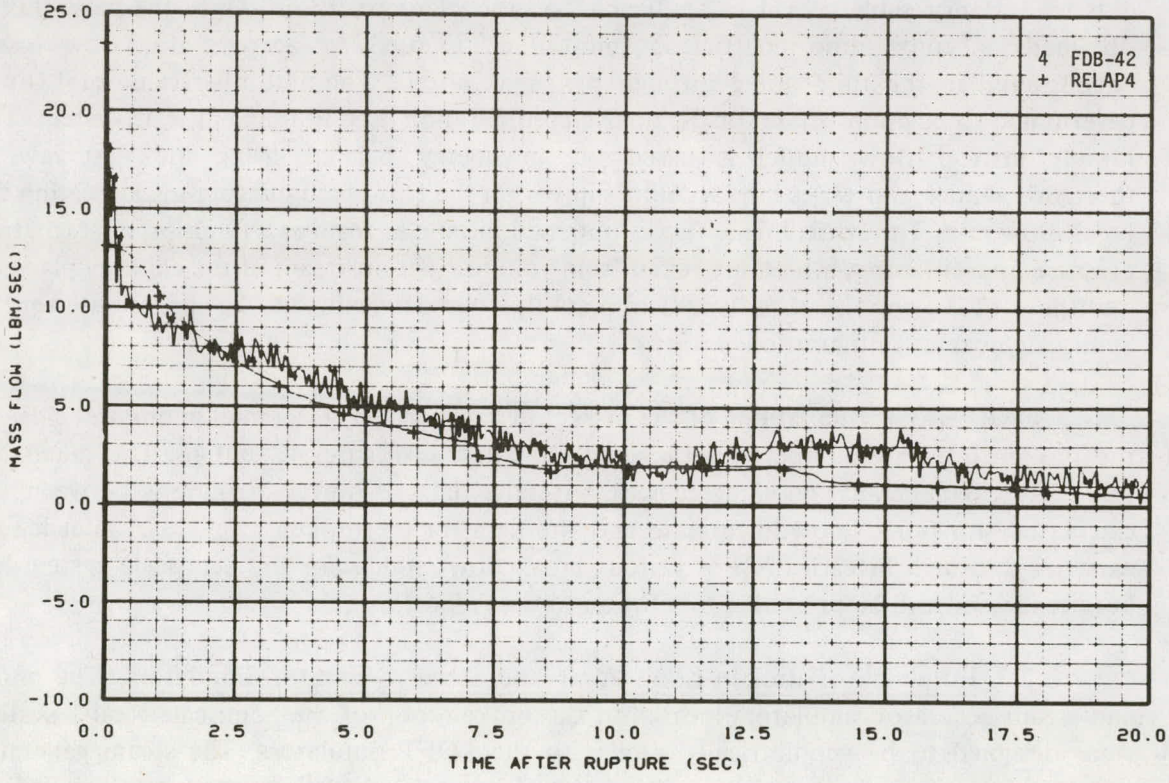

Fig. 48 Mass flow rate upstream of the break nozzle on the vessel outlet side – comparison of RELAP4 calculation with Test S-02-4 data.

orifice plates, seven in each U-leg. The pump simulator consists of a housing in which are installed 14 orifice plates. The orifice plates in each of the simulators are used to obtain a scaled flow resistance representative of the LOFT counterpart. Since the Semiscale simulators were designed directly from their LOFT counterparts, information on the simulator pressure drops as well as an evaluation of the calculated pressure loss across these components will aid in evaluating the broken loop pressure drops in the LOFT system.

The pressure drop across the pump simulator was the largest pressure drop in the Mod-1 system during the blowdown transient. The measured pump simulator differential pressure is presented in Figure 49. Also presented is the differential pressure calculated by the RELAP4 program. The data show an initial sharp rise in the pressure drop caused by fluid accelerating toward the break. After about two seconds, a relatively high two-phase pressure drop occurs, which results in a gradual decline of the pressure differential for the remainder of blowdown. The pressure drop across the pump simulator was considerably underestimated by the RELAP4 calculation. The lower pressure was thought to be caused by the model of the pump simulator in the RELAP4 program, which used only three junctions to represent the total resistance across the 14 orifice plates. However, renodalyzing the pump simulator model in the RELAP4 program to have a larger number of junctions at which the resistances could be applied did not significantly improve the comparison of the calculated and measured pump simulator differential pressure. A complete analysis of this effect is not within the scope of the present study.

The measured pressure difference across the steam generator simulator and that calculated by the RELAP4 program are presented in Figure 50. The initial sharp rise in the differential pressure is caused by the acceleration of fluid toward the break. Between 0.5 and 2.0 seconds, the pressure differential decreased considerably, corresponding to a reduction in the mass flow rate through the steam generator simulator. The gradual increase that occurs after 2.5 seconds is a result of an increase in fluid quality and velocity. The rapid increase in the pressure difference at about nine seconds can be attributed to an increase in the mass flow through the steam generator simulator caused by fluid from the intact loop hot leg. The RELAP4 calculation of the steam generator simulator pressure drop follows the trends of the data quite well for the first eight seconds. However, RELAP4 underestimates the pressure difference after eight seconds, principally because it underestimates the magnitude of the flow reversal that occurs in the intact loop hot leg.

3.3 Pressurizer Performance and Influence on Intact Loop Hot Leg and Core Fluid Response

An analysis of the intact loop pressurizer response has been performed to determine the influence of the pressurizer flow behavior on the intact loop hot leg fluid response and the possible subsequent effect that the hot leg fluid had on core flow behavior. Results of the analysis indicate that during the first eight seconds following rupture the intact loop pump was most influential in controlling the hot leg fluid, whereas the pressurizer response had only minor effect on the hot leg fluid behavior. As a result, the pressurizer response does not have significant effect on core flow during this period. After about 12 seconds, however, a high velocity steam flow from the pressurizer had considerable influence on the

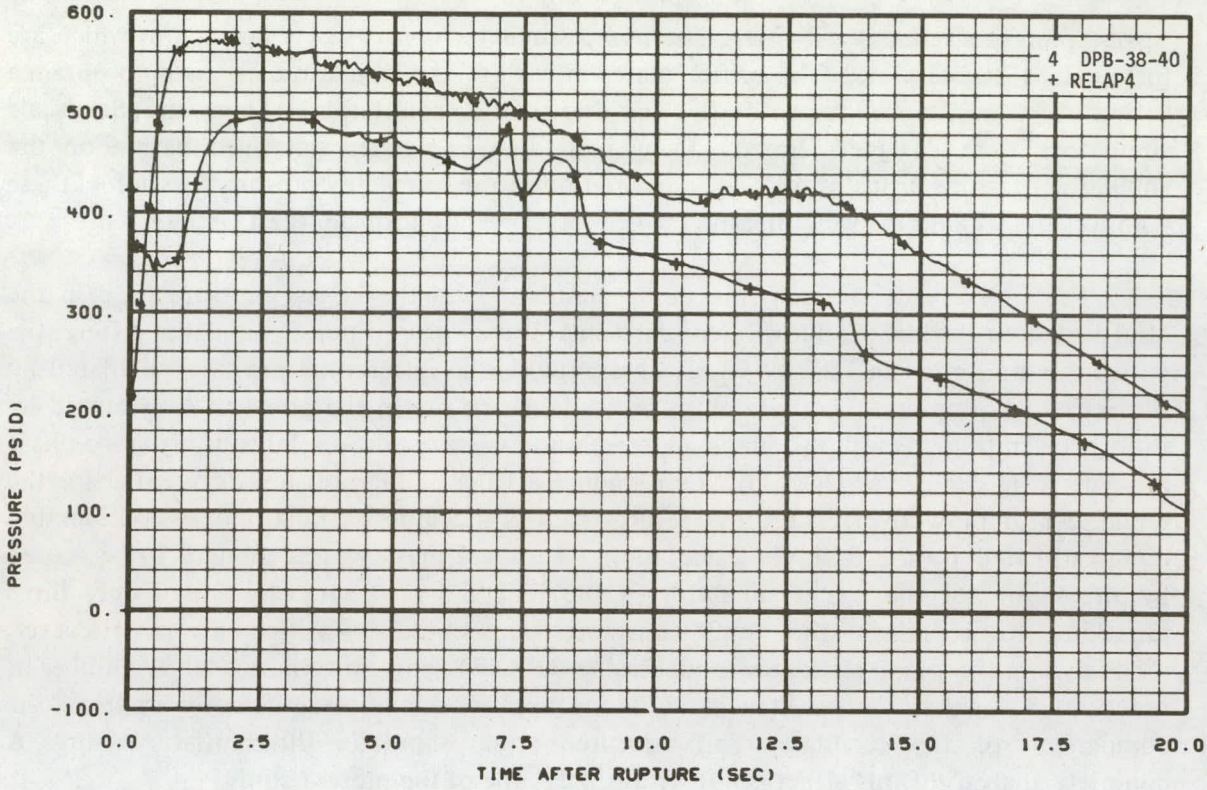

Fig. 49 Differential pressure across the broken loop pump simulator – comparison of RELAP4 calculation with Test S-02-4 data.

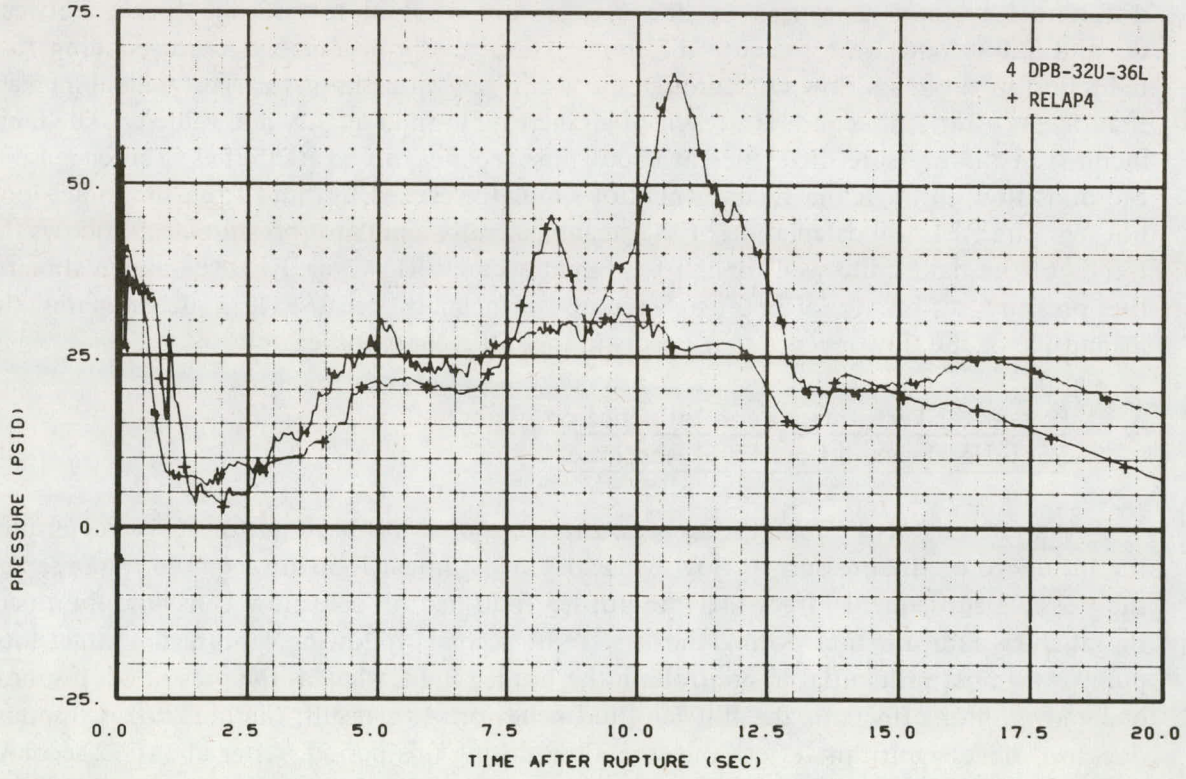

Fig. 50 Differential pressure across the broken loop steam generator simulator – comparison of RELAP4 results with Test S-02-4 data.

intact loop hot leg fluid and apparently influenced the rewetting of the upper portions of several of the core heater rods at that time.

The pressurizer mass flow response for Test S-02-5, shown in Figure 51, illustrates a typical pressurizer blowdown. Figure 52 shows the pressurizer configuration and instrumentation locations. Subcooled water in the pressurizer outlet neck and surge line resulted in the initial high mass flow rate. The decrease in flow between one and two seconds corresponds to the saturated (two-phase) pressurizer fluid reaching the high flow resistance surge line. The two-phase flow continued until about 12 seconds, at which time the fluid cleared the surge line, and a transition to a high velocity steam flow occurred. The sharp decline in mass flow at 11.5 seconds occurs because of the relative locations of the pressurizer density and volumetric flow devices and is not an actual flow condition. The mass flow rate is obtained from both the density and volumetric flow measurements. Since the steam-fluid interface reaches the densitometer location before it reaches the turbine flowmeter location, the calculated mass flow indicates the sharp drop shown in the figure.

The effect of transition from water to steam flow (from the pressurizer) on the hot leg fluid response is illustrated by the comparison shown in Figure 53 of the fluid densities at the vessel outlet and at the steam generator inlet. The transition to steam flow from the pressurizer, at about 12 seconds, is seen to result in a backup of fluid near the steam generator inlet, while fluid between the pressurizer and vessel is essentially swept out. The fluid swept from the hot leg into the vessel upper plenum apparently was responsible for the rewet of the upper portion of several of the core heater rods. Figure 54 shows cladding temperatures in the upper portion of the core for several rods for Test S-02-5. The sudden decrease in temperatures that occur after 11 seconds results from the rewet of the rod surface by fluid from the intact loop hot leg. Penetration of the hot leg fluid into the core region, however, is probably limited to the upper portion of the core. No noticeable change in core inlet flow, due to the pressurizer influence, is apparent during this period of time.

An analysis of the intact loop pressurizer response has been performed for Test S-02-4 using the RELAP4 computer program. The pressurizer model used in the RELAP4 program consisted of a single control volume containing the pressurizer fluid. The pressurizer surge line was represented by a single flow junction, which connected the pressurizer volume to an intact loop hot leg volume. The hydraulic resistance applied to the pressurizer-hot leg junction in the RELAP4 program was calculated on the basis of actual flow measurements.

To determine whether the pressurizer flow response had significant effect on the intact loop hot leg flow behavior, two RELAP4 calculations were performed using different surge line hydraulic resistances. The surge line resistance values used in the calculations were 4,500 and 11,000 $sec^2/ft^3\text{-}in^2$ respectively. The value of 4,500 $sec^2/ft^3\text{-}in^2$ is a measured value derived from the relation $R' = \rho\Delta P/\dot{M}^2$, where ρ is the fluid density, ΔP is the differential pressure across the pressurizer surge line, and $\dot{M}$ is the surge line mass flow rate. Use of the value 11,000 $sec^2/ft^3\text{-}in^2$ resulted in a calculated pressurizer mass flow response which more closely simulated the actual flow response for Test S-02-4. Figures 55 and 56 compare the calculated pressurizer pressure response using the resistance values of 4,500 and 11,000 $sec^2/ft^3\text{-}in^2$, respectively, with Test S-02-4 data. Transition to steam flow from the

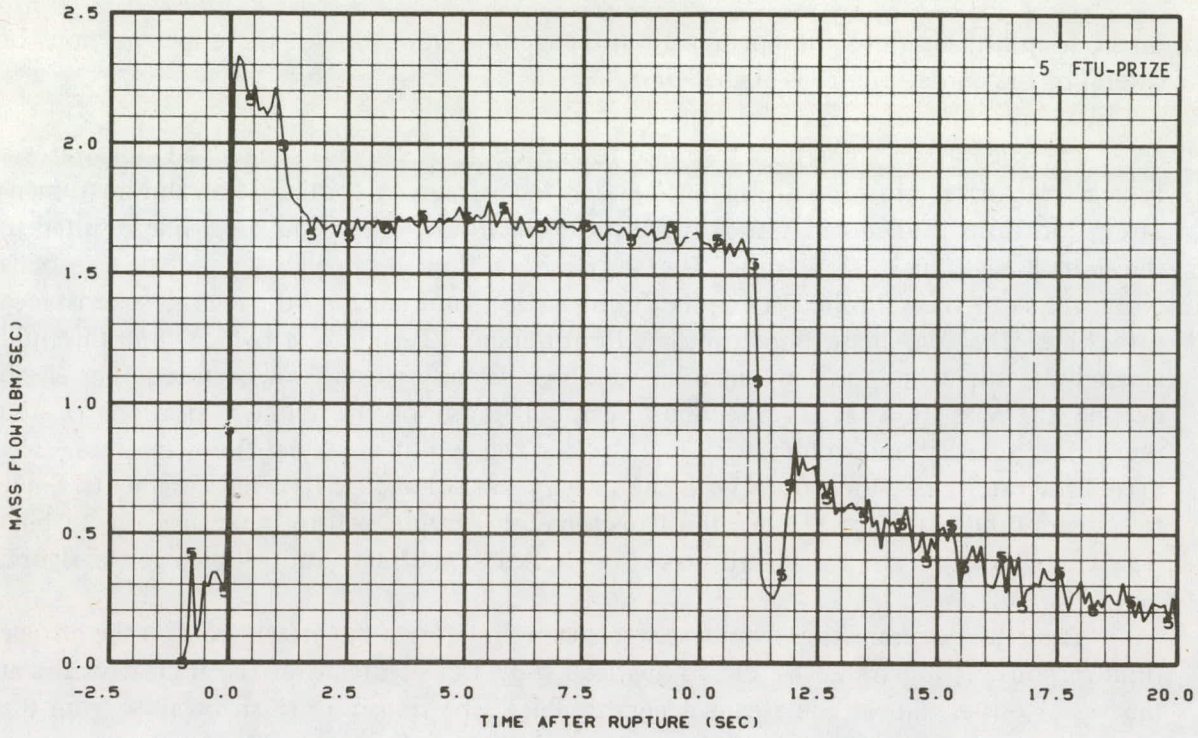

Fig. 51 Mass flow rate in the intact loop pressurizer surge line – Test S-02-5.

pressurizer (as signaled by the abrupt change in slope of the pressure response curves) occurred at about 7.5 seconds and 11.2 seconds for the calculations and at about 11 seconds for the test data. Figures 57 and 58 show the mass flow rates at Stations 1 and 5 for both calculations. Included in the figures for comparison are the measured mass flow rates at the same locations from Test S-02-4. The figures show that small differences in the intact loop hot leg flow responses do occur depending on the pressurizer behavior. However, the magnitude of the differences in flow rates that do occur indicates that the pressurizer response does not significantly affect the flow behavior in other regions of the system.

3.4 Steam Generator Performance

An analysis of the thermal response of the intact loop steam generator has been performed to evaluate the heat transfer occurring in the steam generator during the blowdown transient. Control of the steam generator secondary feedwater flow and inlet temperature for each test established the required primary loop fluid temperature conditions prior to rupture. At about one second after rupture, the steam generator secondary feedwater and discharge valves were closed.

Steam generator instrumentation for the test series provided data for both qualitative and quantitative analyses of steam generator performance during blowdown. Instrumentation within the steam generator included a pressure transducer and four thermocouples to provide an indication of primary-to-secondary and secondary-to-primary heat transfer. The steam generator configuration and secondary-side instrumentation

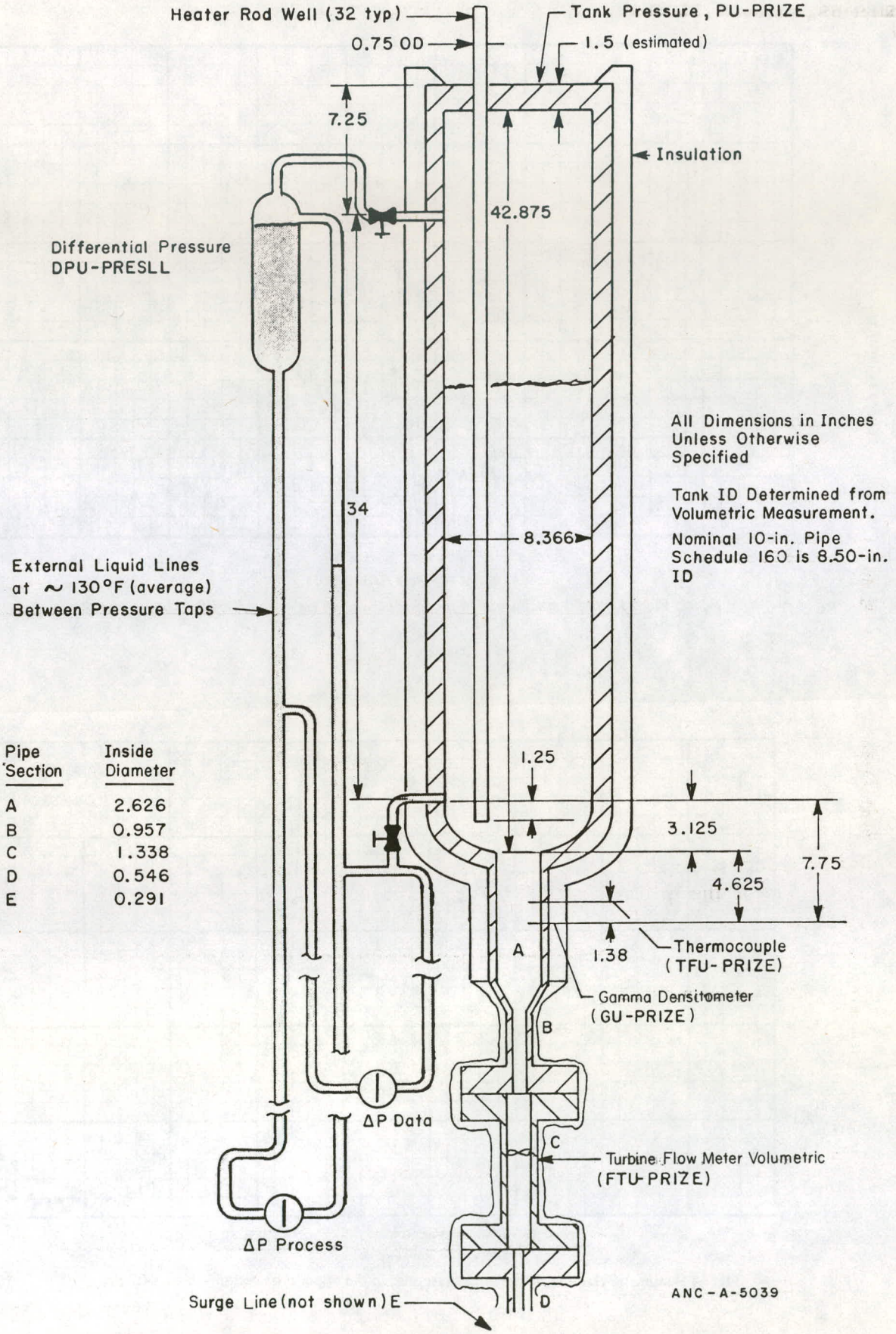

Fig. 52 Intact loop pressurizer schematic.

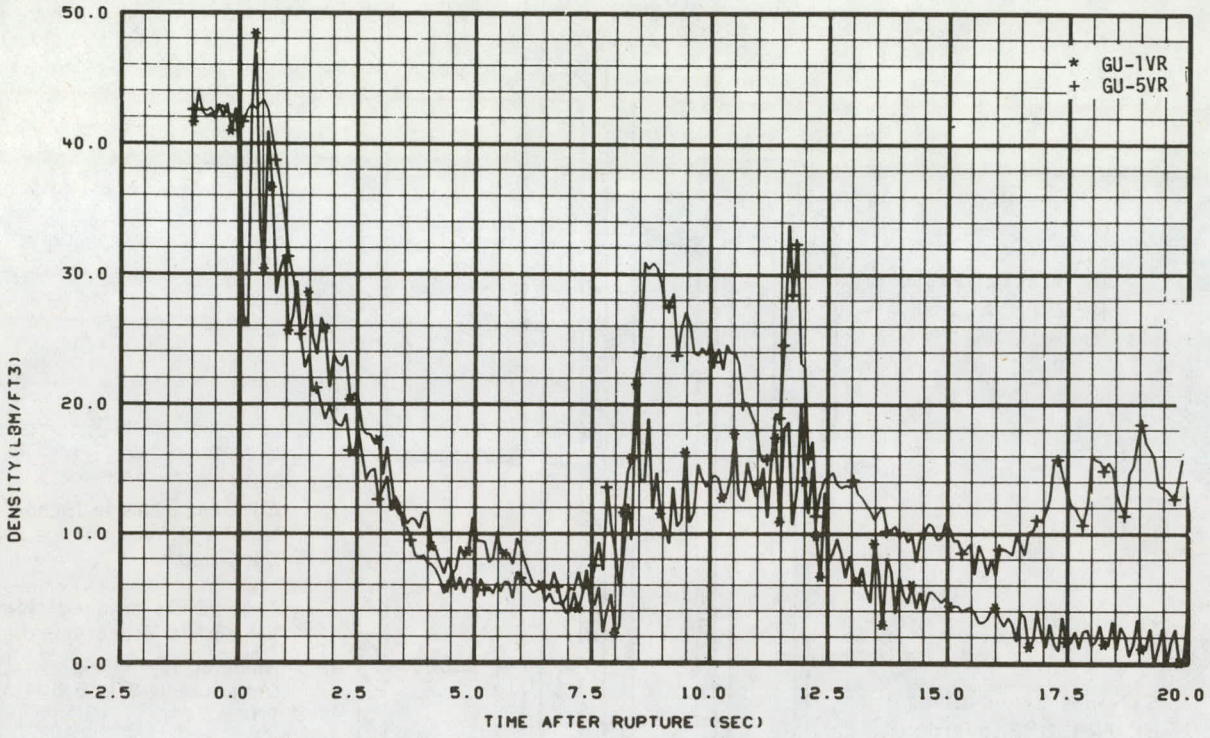

Fig. 53 Fluid densities within the intact loop hot leg – Test S-02-5.

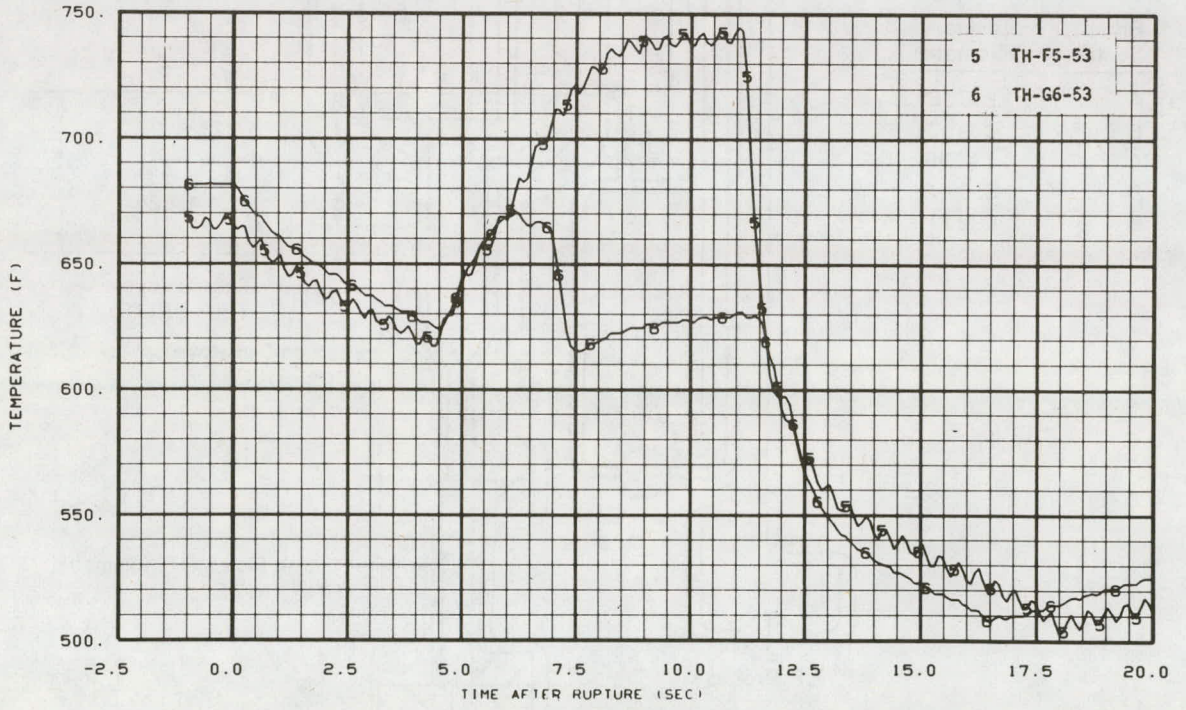

Fig. 54 Heater rod cladding temperature response in the upper core region – Test S-02-5.

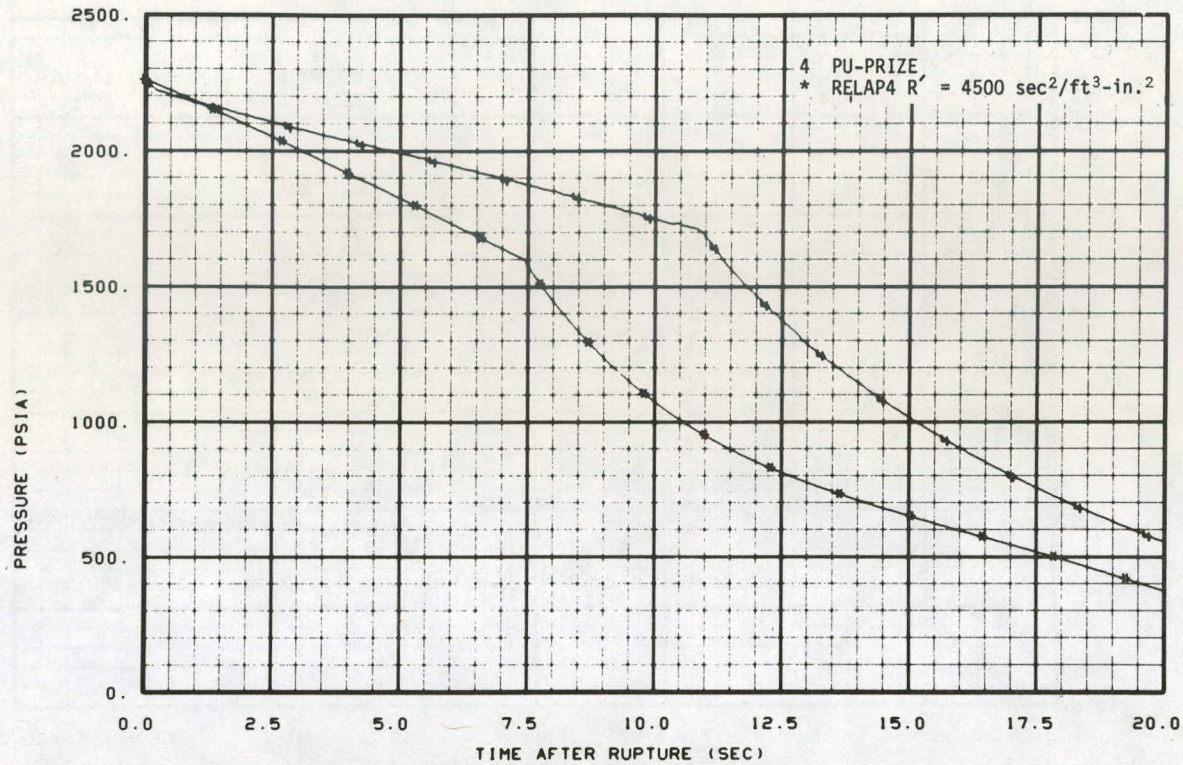

Fig. 55 Pressure response of the intact loop pressurizer – comparison of RELAP4 calculation using pressurizer surge line resistance value of 4,500 sec^2/ft^3-$in.^2$ with Test S-02-4 data.

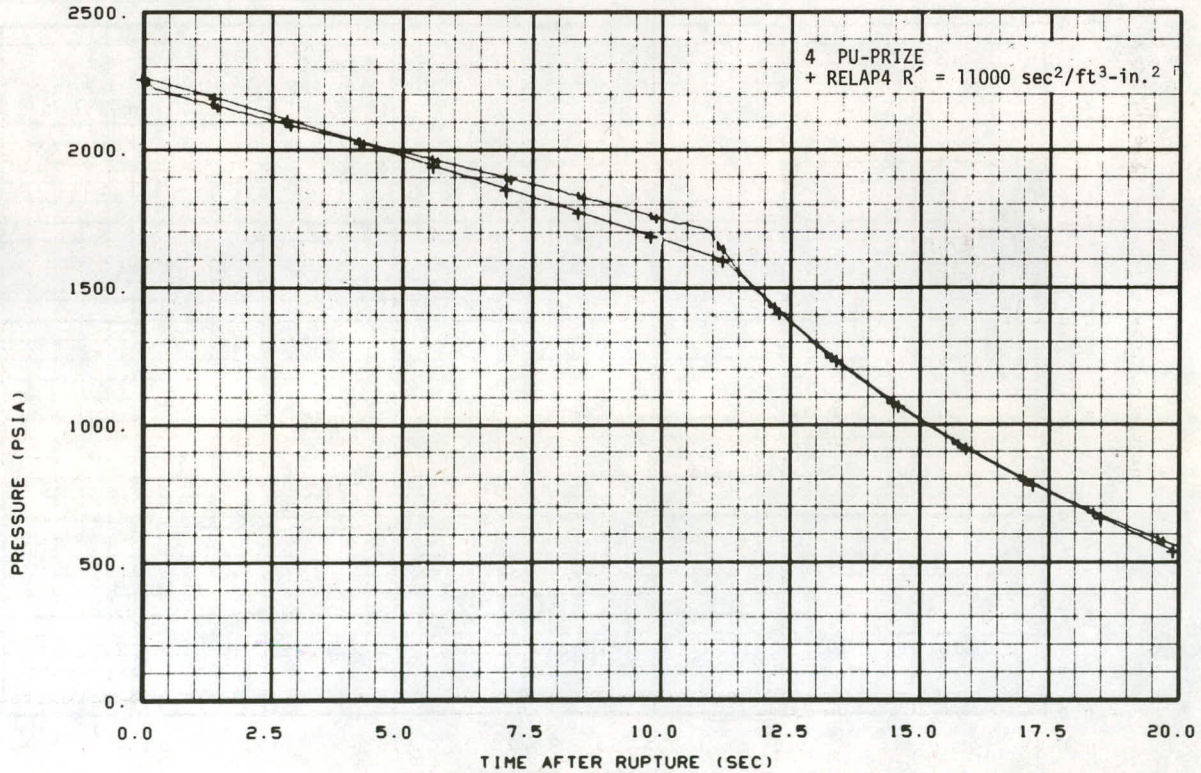

Fig. 56 Pressure response of the intact loop pressurizer – comparison of RELAP4 calculation using pressurizer surge line resistance of 11,000 sec^2/ft^3-$in.^2$ with Test S-02-4 data.

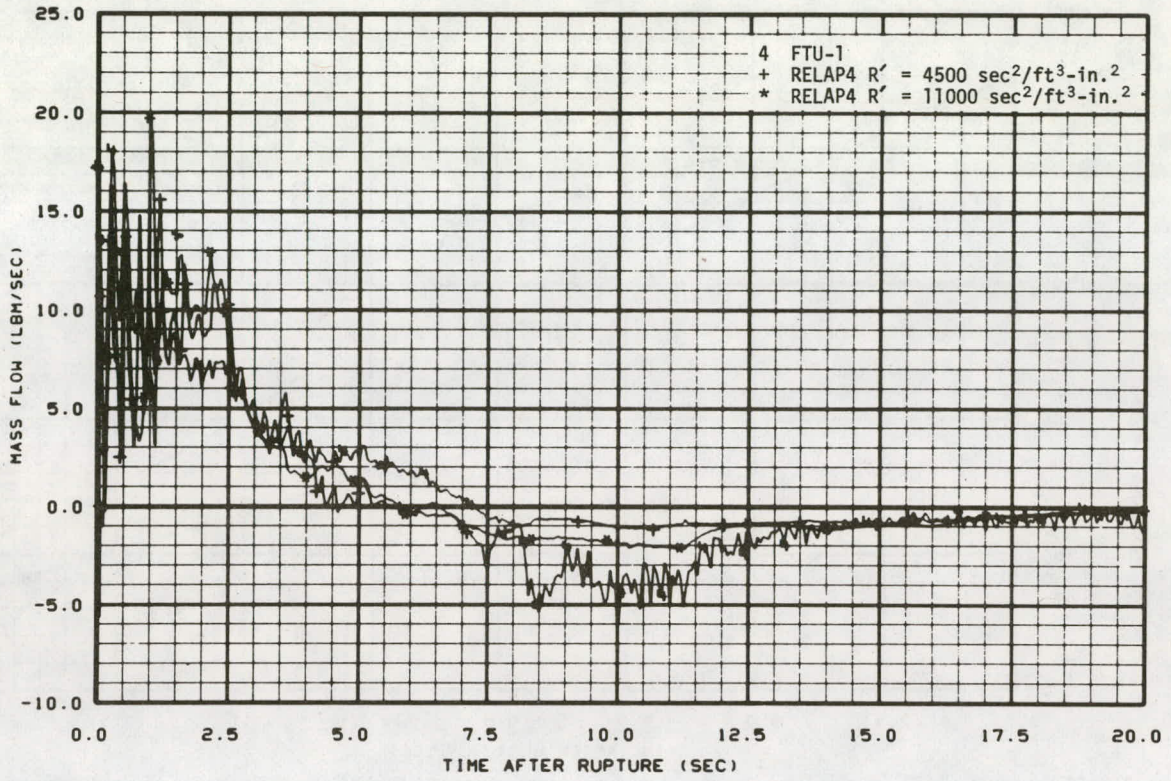

Fig. 57 Mass flow rate near the vessel outlet side of the intact loop – comparison of RELAP4 calculations using pressurizer surge line resistance values of 4,500 and 11,000 $sec^2/ft^3\text{-}in.^2$ with Test S-02-4 data.

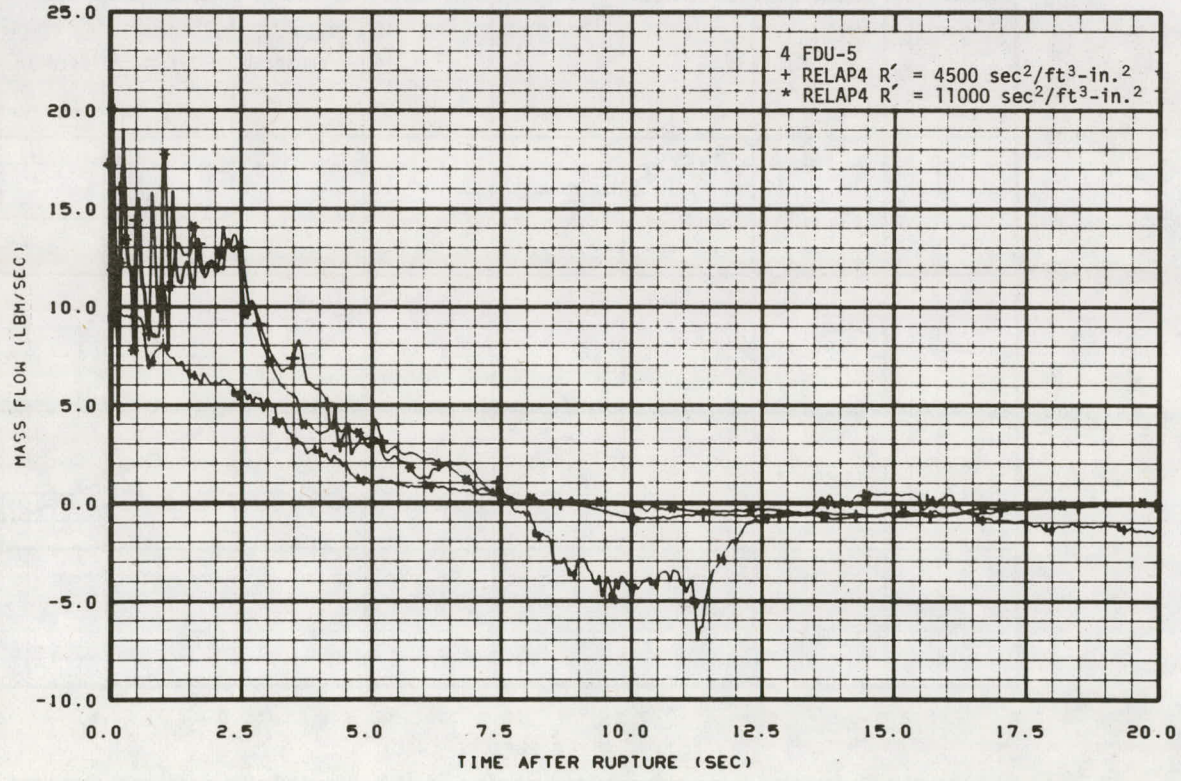

Fig. 58 Mass flow rate downstream of the pressurizer in the intact loop hot leg – comparison of RELAP4 calculations using pressurizer surge line resistance valves of 4,500 and 11,000 $sec^2/ft^3\text{-}in.^2$ with Test S-02-4 data.

locations are shown in Figure 59. Instrumentation located external to the steam generator but near the primary side inlet and outlet provided measurements of fluid density, flow rate, pressure, and temperature at these locations.

The pressure history measured by the transducer located in the steam dome provides a means of analyzing the steam generator thermal response during blowdown. Since the behavior of the steam generator during Test S-02-4 was representative of its behavior for the overall blowdown heat transfer test series, the analysis presented here is limited to that test. The measured secondary pressure (PU-SGSD) obtained during Test S-02-4 is shown in Figure 60. The increase in pressure that occured after the steam generator feedwater and discharge valves were closed is due to the increase in secondary fluid temperature caused by heat transfer from the primary fluid. At about nine seconds after rupture, the primary fluid temperature fell below the secondary fluid temperature and reversal in heat transfer direction occured. As a result, the secondary fluid temperature began to decrease, leading to steam condensation and a corresponding reduction in the secondary pressure.

Analysis of the steam generator thermal response was performed for Test S-02-4 using the RELAP4 computer program. The steam generator model used in the RELAP4 program consisted of four control volumes on the primary side, each with a single two-dimensional heat slab, and one control volume on the secondary side containing the secondary fluid, as shown in Figure 61. Both primary and secondary fluid-to-tube heat transfer coefficients were based on fluid conditions.

To determine the significance of the steam generator heat transfer rate on the overall system blowdown response, RELAP4 calculations were performed using different values of the minimum steam generator secondary-to-primary heat transfer coefficient. The secondary-to-primary heat transfer coefficients used in the calculations were 5 and 250 Btu/hr-ft^2-^{o}F. The heat transfer coefficient of 5 Btu/hr-ft^2-^{o}F is a standard value used in the RELAP4 calculation during the latter portion of blowdown whenever heat transfer from a stagnant fluid volume to an adjacent heat slab was predicted to occur. For this heat transfer condition, the coefficient of 5 Btu/hr-ft^2-^{o}F is the minimum value supplied by the RELAP4 program. Use of a turbulent natural convection heat transfer correlation[15] indicated that a minimum heat transfer coefficient of 250 Btu/hr-ft^2-^{o}F would be more appropriate.

The steam generator secondary pressures resulting from the above calculations are shown in Figure 62 and are compared with results from Test S-02-4. The figure shows that the magnitude of the secondary-to-primary heat transfer has considerable effect on the secondary side pressure response. The sensitivity of the intact loop hot and cold leg pressure responses to the steam generator heat transfer, however, was found to be small. Figures 63 and 64 show the calculated primary side pressures near the inlet and outlet of the steam generator. Results from Test S-02-4 are included in the figures. As shown in these figures, an increase in the minimum secondary fluid-to-tube heat transfer coefficient from 5 Btu/hr-ft^2-^{o}F to 250 Btu/hr-ft^2-^{o}F has very little effect on the resulting primary side pressures. Thus, the conclusion reached is that the steam generator heat transfer has very little effect on the overall system blowdown response.

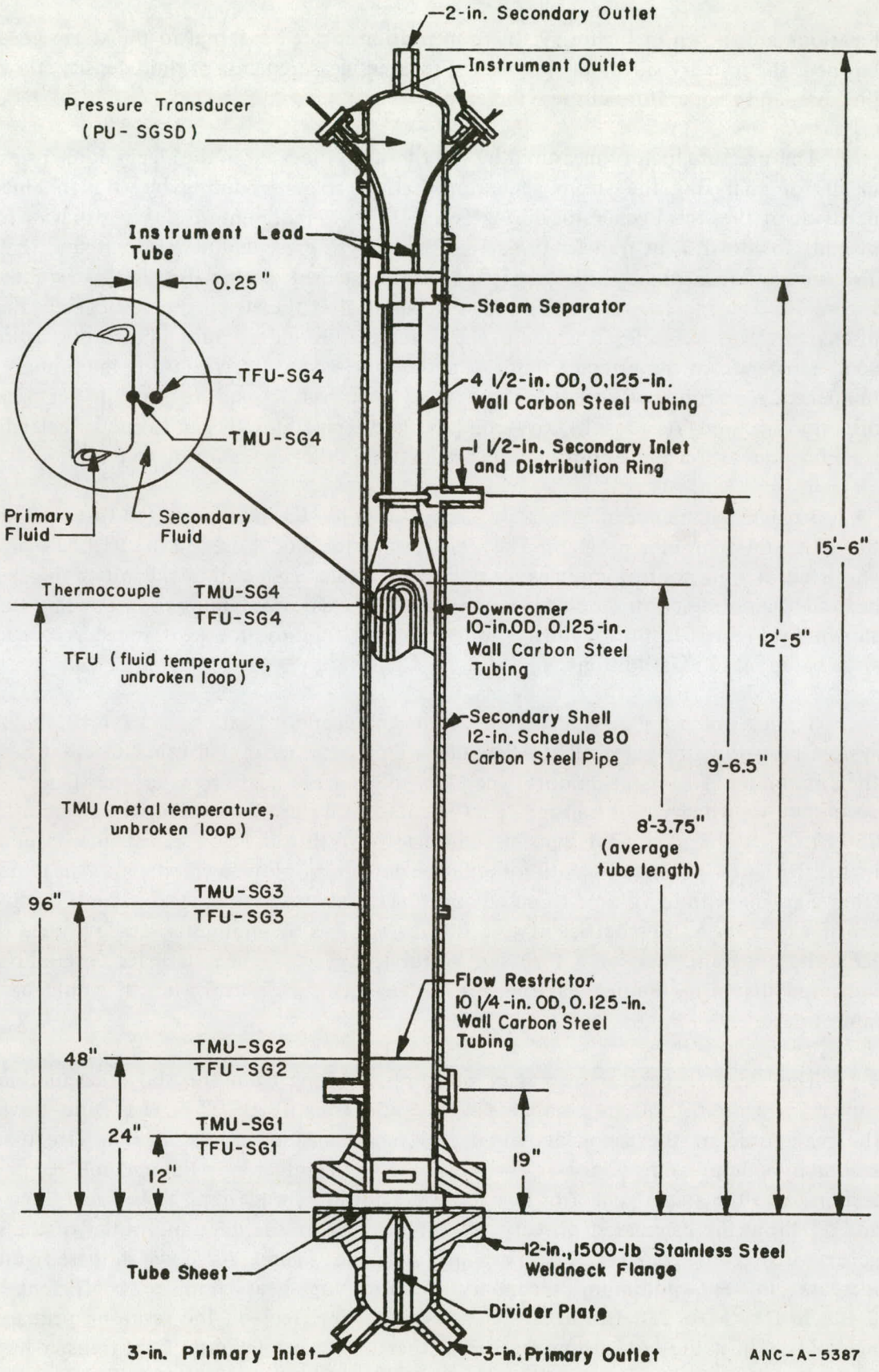

Fig. 59 Intact loop steam generator configuration.

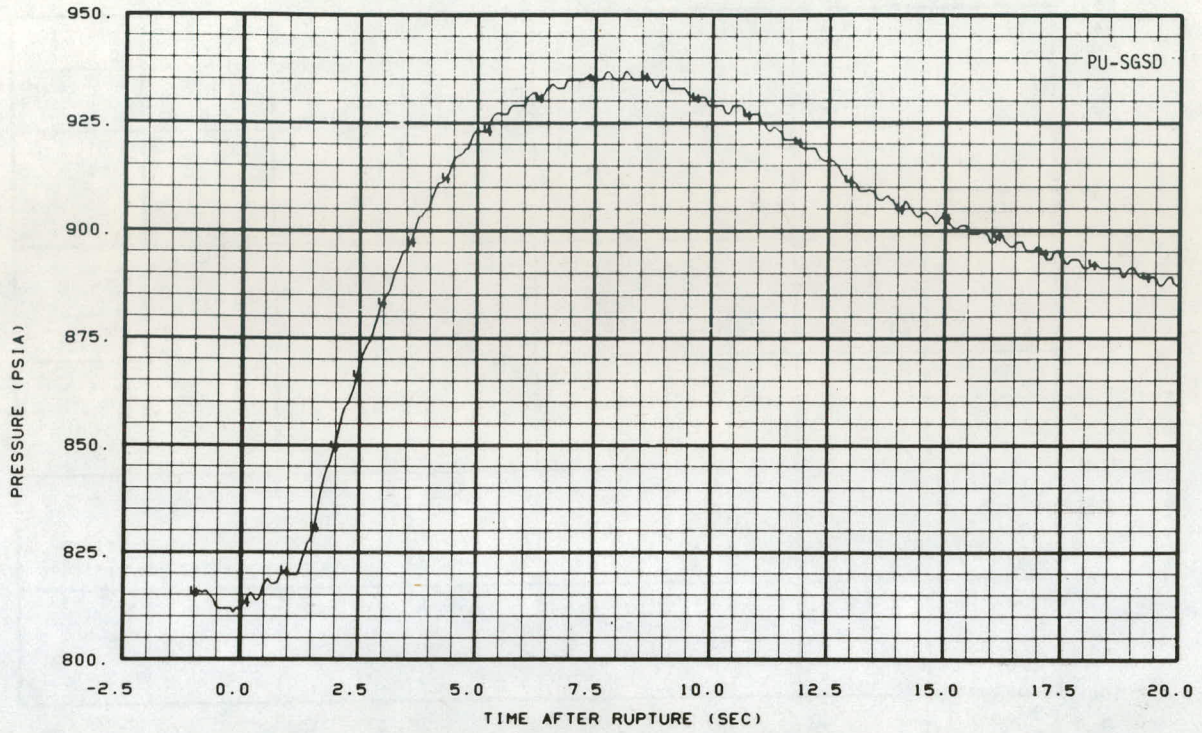

Fig. 60 Pressure response in the intact loop steam generator secondary side – Test S-02-4.

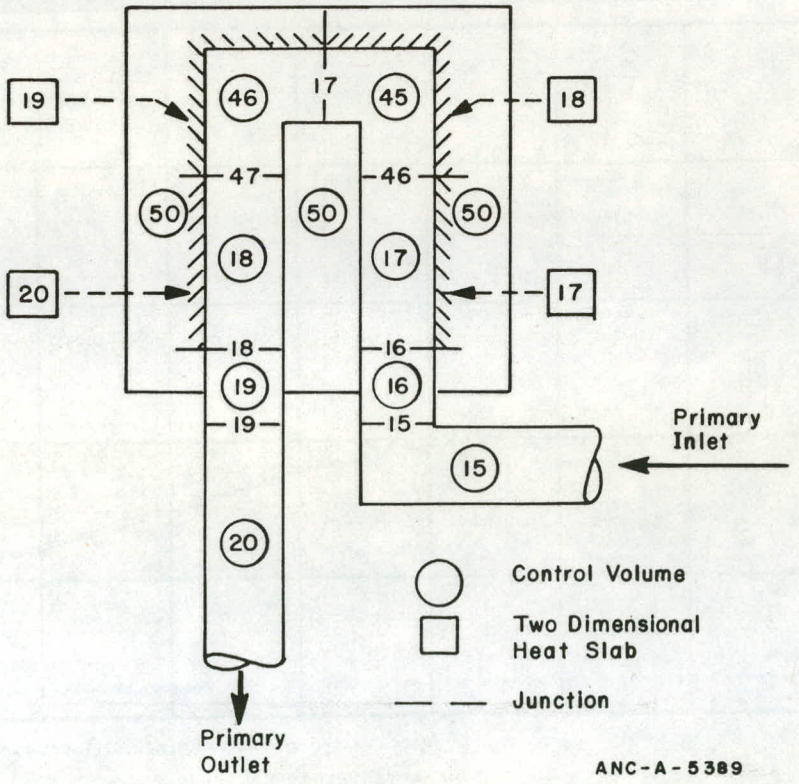

Fig. 61 RELAP4 intact loop steam generator model.

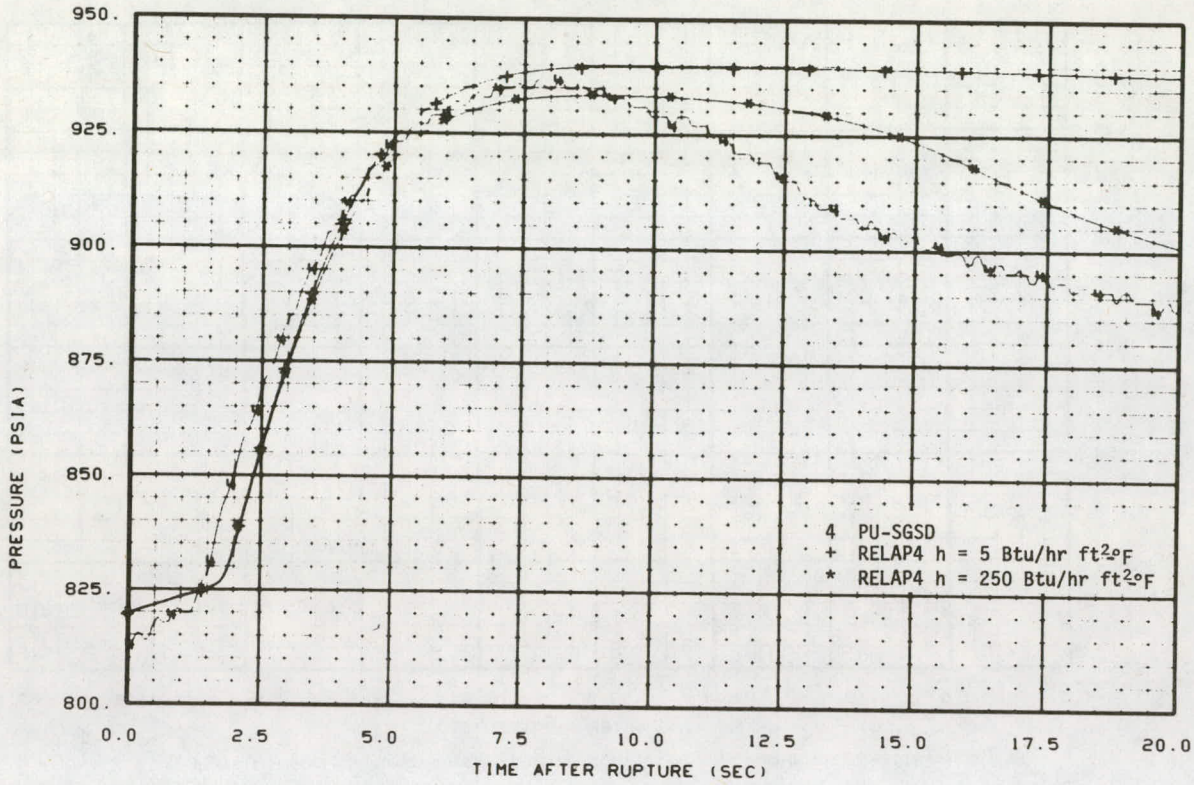

Fig. 62 Pressure response in the intact loop steam generator secondary side – comparison of RELAP4 calculations using secondary-to-primary heat transfer coefficients of 5 and 250 Btu/hr-ft^{2}-^{o}F with Test S-02-4 data.

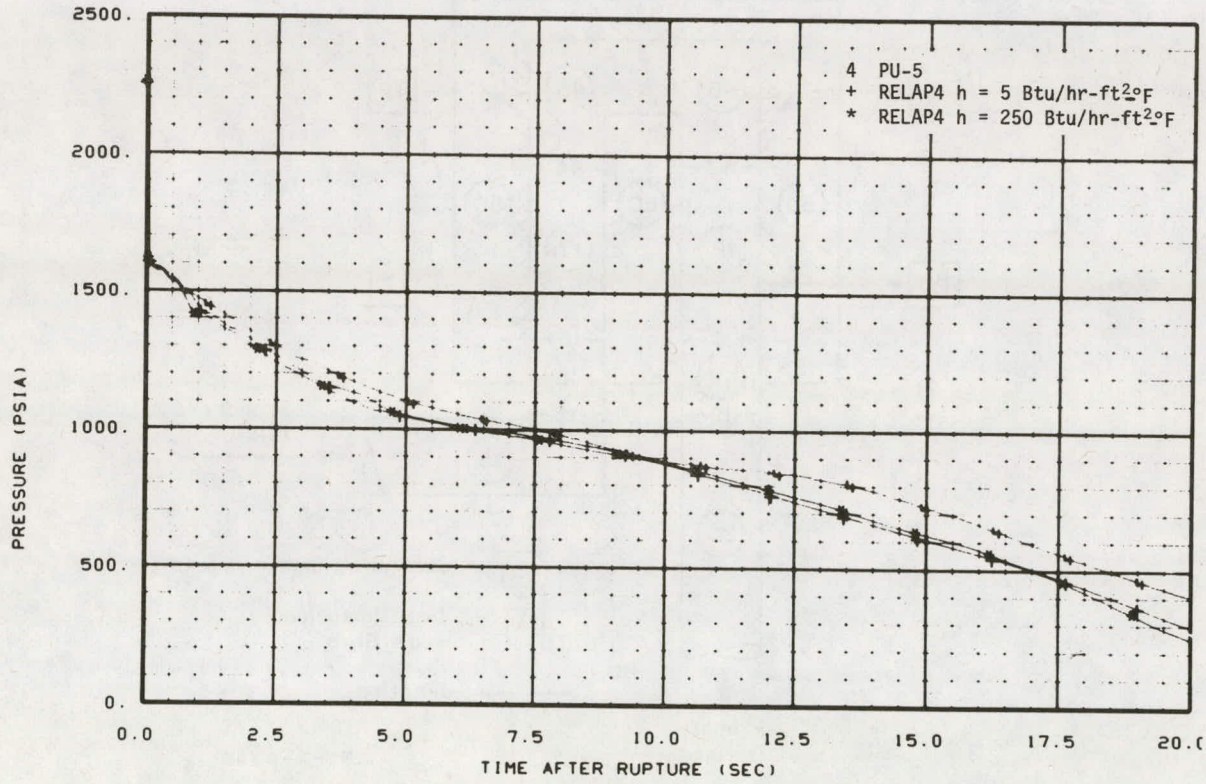

Fig. 63 Pressure response near the inlet to the steam generator in the intact loop – comparison of RELAP4 calculations using secondary-to-primary heat transfer coefficients of 5 and 250 Btu/hr-ft^{2}-^{o}F with Test S-02-4 data.

Calculations were performed to evaluate the amount and direction of the heat transfer occurring in the steam generator during blowdown for Test S-02-4. The calculation consisted of a simple energy balance using the steam generator tube bundle metal and secondary side fluid as a control volume. The change in energy state of the steam generator external structure and external heat losses were neglected. An estimate of the secondary fluid volume capable of acting as a heat sink, or source, was assumed sufficiently large that the heat transfer was regarded as a maximum probable value. Both the heat transfer to the tube bundle metal and secondary fluid during the early portion of the blowdown and the heat transfer from the tube bundle metal and secondary fluid during the latter portion of blowdown were determined.

The results of the steam generator heat transfer calculation for Test S-02-4 indicate that an energy transfer to the tube bundle and secondary fluid of approximately 2,695 Btu occurred between one and nine seconds after rupture, and an energy transfer from the tube bundle and secondary fluid to the primary fluid of approximately 1,435 Btu occurred between 10 and 40 seconds after rupture. Compared to the energy stored in the primary fluid prior to rupture, the energy transfer occurring in the steam generator during blowdown is small (less than 1%). As a result, the steam generator heat transfer is thought to have had little effect on the overall system blowdown performance. This conclusion is consistent with results obtained from Test S-01-4 and Test S-01-5 of the Semiscale Mod-1 isothermal test series[16].

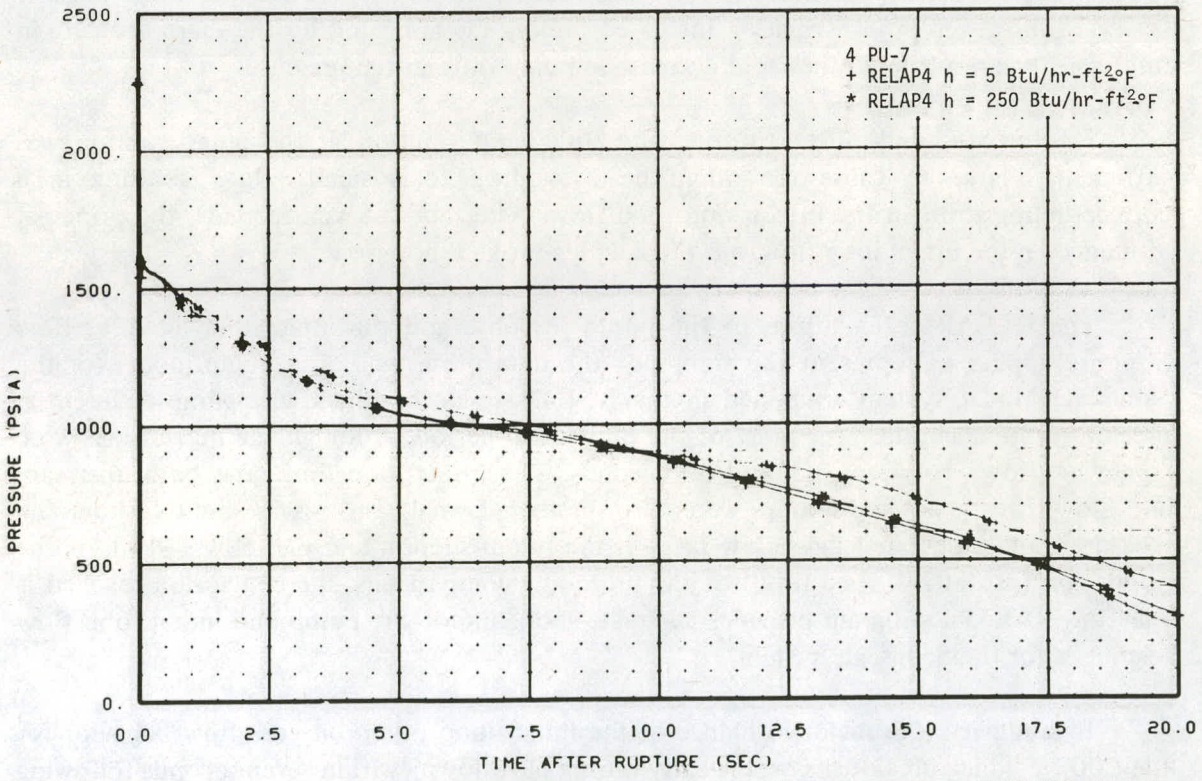

Fig. 64 Pressure response near the outlet to the steam generator in the intact loop – comparison of RELAP4 calculations using secondary-to-primary heat transfer coefficients of 5 and 250 Btu/hr-ft^2-°F with Test S-02-4 data.

3.5 Intact Loop Pump and Cold Leg Response

During the 200% offset shear cold leg break tests, the head generated by the intact loop pump affected loop flow and to a lesser extent the core flow early in blowdown. The capability of the pump to force fluid around the intact loop, and the corresponding influence of the intact loop flow on core fluid response, declined as blowdown progressed, principally due to the degradation of the pump head which resulted from the increasing void fraction at the pump suction. The major effect of the intact loop pump response on core flow behavior during a 200% cold leg break test was the tendency to limit the magnitude of the core flow reversal during the early portion of blowdown. Thus, an understanding of the pump performance and the ability to predict the pump and intact loop flow response are necessary to adequately predict the core flow behavior.

A study of the pump differential pressure curve can be used to illustrate the pump response during a blowdown. Figure 65 shows the pump differential pressure for Test S-02-4 and includes the RELAP4 calculated value. The reduction in the pump differential pressure from rupture to about six seconds after rupture is caused by a decrease in pump speed during this period. After six seconds, however, the sharp drop in pump differential pressure can be attributed to void formation at the pump suction. Figure 66 shows the fluid density at the pump suction for Test S-02-4 and includes the RELAP4 calculated density at the same location for comparison. The fluid at the pump suction remained subcooled until about 5.5 seconds as indicated by the measured fluid density. Once the fluid became saturated, however, void formation increased rapidly (as indicated by the sharp decrease in fluid density), resulting in the rapid decrease in pump differential pressure.

By seven seconds after rupture, the fluid void fraction at the pump suction was sufficiently large to cause the pump head to drop to a small value, resulting in a corresponding drop in the intact loop fluid flow. After about seven seconds, the principal influence on the intact loop flow was the cold leg broken loop flow.

The RELAP4 calculations of the pump response and the intact loop cold leg flow response appear to represent the trends of the data quite well. The pump model for the Semiscale Mod-1 system contained in the RELAP4 code predicted the pump differential pressure quite accurately for most of the blowdown period, although the magnitudes were somewhat low, between 3.5 and 6.5 seconds. The intact loop flow rates both upstream and downstream of the pump were also predicted well. Figures 67 and 68 show the measured and calculated mass flow rates at the pump suction and just downstream of the pump for Test S-02-4. As a result of the preceding comparisons, the conclusion reached is that the RELAP4 program provides adequate modeling of the pump and intact loop flow responses for the Semiscale system.

In summary, the major influence of the intact loop pump on core flow behavior for the 200% cold leg break tests occurs early during blowdown (within seven seconds following rupture) and results in limiting the magnitude of the core flow reversal. The RELAP4 code calculates both the intact loop pump and cold leg response well for the Semiscale system.

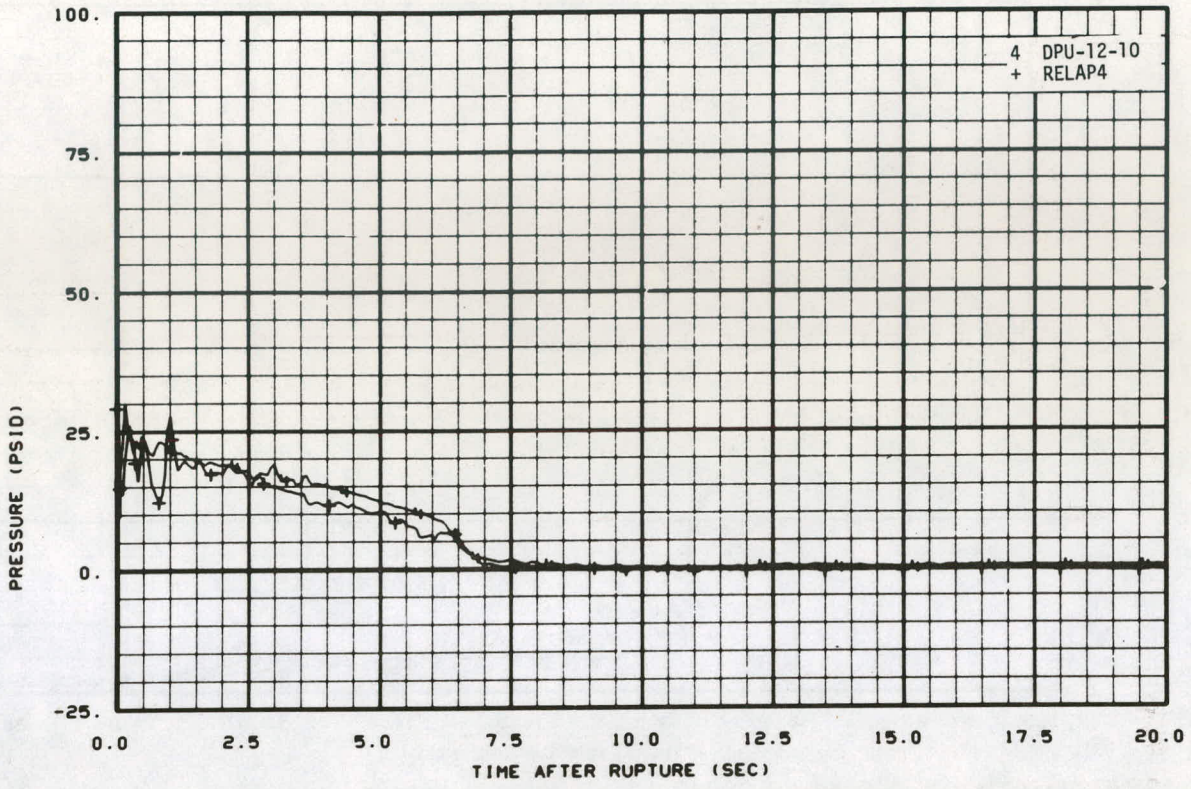

Fig. 65 Differential pressure across the intact loop pump – comparison of RELAP4 calculation with Test S-02-4 data.

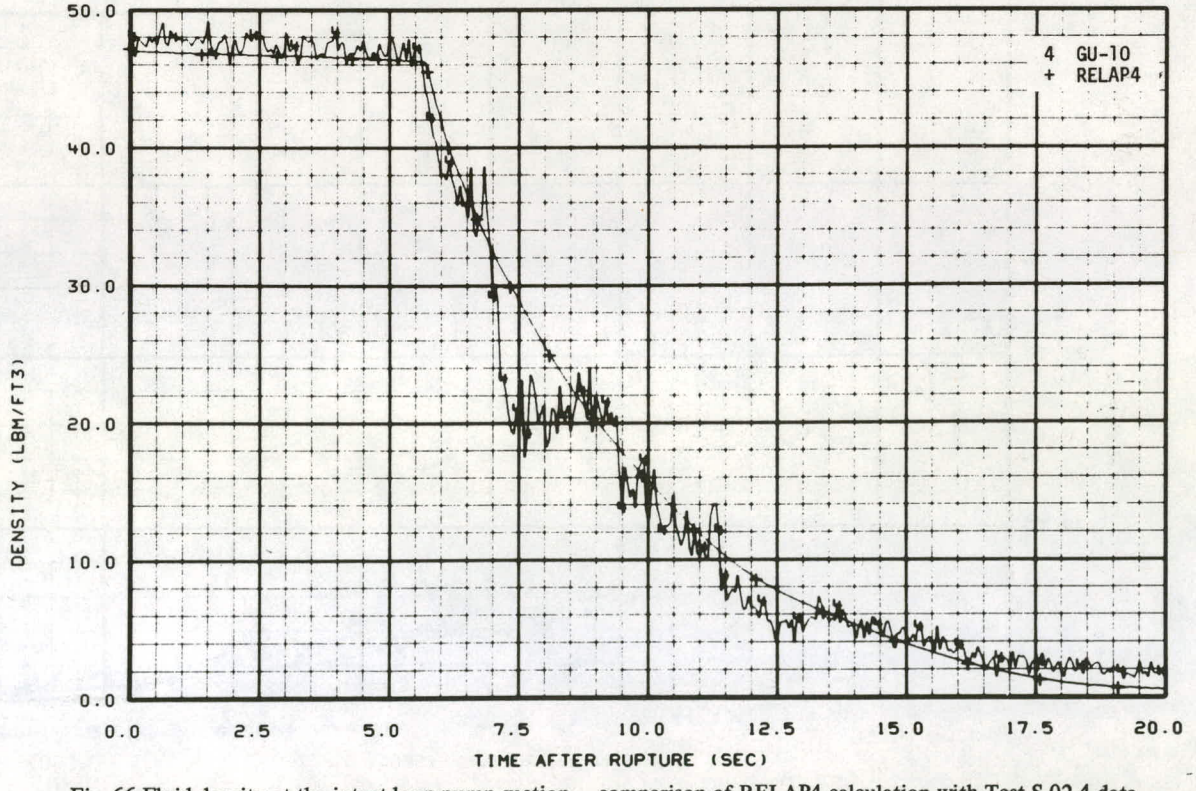

Fig. 66 Fluid density at the intact loop pump suction – comparison of RELAP4 calculation with Test S-02-4 data.

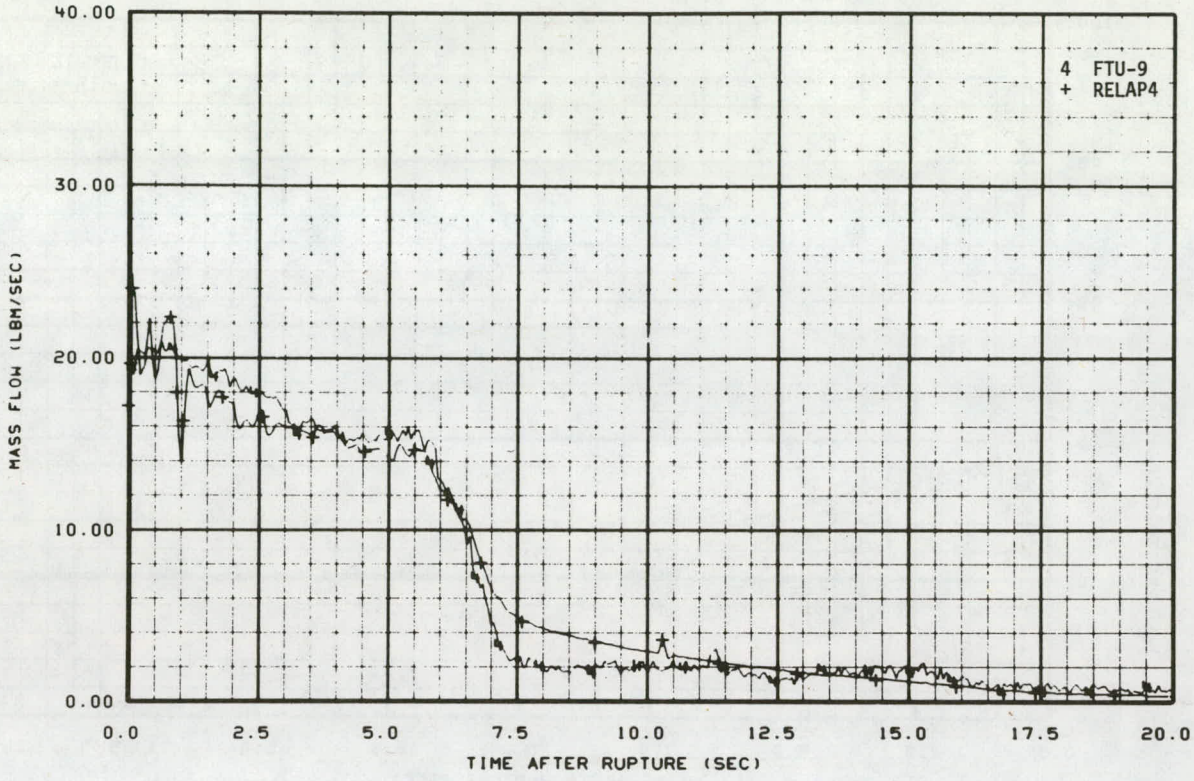

Fig. 67 Mass flow rate at the intact loop pump suction – comparison of RELAP4 calculation with Test S-02-4 data.

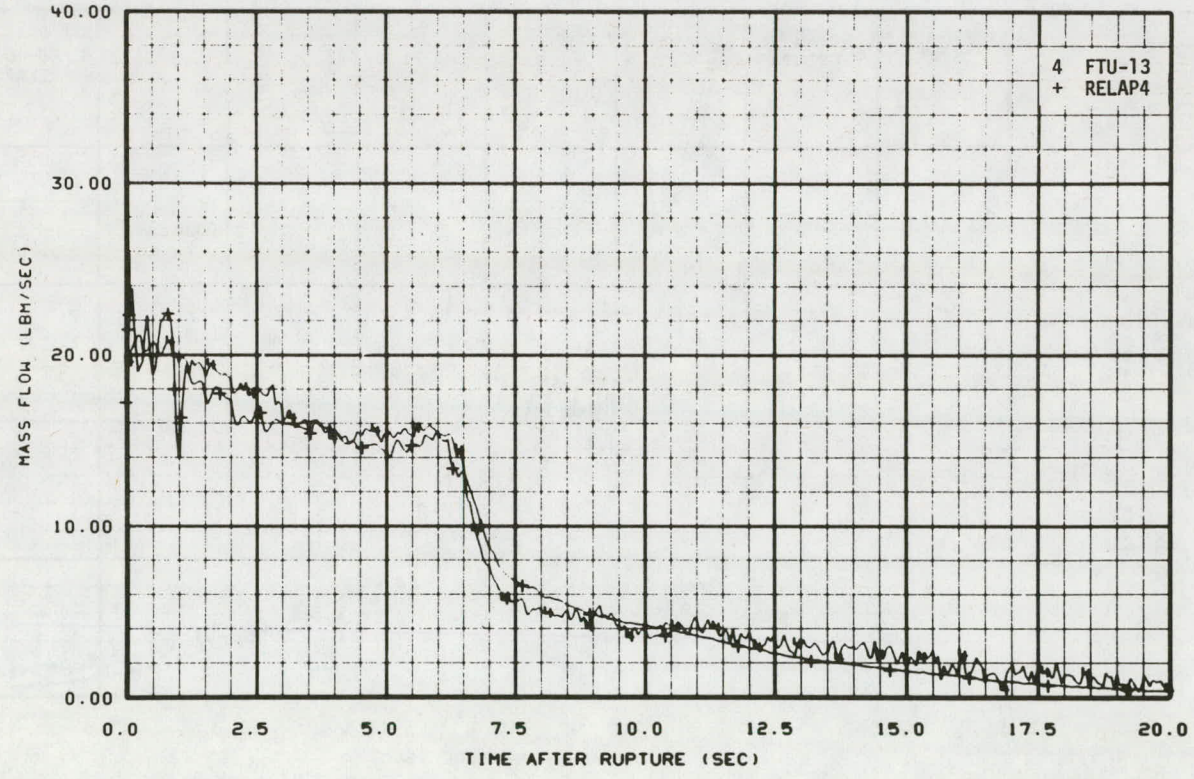

Fig. 68 Mass flow in intact loop cold leg downstream of the intact loop pump – comparison of RELAP4 calculation with Test S-02-4 data.

IV. CONCLUSIONS

The thermal hydraulic response of the Semiscale Mod-1 system during tests of the blowdown heat transfer test series has been investigated. The results from the blowdown heat transfer tests have led to an increased understanding of the heat transfer and flow processes that occur in the Semiscale Mod-1 system during the blowdown portion of a simulated LOCA. Results from these tests have been valuable also for evaluating the adequacy and improving the predictive capability of analytical models developed to predict system response during a LOCA.

Analysis of the data from the Semiscale Mod-1 blowdown heat transfer test series has resulted in the following conclusions.

1. CORE FLUID BEHAVIOR

During blowdown resulting from a 200% offset shear cold leg break, the core fluid response is principally a function of the break flow distribution. The large subcooled flow in the vessel inlet side of the broken loop causes core flow to become negative within 100 msec following rupture. The core flow remained negative until about six seconds after rupture, at which time it approached zero.

2. INFLUENCE OF INITIAL CONDITIONS AND BREAK LOCATION ON CORE FLOW BEHAVIOR

The 200% offset shear cold leg break configuration is much more serious with respect to core thermal response than is the 200% offset shear hot leg break configuration. The 200% cold leg break results in an immediate reversal of core flow and a high rate of generation of steam within the core region, resulting in poor core heat transfer conditions. For the 200% hot leg break, however, a high density positive core flow existed throughout the blowdown period.

The core temperature differential prior to rupture for a 200% offset shear cold leg break test has a significant effect on the overall system hydraulic response and, in particular, on the vessel side break flow during subcooled blowdown. The core flow, being highly sensitive to the vessel side break flow, is thus strongly affected by the initial core temperature differential.

Within the range tested, the initial core power has little effect on the resulting system fluid thermal-hydraulic response. The higher rod energy is stored within the core region during blowdown.

3. RESPONSE OF SYSTEM COMPONENTS

The intact loop pressurizer response was found to have only a minor effect on the hot leg flow response during the time in which two-phase flow existed in the pressurizer surge line. Once the two-phase liquid cleared the pressurizer surge line, a high velocity steam flow from the pressurizer essentially swept hot leg fluid into the vessel upper plenum, resulting in the rewet of the upper portions of several heater rods.

Intact loop secondary-to-primary heat transfer was found to be small during the blowdown period and thus did not have a significant effect on overall system response.

The effect of the intact loop pump on core flow behavior was to limit the magnitude of the core flow reversal early in blowdown. The pump head became degraded by approximately 6.5 seconds after rupture for the 200% cold leg break test and approximately five seconds after rupture for the 200% hot leg break test.

V. REFERENCES

1. H. S. Crapo, M. F. Jensen, and K. E. Sackett, *Experimental Data Report for Semiscale Mod-1 Test S-02-1 (Blowdown Heat Transfer Test),* ANCR-1231 (July 1975).

2. H. S. Crapo, M. F. Jensen, and K. E. Sackett, *Experiment Data Report for Semiscale Mod-1 Test S-02-2 (Blowdown Heat Transfer Test),* ANCR-1232 (August 1975).

3. H. S. Crapo, M. F. Jensen, and K. E. Sackett, *Experiment Data Report for Semiscale Mod-1 Test S-02-3 (Blowdown Heat Transfer Test),* ANCR-1233 (September 1975).

4. H. S. Crapo, M. F. Jensen, and K. E. Sackett, *Experiment Data Report for Semiscale Mod-1 Test S-02-4 (Blowdown Heat Transfer Test),* ANCR-1234 (November 1975).

5. H. S. Crapo, M. F. Jensen, and K. E. Sackett, *Experiment Data Report for Semiscale Mod-1 Test S-02-5 (Blowdown Heat Transfer Test),* ANCR-1235 (December 1975).

6. H. S. Crapo, M. F. Jensen, and K. E. Sackett, *Experiment Data Report for Semiscale Mod-1 Test S-02-7 (Blowdown Heat Transfer Test),* ANCR-1237 (November 1975).

7. H. S. Crapo, M. F. Jensen, and K. E. Sackett, *Experiment Data Report for Semiscale Mod-1 Tests S-02-9 and S-02-9A (Blowdown Heat Transfer Tests),* ANCR-1236 (January 1976).

8. K. V. Moore and W. H. Rettig, *RELAP4 – A Computer Program for Transient Thermal-Hydraulic Analysis,* ANCR-1127 Rev. 1 (December 1973).

9. T. K. Larson, *Core Thermal Response During Semiscale Mod-1 Blowdown Heat Transfer Tests,* ANCR-NUREG-1285 (June 1976).

10. E. M. Feldman and D. J. Olson, *Semiscale Mod-1 Program and System Description for the Blowdown Heat Transfer Tests (Test Series 2),* ANCR-1230 (August 1975).

11. C. E. Cartmill, *Thermal-Hydraulic Response of the Semiscale Mod-1 System Isothermal Test Series,* ANCR-1228 (October 1975).

12. H. S. Crapo, M. F. Jensen, and K. E. Sackett, *Experimental Data Report for Semiscale Mod-1 Test S-01-6 (Isothermal Blowdown with 40-Rod Heater Core),* ANCR-1253 (September 1975).

13. R. E. Henry and H. K. Fauske, "The Two-Phase Critical Flow of One-Component Mixtures in Nozzles, Orifices, and Short Tubes," *Journal of Heat Transfer,* Trans. ASME (May 1971).

14. F. J. Moody, "Maximum Flow Rate of a Single Component, Two-Phase Mixture," *Journal of Heat Transfer,* Trans. ASME (February 1965).

15. W. H. McAdams, *Heat Transmission*, New York: McGraw-Hill Book Company, Inc. (1954).

16. R. T. French, *An Evaluation of Piping Heat Transfer, Piping Flow Regimes, and Steam Generator Heat Transfer for the Semiscale Mod-1 Isothermal Tests*, ANCR-1230 (August 1975).

APPENDIX A

RELAP4 COMPUTER CODE AS APPLIED TO SEMISCALE MOD-1 THERMAL-HYDRAULIC ANALYSIS

THIS PAGE

WAS INTENTIONALLY

LEFT BLANK

APPENDIX A

RELAP4 COMPUTER CODE AS APPLIED TO SEMISCALE MOD-1 THERMAL-HYDRAULIC ANALYSIS

The RELAP4 computer program[A-1] was developed primarily to describe the transient behavior of water-cooled nuclear reactors subjected to postulated accidents such as those resulting from loss of coolant, pump failure, or nuclear power variations. Since features of the program that describe the nuclear reactor are optional, the program can be applied to experimental water-reactor simulators such as the Semiscale Mod-1 system.

The Semiscale Mod-1 system is modeled in RELAP4 as a set of fluid control volumes connected by flow junctions. Numerical methods calculate the fluid conditions within the control volumes during an assumed depressurization, such as would occur from a double-ended offset shear of a primary coolant pipe.

The geometric and thermodynamic features of the system to be analyzed are input to the program. Geometric features necessary to describe the volumes are fluid volume, elevation, flow area, hydraulic flow resistance, and surface areas and volumes of hardware which exchange energy with the fluid. Power generation in the components, thermal properties of the components, and initial conditions of the fluid are input thermodynamic features. Other required inputs include junctions connecting the fluid volumes, pump models, bubble rise models, and choices of heat transfer correlations and flow-choking models. Given the mechanical and thermodynamic features and initial conditions of the system, RELAP4 then solves an integral form of the one-dimensional momentum, energy, and mass conservation equations of each control volume.

The version of the RELAP4 computer code used for the calculations presented in this report was an amended version of RELAP4/005(26). The code was modified by means of the update procedure to incorporate several features required by the Semiscale system as well as to change the heat transfer logic. The modifications to the code consisted of:

(1) A provision to preclude the intact loop coolant pump speed from coasting down to less than 61% of initial speed

(2) A special 'trip' to shut down core power should a high power rod hot spot temperature exceed a fixed critical value

(3) Substitution of a heat transfer coefficient of 25 Btu/hr-ft^2-^{o}F in place of the Berenson[A-1] pool film boiling correlation.

In addition, a core heat slab configuration was provided in the model to represent the forty electrically heated rods.

The RELAP4 model of the Semiscale Mod-1 system used for the test predictions presented in this report consisted of 68 control volumes interconnected with 80 flow junctions. The flow junctions occurred at the approximate location of the experimental measurements to facilitate comparisons between calculations and data. In addition, the model included 50 heat conductor slabs to account for heat transfer to and from the fluid in a given volume. The RELAP4 test prediction model of the Semiscale Mod-1 system in the 200% cold leg break configuration is shown in Figure A-1. Table A-I gives a description of the control volumes corresponding to Figure A-1. A slightly modified versionof the pretest RELAP4 model containing 63 control volumes, 71 junctions, and 47 heat conductor slabs was used for the posttest calculations presented in this report. This model is shown in Figure A-2. A description of the control volumes corresponding to Figure A-2 can be obtained by referring to the corresponding volume differences between Figures A-1 and A-2.

The core heat slab configuration used for both the pretest and posttest calculation models simulated both the high- and low-powered rods of the Semiscale system. The four high-power rods were represented by ten core heat slabs and the 35 low-power rods by five core heat slabs as shown in Figure A-3. Power fractions for each heat slab were specified to represent the exact axial power profile for the high- and low-power rods. The heated core region of the models was divided into average and hot channels to allow the ten high-power slabs to be in contact with the hot channel and the five low-power slabs to be in contact with the average channel. The fluid volumes in both channels were sized in proportion to the number of hot and cold rods.

Use of the RELAP4/005(26) computer code for the pretest and posttest calculations permitted the incorporation of separate break flow coefficient multipliers for the extended Henry[A-2] (subcooled) and Moody[A-3] (saturated) models. Sensitivity studies conducted early in the blowdown heat transfer test series indicated that multipliers of 1.0 for the Henry model and 0.6 for the Moody model gave the best RELAP4 model calculations for the break flow rate.

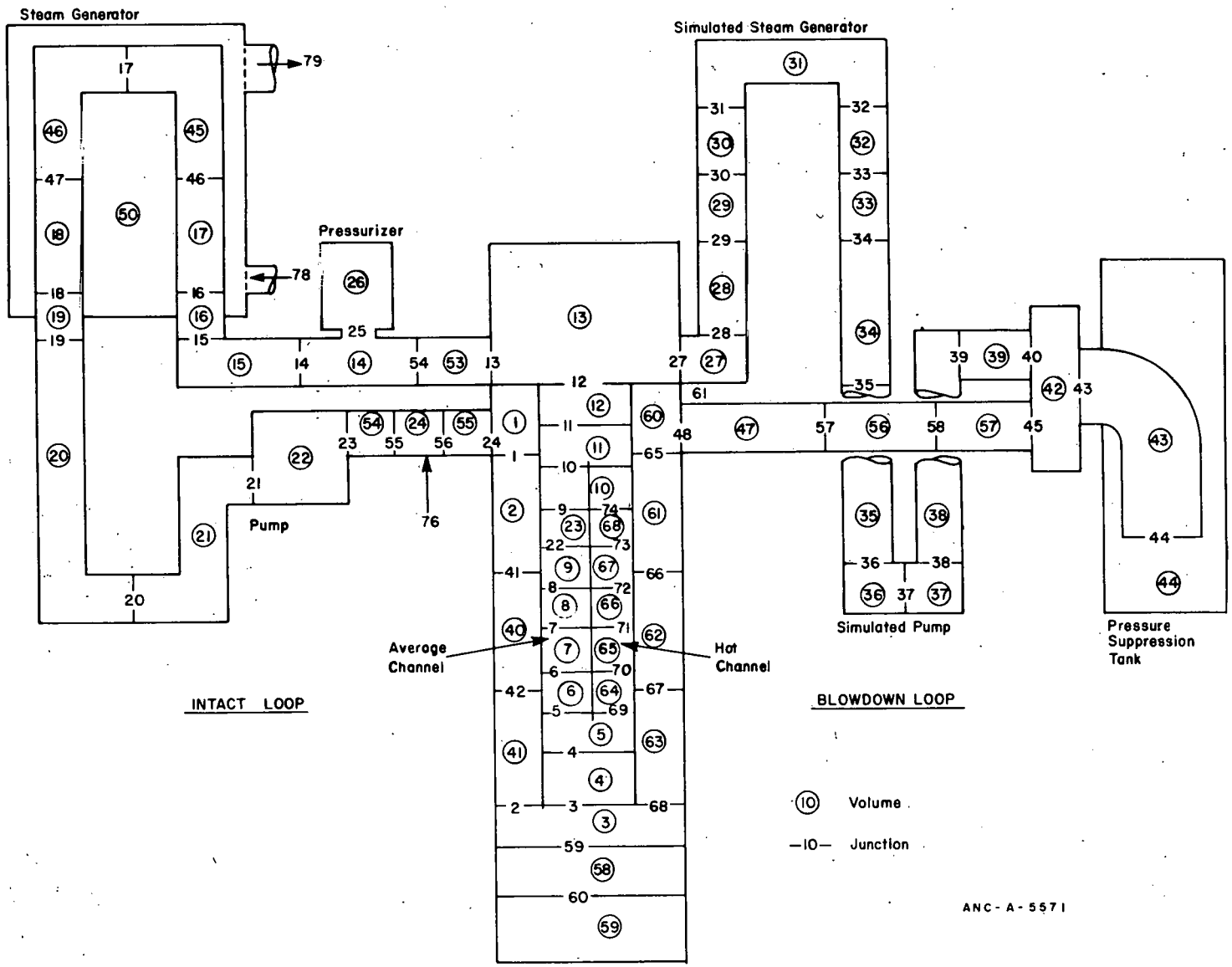

Fig. A-1 RELAP4 Semiscale Mod-1 nodalization diagram for Test S-02-4 test prediction – 200% cold leg break configuration.

TABLE A-I

RELAP4 MODEL FOR BLOWDOWN HEAT TRANSFER TEST S-02-4

Volume No.	Description
1, 60	Innlet annulus
2, 61	Top third of downcomer
40, 62	Middle third of downcomer
41, 63	Bottom third of downcomer
3, 58, 59	Lower plenum
4 5	Core mixer region and instrumentation
6, 64 7, 65 8, 66 9, 67	Heated core region
10 11 12	Inactive core region
13	Upper plenum
53	First third intact loop hot leg
14	Second third intact loop hot leg
15	Last third intact loop hot leg
16	Steam generator inlet plenum
17 45 46 18	Steam generator tubes
19	Steam generator outlet plenum
20 21	Pump suction leg
22	Intact loop pump
23, 68	Heated core region
54	First third intact loop cold leg
24	Second third intact loop cold leg
55	Last third intact loop cold leg
25	Not used
26	Pressurizer
47	First third broken loop cold leg
56	Second third broken loop cold leg

TABLE A-I (contd.)

Volume No.	Description
57	Last third broken loop cold leg
42	Pressure suppression system header
27	Broken loop hot leg
28	Simulated steam generator inlet plenum
29 30 31 32 33	Simulated steam generator
34	Simulated steam generator outlet plenum
35	Simulated pump inlet
36 37	Simulated pump
38	Simulated pump outlet
39	Simulated pump to break
43	Pressure suppression system downcomer
44	Pressure suppression tank

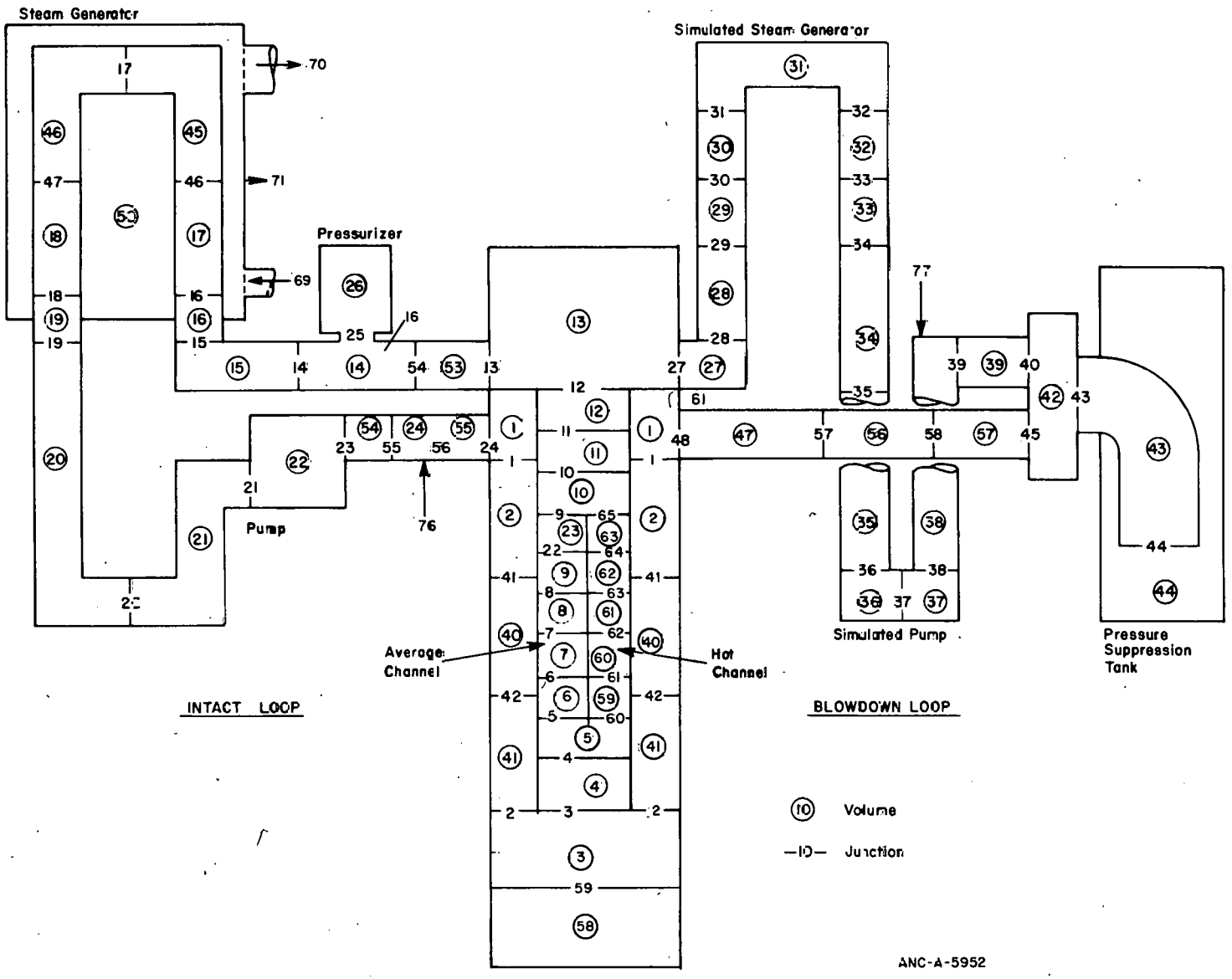

Fig. A-2 RELAP4 Semiscale Mod-1 nodalization diagram for Test S-02-4 posttest calculation – 200% cold leg break configuration.

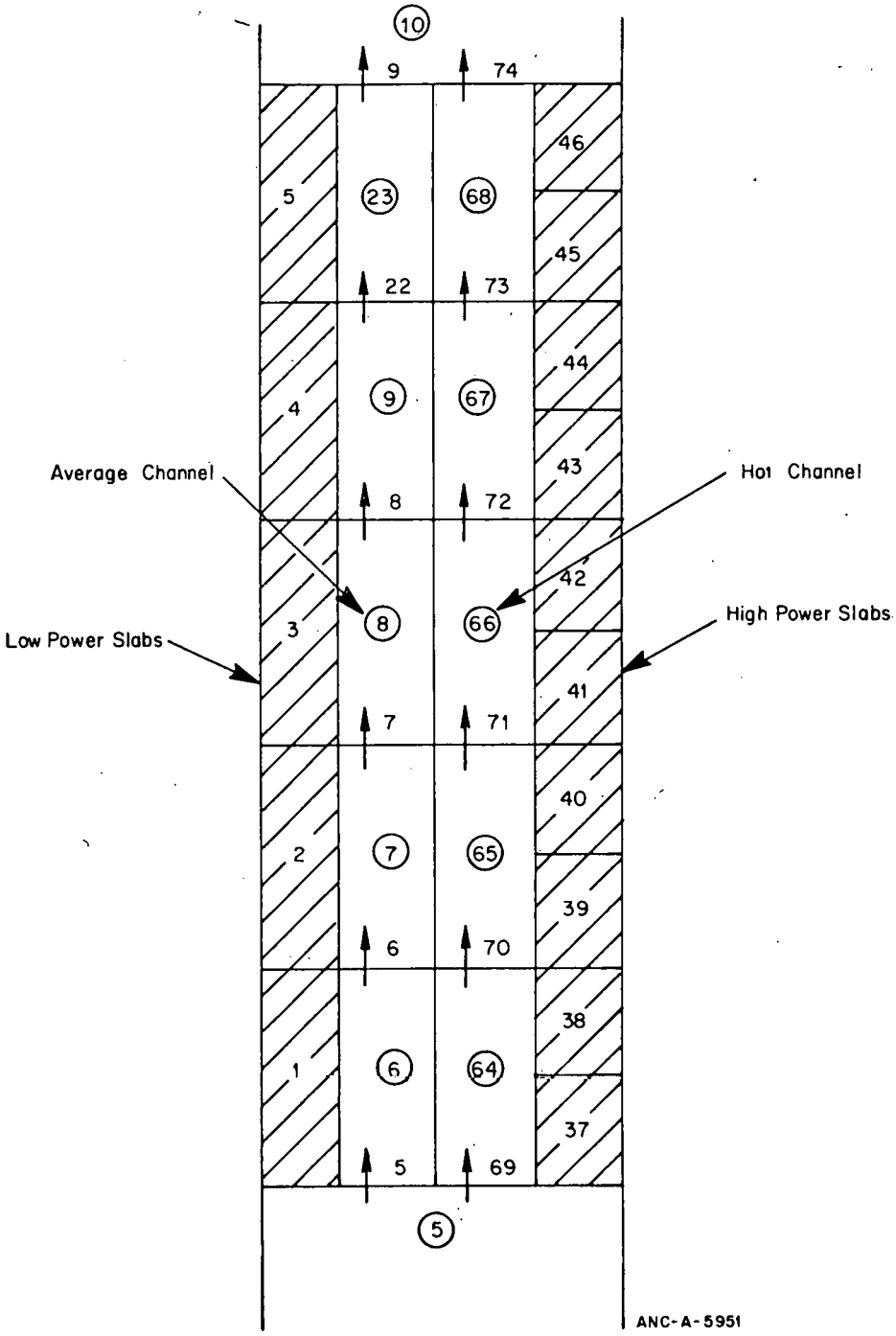

Fig. A-3 Semiscale RELAP4 model heated core configuration with hot channel.

1. REFERENCES

A-1. K. V. Moore and W. H. Rettig, *RELAP4 – A Computer Program for Transient Thermal-Hydraulic Analysis,* ANCR-1127 Rev. 1 (December 1973).

A-2. R. E. Henry and H. K. Fauske, "The Two-Phase Critical Flow of One-Component Mixtures in Nozzles, Orifices, and Short Tubes", *Transactions of the ASME Journal of Heat Transfer,* April 1969.

A-3. F. J. Moody, "Maximum Flow Rate of a Single Component, Two-Phase Mixture", *Journal of Heat Transfer-Trans. ASME,* December 1973.

APPENDIX B

DATA RELIABILITY

THIS PAGE

WAS INTENTIONALLY

LEFT BLANK

APPENDIX B

DATA RELIABILITY

Data obtained during the Semiscale Mod-1 blowdown heat transfer test series have been evaluated for reliability. Checks of the prerupture continuity of pressures, temperatures, and flow measurements around the system, as well as checks of the prerupture fluid densities, were performed for each test to determine whether any of the measurements were not in agreement with the expected values. In addition, results of the transient data were studied to determine whether any of the measurements were not consistent with the response measured by other instruments at nearby locations. In general, measurements of pressures (both gauge and differential), fluid densities, flow measurements, and metal and fluid temperatures from the Semiscale system were found to be consistent with expected results both prior to and during the blowdown transient and are considered to be highly representative of the phenomena being measured. However, at several locations in the system, disagreements between flow measurement comparisons obtained from the drag discs and turbine flowmeters did occur.

The use of two types of flow measuring devices (turbine flowmeters and drag discs) at several locations in the Semiscale system provides alternative methods for determining the fluid flow response. Figures B-1 through B-5 illustrate the mass flow rates for Test S-02-4 at several locations in the system where results from both a drag disc and a turbine flowmeter were available. The figures indicate that the drag disc and turbine flowmeter results agree quite well during the early portion of blowdown but tend to diverge considerably as the blowdown progresses. The disagreement between results during the latter portion of blowdown can be attributed to the effect of fluid flow regimes on the measuring devices. The drag disc devices basically consist of a strain-gauged cantilever beam with an enlarged target area on one end which protrudes into a flowing fluid. The area of the target, however, is small compared to the cross-sectional area of the flow channel. Thus, under flow conditions in which a nonhomogeneous or stratified-type flow exists, the drag disc is not expected to provide an accurate measurement of flow conditions. The turbine flowmeter, however, consists of a device through which all fluid in a given flow channel passes. Thus turbine flowmeter results are considered to be more representative of the flow rate of the mixture than the drag disc results when a nonhomogeneous or stratified flow exists.

Overall, results from turbine flowmeter measurements for the entire blowdown period and results from drag disc measurements during the early portion of blowdown were in agreement with expected values. Prerupture values of the flow measurements in the intact loop and vessel were consistent with the specified initial flow conditions. In addition, results of mass balances on various system volumes during the blowdown transient indicate that the turbine flowmeters (and drag discs early in blowdown) provide accurate measurements of flow conditions in the system.

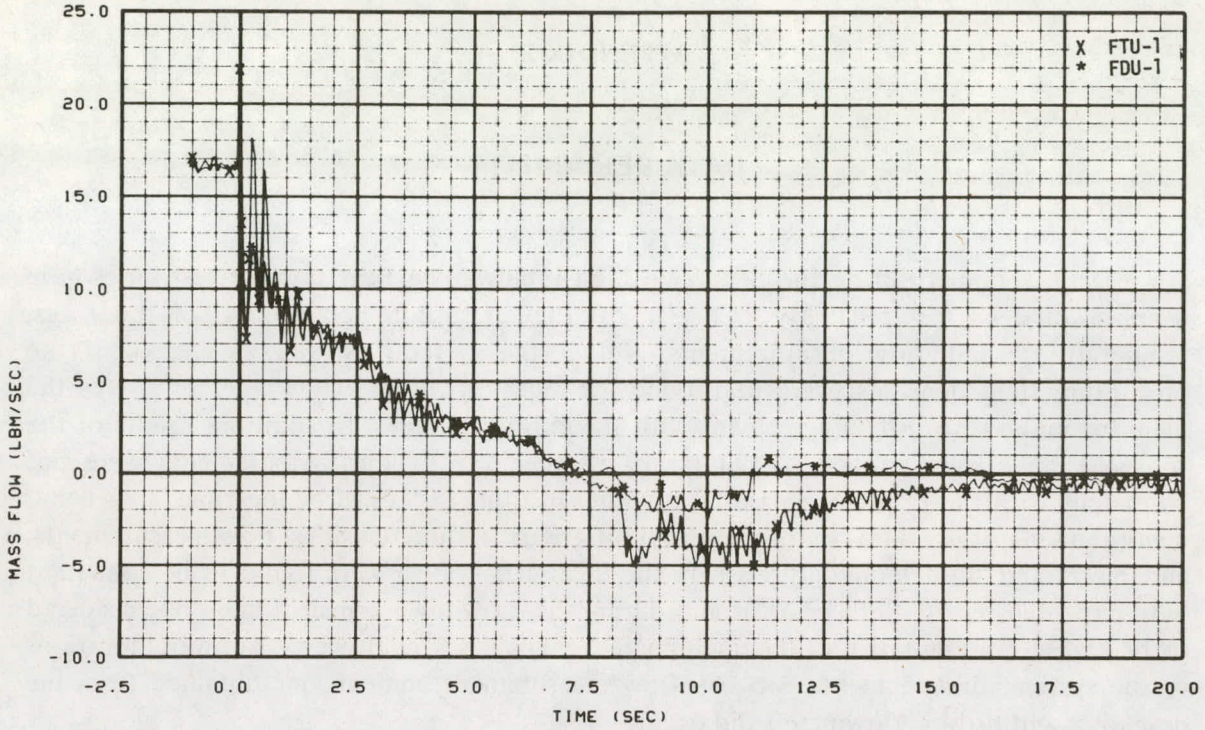

Fig. B-1 Mass flow rate near the vessel on the outlet side of the intact loop – comparison of drag disc and turbine flowmeter results – Test S-02-4.

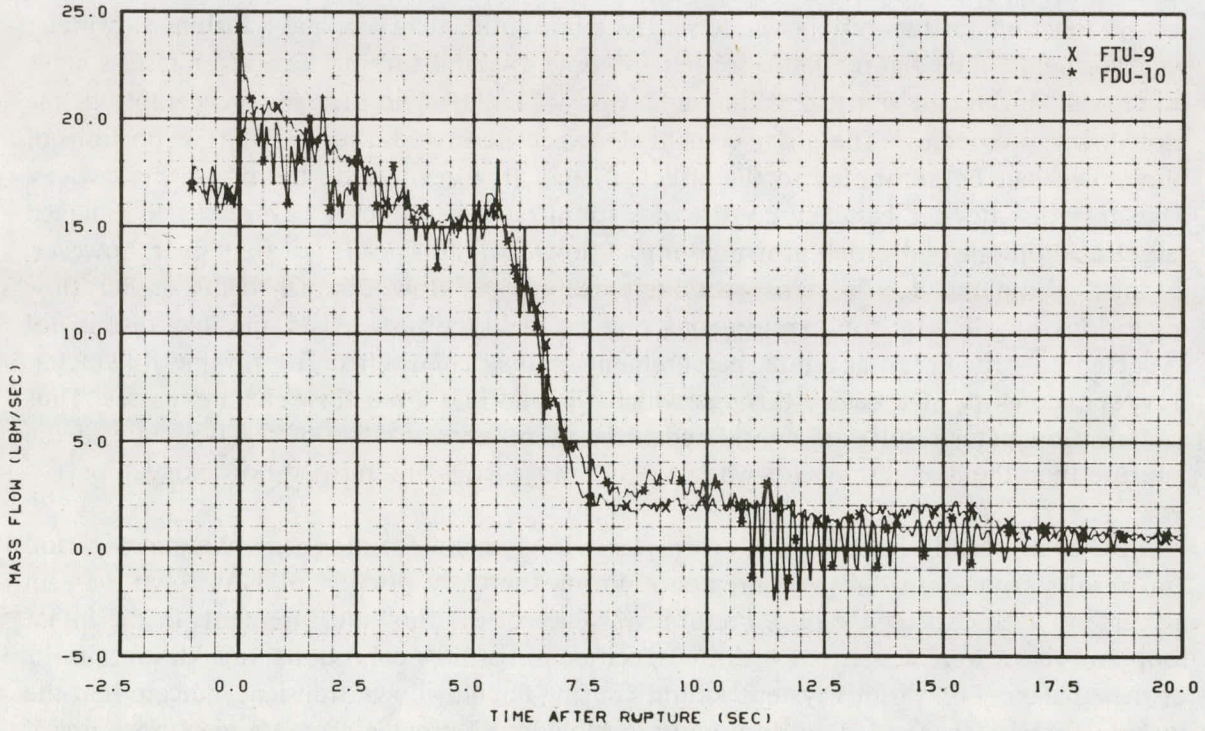

Fig. B-2 Mass flow rate at the intact loop pump suction – comparison of drag disc and turbine flowmeter results – Test S-02-4.

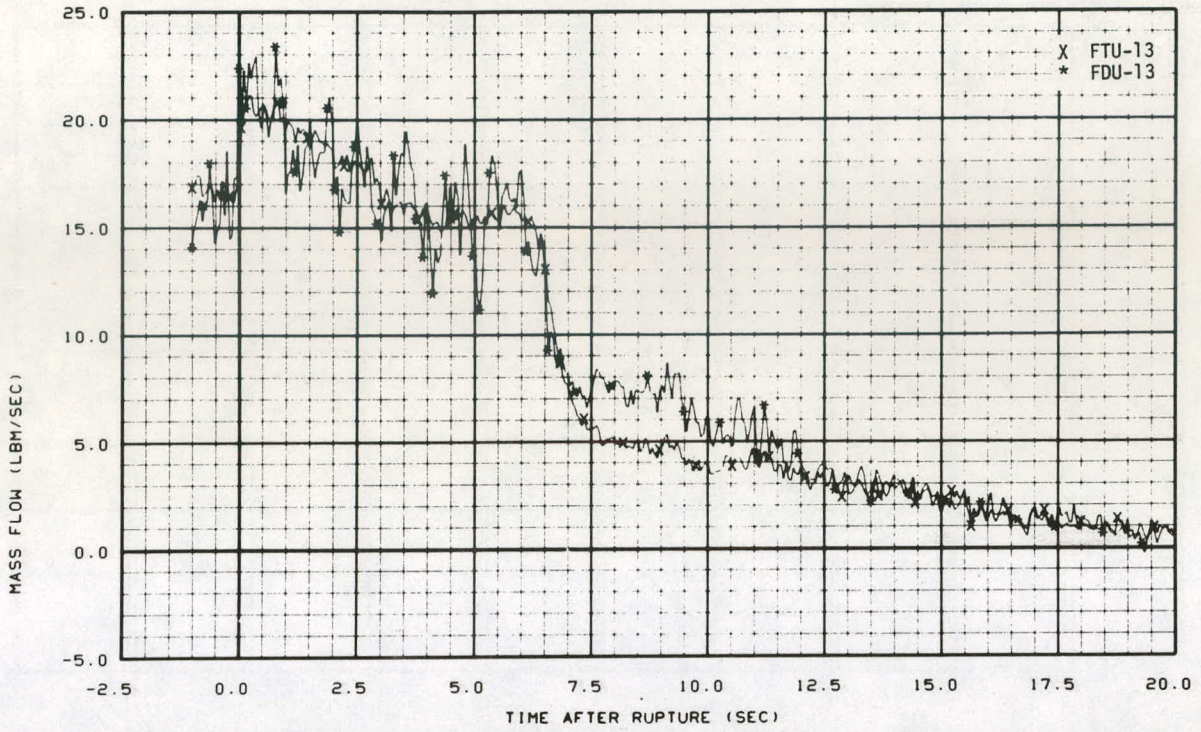

Fig. B-3 Mass flow rate downstream of the intact loop pump – comparison of drag disc and turbine flowmeter results – Test S-02-4.

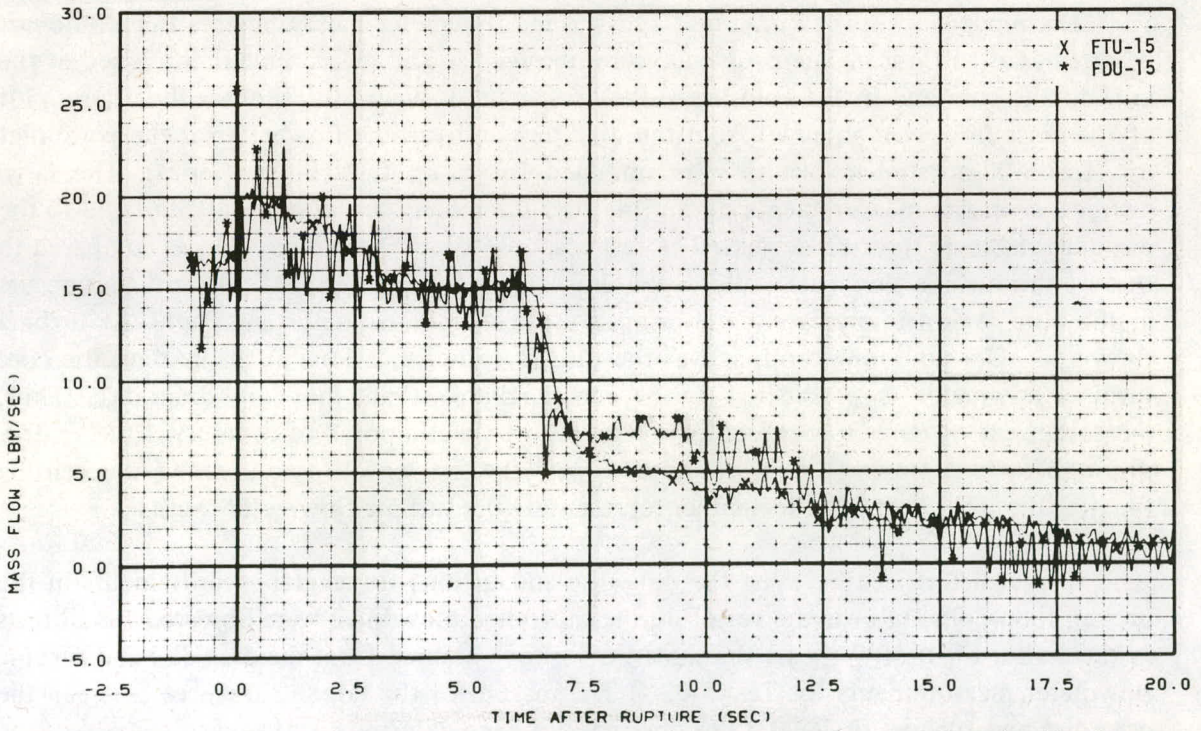

Fig. B-4 Mass flow rate near the vessel on the inlet side of the intact loop – comparison of drag disc and turbine flowmeter results – Test S-02-4.

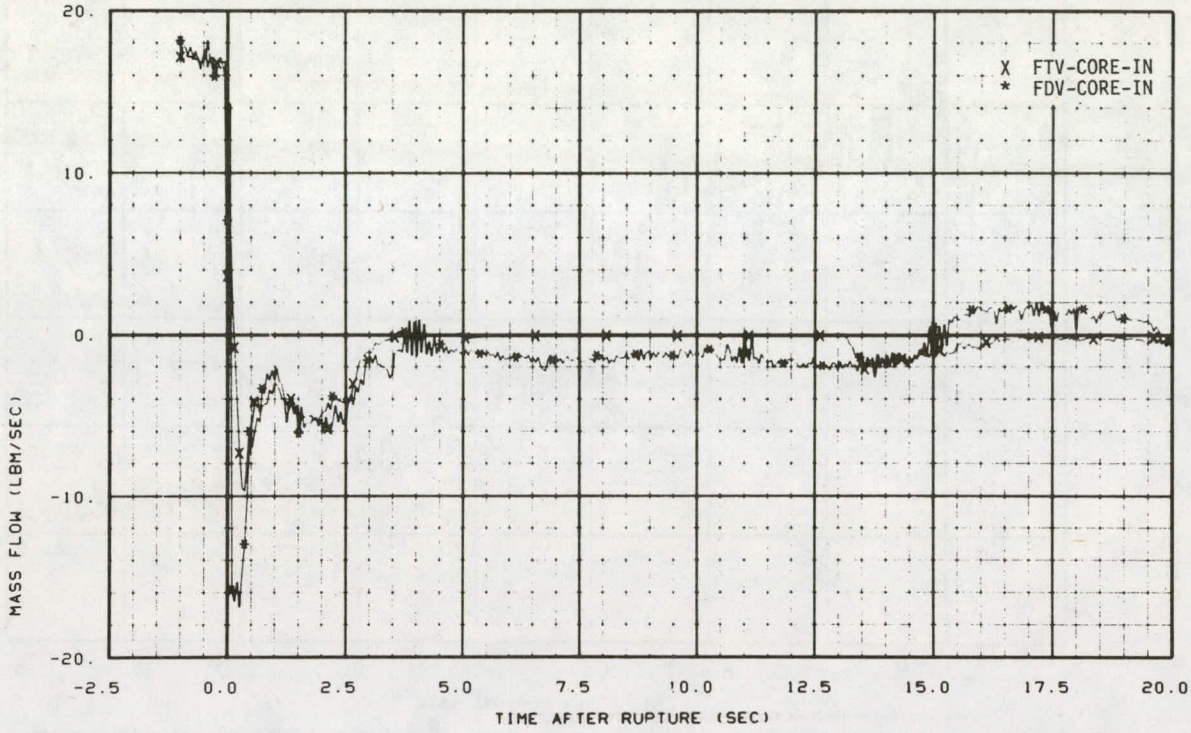

Fig. B-5 Mass flow rate at the inlet to the core – comparison of drag disc and turbine flowmeter results – Test S-02-4.

Discrepancies between drag disc and turbine flowmeter measurements that could not be attributed to flow regime problems were observed in the measurements obtained at the inlet to the core and in the cold leg of the broken loop. Figure B-6 shows a short term plot of the mass flowrates obtained from the drag disc and turbine flowmeter at the core inlet for Test S-02-4 (similar results were obtained for other tests in the series). The large differences in the measurements during the first 0.5 second are directly attributable to the response times of the two devices. The fast response time of the drag disc, as compared to that of the turbine flowmeter, allows the drag disc to follow the rapid transient that occurs in the core region immediately following rupture more accurately than could the turbine flowmeter. Over the long term, as was the case for other locations in the system, the core turbine flowmeter is considered to be more reliable than the core drag disc. Thus, measurements of core flow presented in this report are composed of composites of the drag disc and turbine flowmeter measurements, with the first one to two seconds representing the drag disc results and the remainder representing the turbine flowmeter results.

Large differences between the drag disc and turbine flowmeter measurements in the broken loop cold leg near the vessel during subcooled blowdown were observed for all tests in the series. Figure B-7 shows the mass flow rates obtained from the drag disc and turbine flowmeter measurements for Test S-02-4. The reason for the large differences between the drag disc and turbine flowmeter response has not been determined. However, a study of the flow data has been performed to determine which instrument provided the most accurate measurement of the flow in the broken loop cold leg. A mass balance over the blowdown

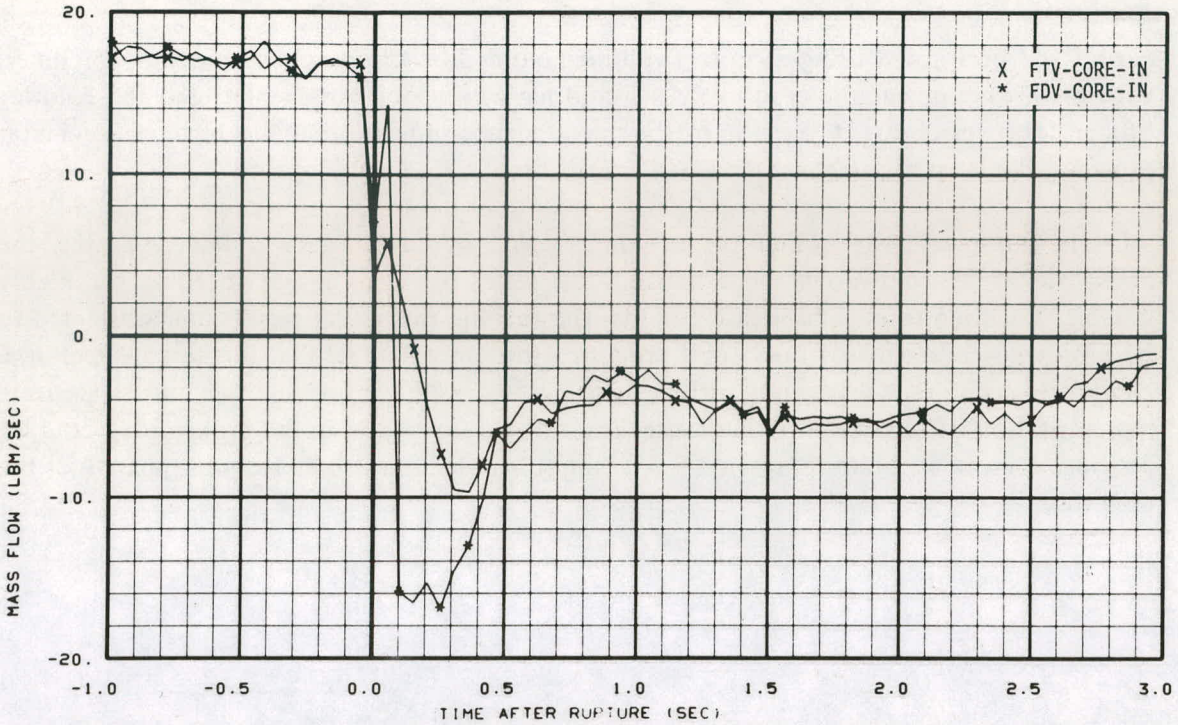

Fig. B-6 Mass flow rate at the inlet to the core (short term) – comparison of drag disc and turbine flowmeter results – Test S-02-4.

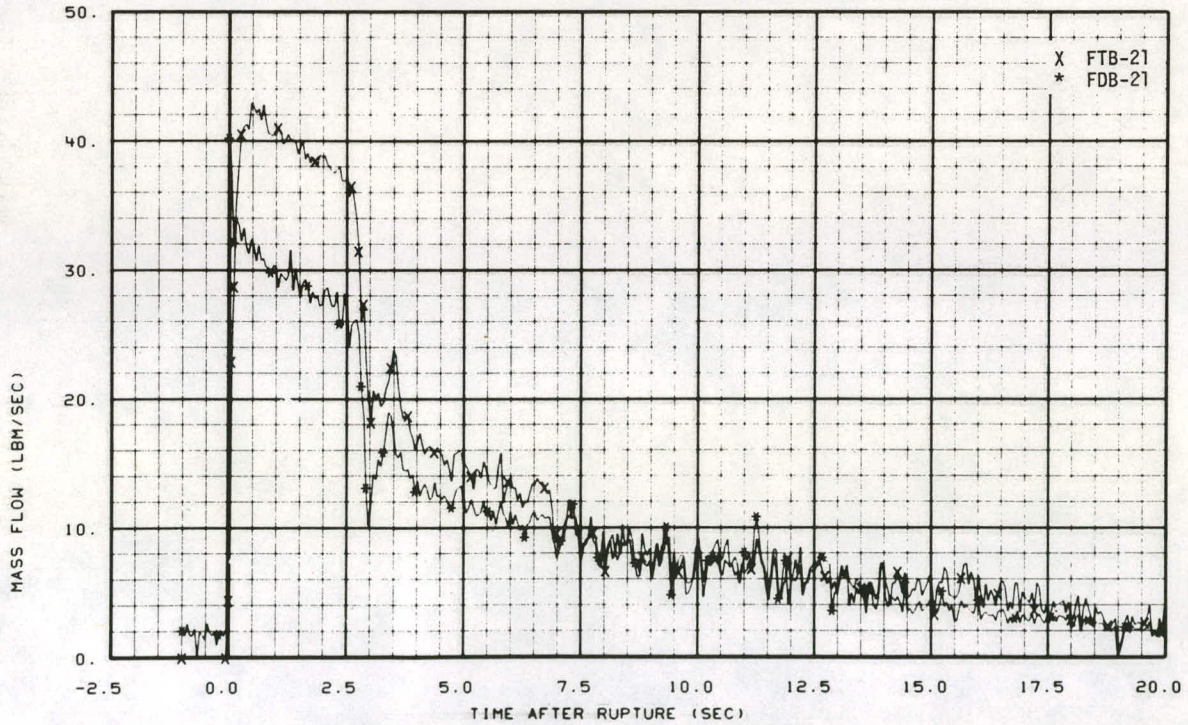

Fig. B-7 Mass flow rate near the vessel on the inlet side of the broken loop – comparison of drag disc and turbine flowmeter results – Test S-02-4.

period was performed using a control volume bounded by the vessel and vessel downcomer, with flow junctions at the core inlet, the cold leg intact loop vessel inlet, and the cold leg broken loop vessel outlet. Results of the mass balance indicate that the turbine flowmeter provided the most accurate measurement of the broken loop cold leg flow.

In summary, an evaluation of the thermal-hydraulic data obtained during the Semiscale Mod-1 blowdown heat transfer test series has shown that the data are highly reliable. For long term flow measurements, the turbine flowmeter results are considered to be more representative of flow conditions than the drag disc results. In the core region, a composite of drag disc and turbine flowmeter results provides the most accurate representation of the core flow response. The turbine flowmeter in the broken loop cold leg provides a more accurate representation of the subcooled blowdown response than does the drag disc.

APPENDIX C

REPEATABILITY OF RESULTS

THIS PAGE

WAS INTENTIONALLY

LEFT BLANK

APPENDIX C

REPEATABILITY OF RESULTS

Experimental data from the Semiscale Mod-1 blowdown heat transfer tests have been evaluated to determine the repeatability of phenomena occurring in the Semiscale system when the system is subjected to similar blowdown environments. Determination of the repeatability of the data for tests with similar conditions is important in evaluating the adequacy and improving the predictive capability of analytical models developed to predict the system response during a blowdown transient. In addition, repeatability of phenomena is important to the Semiscale program because many of the objectives of the Semiscale tests are related to comparing results from two or more differential tests. In these differential tests, either the initial conditions or configuration were changed to determine the effect of the change on the system response. A discussion of the repeatability of the results for the Semiscale Mod-1 blowdown heat transfer test series is discussed in this appendix.

Tests S-02-9 and S-02-9A provided an excellent basis for assessing the repeatability of results during the blowdown transient for tests with similar initial conditions. Test S-02-9 was a rerun of Test S-02-9A, which was necessitated because a valve in the emergency core coolant line to the lower plenum was inadvertently left open during the earlier test. The initial fluid conditions for the two tests were essentially the same. In general, the two tests provided data which were in excellent agreement for the entire blowdown period. Figure C-1 shows the system depressurization rates for the two tests. As can be seen from the figure, the system pressure responses for the two tests were essentially identical. Figures C-2 and C-3 show the mass flow rates near the vessel in the intact loop cold leg and broken loop cold leg, respectively, and Figure C-4 shows the mass flow rates at the inlet to the core. These figures illustrate the high degree of repeatability of system mass flow rates for the tests. The fluid density measurements within the system likewise showed a high degree of repeatability. Figures C-5 and C-6 show the fluid density at the core inlet and in the vessel lower plenum, and Figures C-7 and C-8 show the density at the intact loop pump suction and near the vessel in the broken loop hot leg.

Comparisons of results from other tests in the series which had similar initial conditions, including Tests S-02-4 and S-02-5 and Tests S-02-7 and S-02-9A, also showed a high degree of data repeatability. In certain cases, however, the repeatability of results was affected by unexpected differences in the preblowdown initial conditions or by such factors as slight differences between the pump coastdown speeds during the blowdown transient for two tests.

From the test comparisons previously discussed, the conclusion is reached that the repeatability of the thermal-hydraulic response of the system during the blowdown heat transfer test series was excellent.

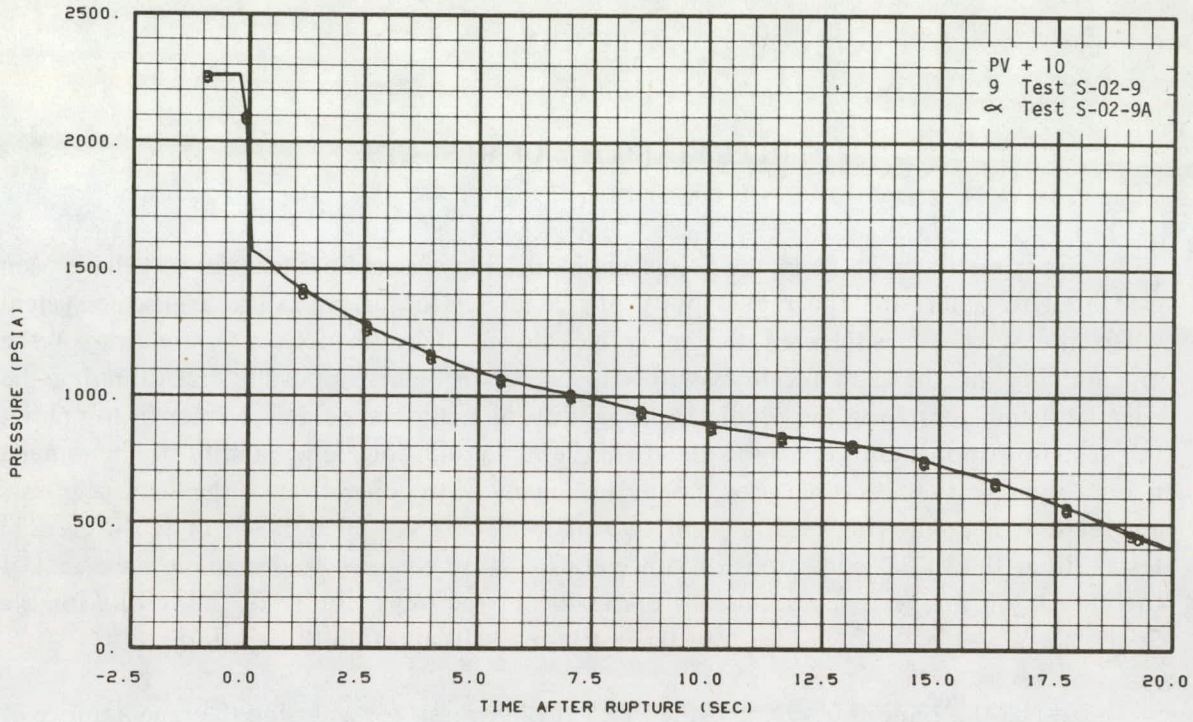

Fig. C-1 System pressure response – showing repeatability of results – Tests S-02-9 and S-02-9A.

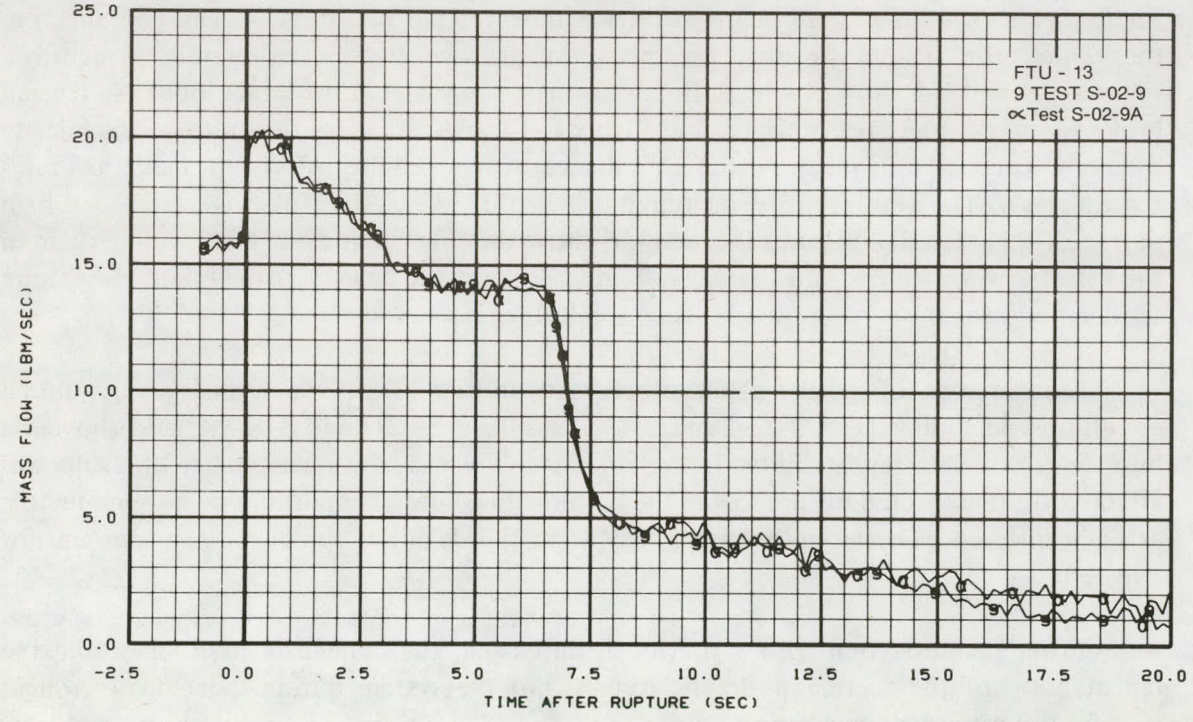

Fig. C-2 Mass flow rate downstream of the intact loop pump – showing repeatability of results – Tests S-02-9 and S-02-9A.

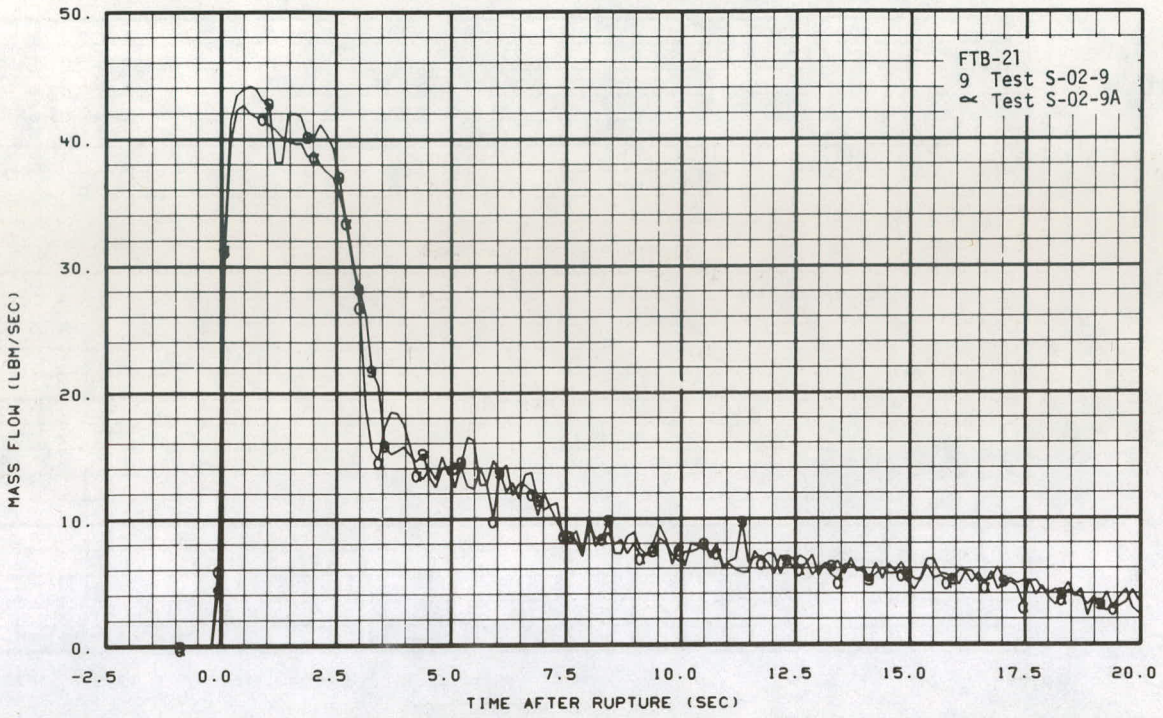

Fig. C-3 Mass flow rate near the vessel on the inlet side of the broken loop – showing repeatability of results – Tests S-02-9 and S-02-9A.

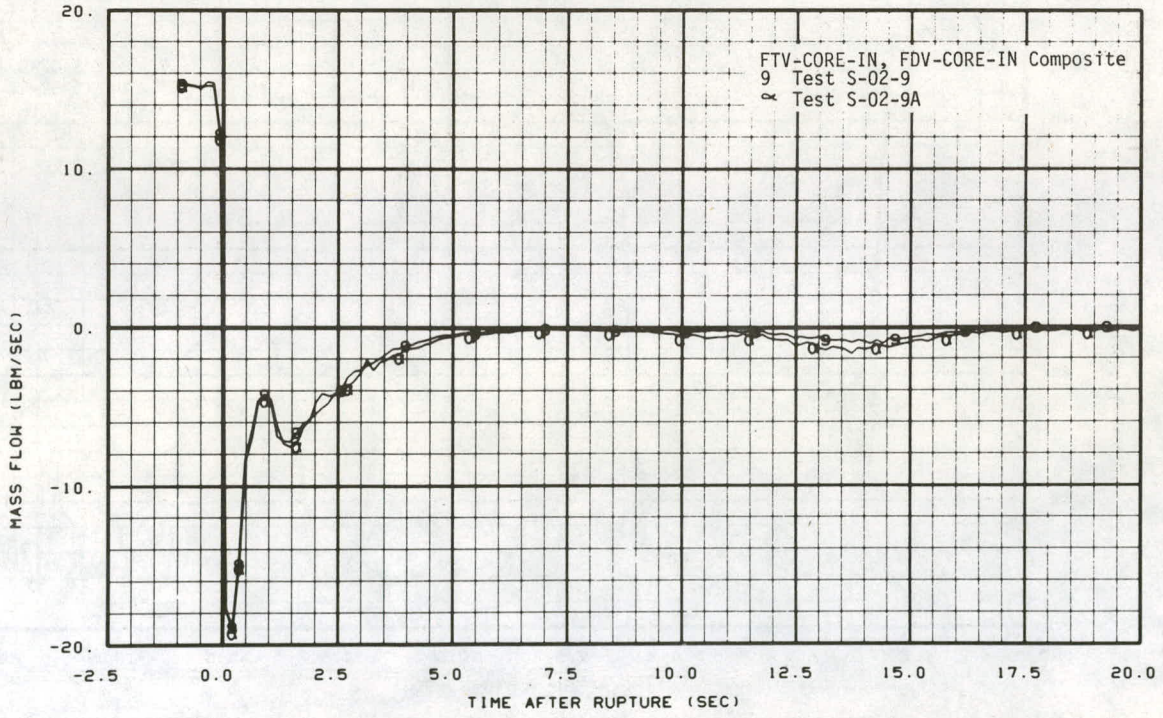

Fig. C-4 Mass flow rate at the inlet to the core – showing repeatability of results – Tests S-02-9 and S-02-9A.

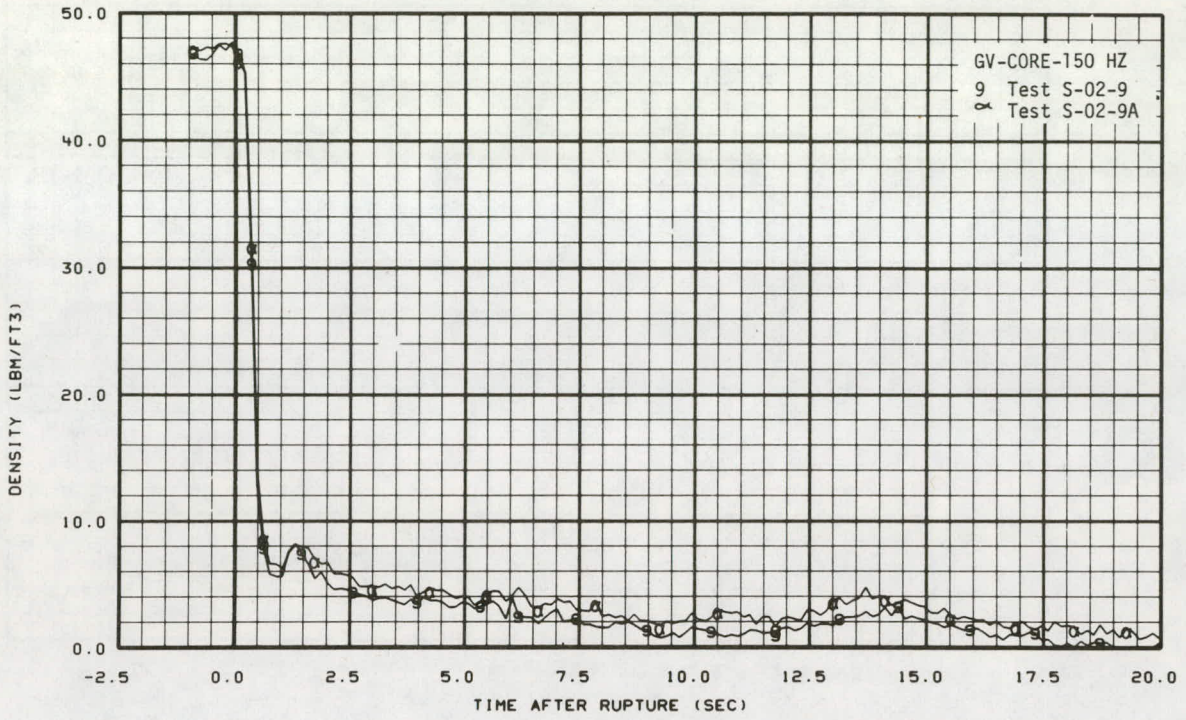

Fig. C-5 Fluid density at the inlet to the core – showing repeatability of results – Tests S-02-9 and S-02-9A.

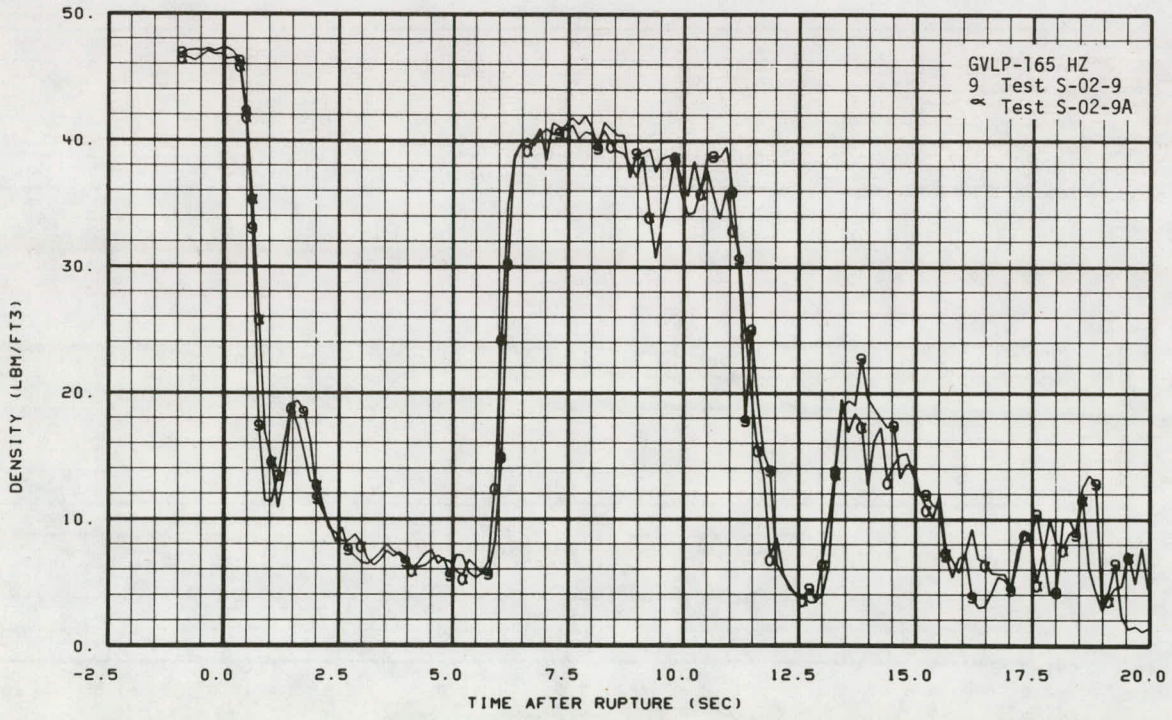

Fig. C-6 Fluid density in the vessel lower plenum 165 inches below the cold leg centerline – showing repeatability of results – Tests S-02-9 and S-02-9A.

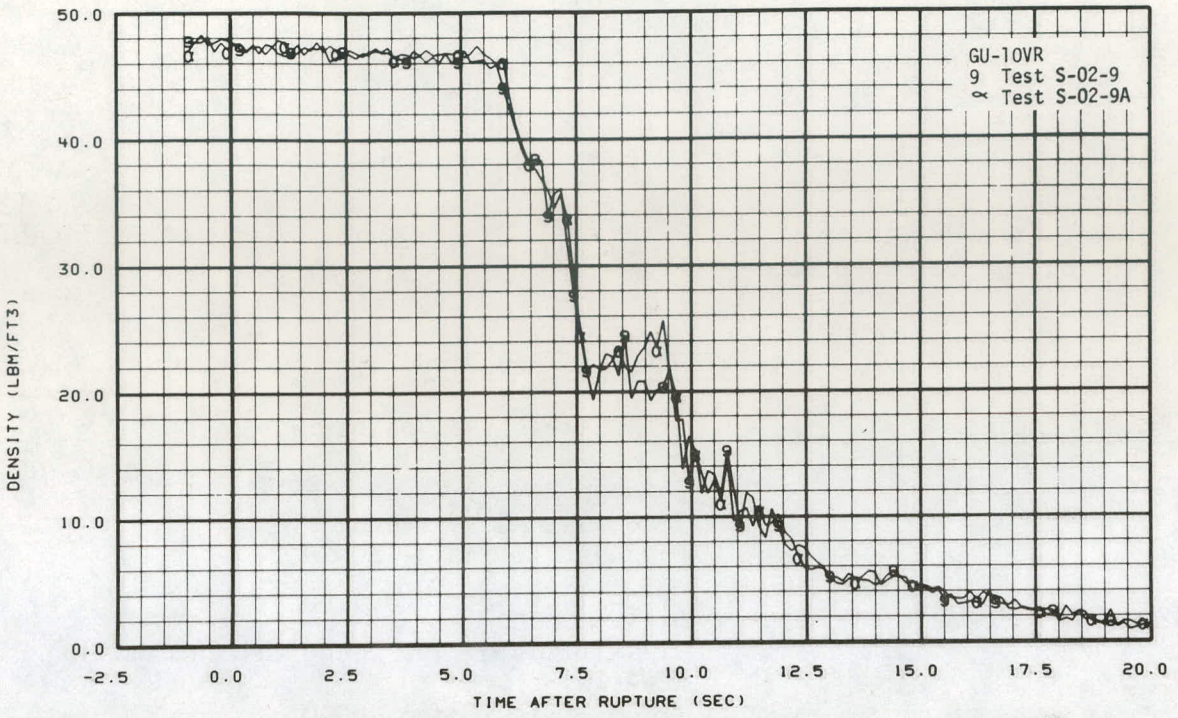

Fig. C-7 Fluid density at the intact loop pump suction – showing repeatability of results – Tests S-02-9 and S-02-9A.

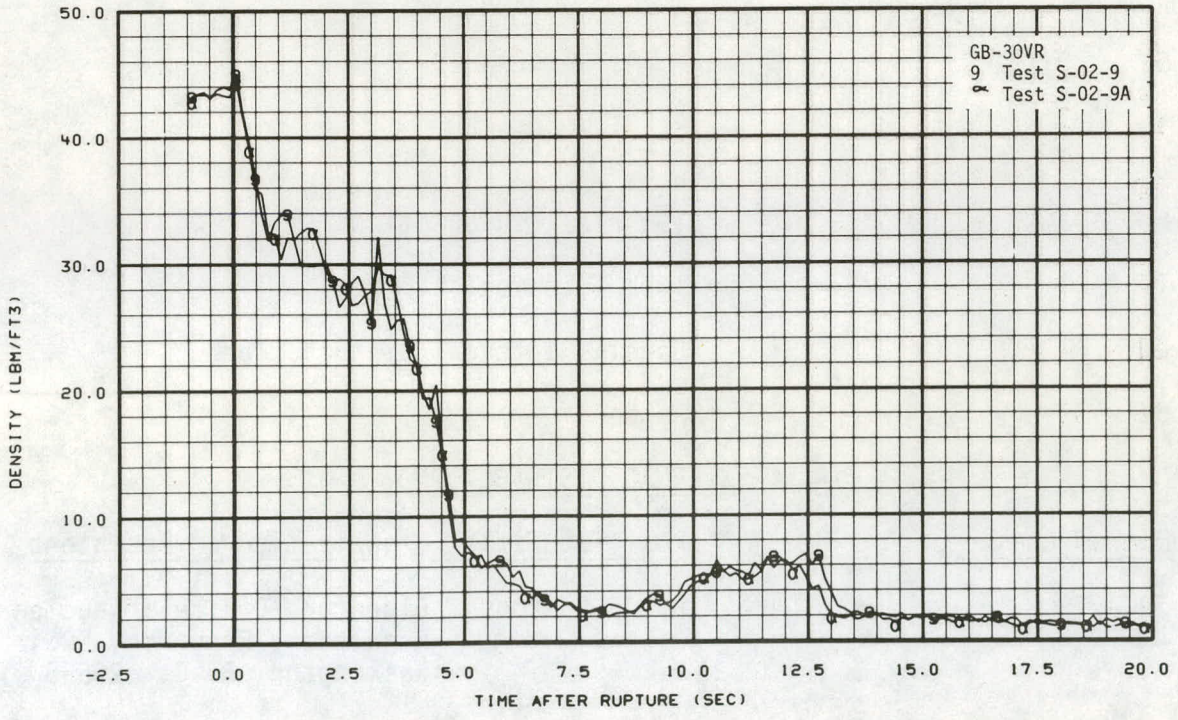

Fig. C-8 Fluid density near the vessel on the outlet side of the broken loop – showing repeatability of results – Tests S-02-9 and S-02-9A.

Report No. ANCR-NUREG-1287
Volume, Part, Revision Not Applicable
Distribution Category No. NRC-2

INTERNAL DISTRIBUTION

No. of Copies	Name of Recipient
1	Chicago Patent Group - ERDA 9800 South Cass Avenue Argonne, Illinois 60439
2 - 4	A. T. Morphew Classification and Technical Information Officer ERDA-ID Idaho Falls, Idaho 83401
5	R. J. Beers, ID
6	P. E. Litteneker, ID
7	R. E. Swanson, ID
8	V. A. Walker, ID
9	R. E. Wood, ID
10	H. P. Pearson, Supervisor Technical Information
11 - 20	INEL Technical Library
21 - 57	Special Internal Distribution
58 - 77	Author

EXTERNAL DISTRIBUTION

No. of Copies	Position Title, Organization of Recipient
78 - 79	H. J. C. Kouts, Director, Office of Nuclear Regulatory Research, NRC, Washington, D. C. 20555
80 - 383	Distribution under NRC-2